Uncovering Spatial and Temporal Patterns of Micropollutants Through Nontarget Analysis of Treatment Systems

By

MADISON ERIN HATTAWAY

DISSERTATION

Submitted in partial satisfaction of the requirements for the degree of

DOCTOR OF PHILOSOPHY

in

Civil and Environmental Engineering

in the

OFFICE OF GRADUATE STUDIES

of the

UNIVERSITY OF CALIFORNIA

DAVIS

Approved:

Thomas Young, Chair

Heather Bischel

Ilias Tagkopoulos

Committee in Charge

2022

Abstract

Treatment systems for wastewater and agricultural runoff serve to protect environmental water quality. However, with the proliferation of new compounds in consumer products and growing acknowledgment of the environmental implications of transformation products of parent compounds, conventional targeted mass spectrometry approaches are no longer sufficient in assessing the efficacy of these systems. Therefore, broad-scope methods such as suspect screening and nontarget analysis must be employed to gain a better understanding of the complex processes occurring within these systems.

This dissertation considers both a municipal wastewater catchment and a scaled-down version of a woodchip bioreactor, and finds that both are comprised of competing physical, chemical, and biological processes. In the first chapter, suspect screening is used to find many different classes of compounds within a set of samples collected at seven different time points and eight different locations within a sewer catchment and at the wastewater treatment plant. In the second chapter, the same set of samples is considered in terms of the bulk nontarget features. However, due to the duration of the sampling campaign, wastewater samples had been run on the LC-QTOF-MS in multiple batches, which then required implementation of an empirical Bayes method to correct for batch effects. The success of this method is explored. Finally, the third chapter uses time-series data from microcosm-scale versions of woodchip bioreactors for agricultural run-off to identify examples of key processes that occur within the system.

ACKNOWLEDGEMENTS

If not for all the people I'm about to list here, I don't know where I'd be or what I'd be doing. Certainly not putting the finishing touches on a dissertation. When I arrived in Davis in 2017, I was deeply sad and very unsure of myself. My miraculous transformation into a contented, slightly more sure of herself person is due entirely to being held in the loving compassion of my community in Davis and afar. I can never say thank you enough.

To Tom Young and Heather Bischel, thank you. Not only have I learned so much from working with both of you, but I have deeply enjoyed it too. To Gabby, Chris, Luann, and Berkley, your willingness to lend a hand and cheerful camaraderie taught me that I don't have to be afraid to ask for help. To Cami, Wenting, and Olivia, my office ladies, thank you for all the chocolate, laughs, and inspiration that helped me push on, even when I wanted to give up. To Hannah, thank you for always having the time to listen, even when your schedule was jam packed.

To my mother and father, who drove three days with me from Prairie Village, Kansas to Davis and helped me move in, after years of moving me in and out of dorms at Vanderbilt and making a million other sacrifices to give me the best start in life that you could, thank you. On the hardest days, I remembered that you believed in me, and that was enough. To Carter, my person, who has loved me steadfastly and been doing most of the cooking, thanks for the free stats consults. I can't wait to see what the future has in store for us.

Dedication

For my parents.

Table of Contents

List of Tables

List of Figures

CHAPTER 1 INTRODUCTION

Despite the fact that 140,000 new chemicals have been synthesized since 1950, we do not have a clear understanding of their effects on human health or environmental health [1]. In the United States, only 126 chemicals are regulated by the Clean Water Act, whereas thousands of chemicals have been detected in the environment and many have yet to be detected [2]. To improve our knowledge of these emerging contaminants (ECs), more environmental monitoring studies and the advancement of detection capabilities through analysis of high-resolution mass spectrometry (HRMS) data is key. Significant sources of anthropogenic chemicals in environmental waters include treated wastewater effluent and agricultural run-off, and thus this dissertation will examine both a municipal wastewater catchment and a treatment system for agricultural run-off through the lens of HRMS.

As one would expect, pharmaceuticals and personal care products abound in wastewater, along with food and beverage-related compounds such as caffeine and sucralose. But consider the other inputs of wastewater—the dishwasher, the laundry machine—and then you get an even greater range of chemicals, including benzotriazole [3] and organophosphate esters [4], compounds which are also subject to variable removal during wastewater treatment. Wastewater treatment plants were not designed to remove these compounds, which are now being detected in surface waters at significant concentrations around the world [5]. Not only is this of concern for aquatic ecosystems, but also for communities that find their drinking water downstream of someone else's wastewater treatment, especially when it comes to persistent and mobile ECs [6].

Agricultural run-off also contains substituents such as nutrients and pesticides that are harmful to the receiving environments, but woodchip bioreactors have shown promise as a potential best management practice to mitigate the discharge of these pollutants [7]. The primary

function of these bioreactors is to leverage the microbial reduction of nitrate (NO_3^-) to nitrogen gas while the microbial community uses the woodchips as a carbon source, thus reducing the nutrient load that is released to the environment [8]. One added benefit may also be the removal of pesticides [9], but measuring reactor efficacy can be challenging with changing patterns in pesticide use and the presence of pesticide transformation products. For example, toxicity identification evaluation studies on agricultural areas of California identified organophosphate pesticides as the main contributors to ambient aquatic toxicity and linked pyrethroid insecticides to both surface water and sediment toxicity in 2010 [10]. However, with increased regulation of organophosphate pesticides, surface water monitoring studies have seen an increase in the frequency of neonicotinoid and pyrethroid detections [11]–[13]. Additionally, environmental transformation of the parent compounds may result in the accumulation of possibly toxic byproducts, rather than the complete mineralization of the parent [14]–[17]. For both these reasons, it is important to consider more broad-scope approaches than the traditional targeted analysis of chemicals.

While conventional targeted screening of liquid chromatography (LC) and gas chromatography (GC) mass spectral (MS) data relies on comparison against analytical standards to identify compounds, limiting analysis to only the chemicals the researcher chooses to consider, “nontarget” approaches rely on first aligning peaks across samples and subsequently attempting to assign molecular formulae and structures. Opting for this broad-screen approach is not without sacrifices, because targeted analysis allows compounds to be identified with the highest degree of confidence [18], has higher sensitivity, and allows for quantification. Additionally, suspect screening, which can compare experimental MS1 and MS2 data against structure and spectral libraries, exists on the spectrum between target and nontarget analysis [19].

Therefore, all approaches will remain important and be used in this research. Nontarget analysis and suspect screening will be beneficial when an analytical standard for a transformation product is not commercially available, or the product is unknown. Furthermore, development of nontarget screening methods will be more broadly applicable to other systems where biological transformation of complex compounds may occur, such as in bioremediation scenarios or wastewater treatment.

This dissertation focuses on two different treatment systems at the interface of the built and natural environments, with insights that may improve our understanding of chemical contributions to natural waters. Chapters 2 and 3 take two different approaches to analyzing a unique set of wastewater samples that were collected at seven timepoints from six sub-sewershed locations and at the WWTP influent and effluent. Chapter 2 begins with an overview of the sewer system through the lens suspect screening to find anthropogenic chemicals reflecting different use classes and down-the-drain pathways. Chapter 3 of this dissertation then looks at the same dataset through a nontarget lens, which requires the evaluation of a statistical method for the removal of analytical batch effects, as the obscuring variation of multiple analytical batches presents a major challenge in identifying true spatiotemporal trends in nontarget features within complex environmental datasets. Chapter 4 focuses on the complex system contained in woodchip bioreactors used for the treatment of agricultural run-off, applying some of the same tools from the previous two chapters to examine time-series data from small-scale batch studies. Finally, Chapter 5 closes with discussion, recommendations for future research, and reflection.

References

[1] P. J. Landrigan *et al.*, “The Lancet Commission on pollution and health,” *Lancet*, vol. 391, no. 10119, pp. 462–512, Feb. 2018, doi: 10.1016/S0140-6736(17)32345-0.

[2] J. Hollender, E. L. Schymanski, H. P. Singer, and P. L. Ferguson, “Nontarget Screening with High

Resolution Mass Spectrometry in the Environment: Ready to Go?," *Environ. Sci. Technol.*, vol. 51, no. 20, pp. 11505–11512, Oct. 2017, doi: 10.1021/acs.est.7b02184.

[3] T. Reemtsma, U. Miehe, U. Duennbier, and M. Jekel, "Polar pollutants in municipal wastewater and the water cycle: Occurrence and removal of benzotriazoles," *Water Res.*, vol. 44, no. 2, pp. 596–604, 2010, doi: https://doi.org/10.1016/j.watres.2009.07.016.

[4] A. Saini, C. Thaysen, L. Jantunen, R. H. McQueen, and M. L. Diamond, "From Clothing to Laundry Water: Investigating the Fate of Phthalates, Brominated Flame Retardants, and Organophosphate Esters," *Environ. Sci. Technol.*, vol. 50, no. 17, pp. 9289–9297, Sep. 2016, doi: 10.1021/acs.est.6b02038.

[5] B. Petrie, R. Barden, and B. Kasprzyk-Hordern, "A review on emerging contaminants in wastewaters and the environment: Current knowledge, understudied areas and recommendations for future monitoring," *Water Res.*, vol. 72, pp. 3–27, 2015, doi: https://doi.org/10.1016/j.watres.2014.08.053.

[6] T. Reemtsma *et al.*, "Mind the Gap: Persistent and Mobile Organic Compounds—Water Contaminants That Slip Through," *Environ. Sci. Technol.*, vol. 50, no. 19, pp. 10308–10315, Oct. 2016, doi: 10.1021/acs.est.6b03338.

[7] L. Christianson, J. Tyndall, and M. Helmers, "Financial comparison of seven nitrate reduction strategies for Midwestern agricultural drainage," *Water Resour. Econ.*, vol. 2–3, pp. 30–56, 2013, doi: https://doi.org/10.1016/j.wre.2013.09.001.

[8] L. E. Christianson, A. Bhandari, and M. J. Helmers, "A practice-oriented review of woodchip bioreactors for subsurface agricultural drainage," *Applied Engineering in Agriculture*. 2012.

[9] Z. Mortensen *et al.*, "Isolation of Microbial Populations with the Ability To Use Pesticides as a Sole Carbon Source in Multichannel Woodchip Bioreactors under a Controlled Environment," 2019.

[10] B. Anderson, J. Hunt, D. Markiewicz, and K. Larsen, "Toxicity in California Waters," Sacramento, CA, 2010.

[11] X. Deng, "Surface Water Monitorin for Pesticides in Agricultural Areas in the Central Coast and Southern California, 2020," 2021.

[12] X. Deng, "Surface Water Monitoring for Pesticides in Agricultural Areas of California, 2015," 2016. [Online]. Available: https://www.cdpr.ca.gov/docs/emon/pubs/ehapreps/report_297_deng.pdf.

[13] K. Moran *et al.*, "Water Quality Impairments Due to Aquatic Life Pesticide Toxicity: Prevention and Mitigation in California, USA," *Environ. Toxicol. Chem.*, vol. 39, no. 5, pp. 953–966, May 2020, doi: https://doi.org/10.1002/etc.4699.

[14] A. S. Gunasekara, T. Truong, K. S. Goh, F. Spurlock, and R. S. Tjeerdema, "Environmental fate and toxicology of fipronil," *J. Pestic. Sci.*, pp. 189–199, 2007.

[15] J. Neuwoehner, T. Zilberman, K. Fenner, and B. I. Escher, "QSAR-analysis and mixture toxicity as diagnostic tools: Influence of degradation on the toxicity and mode of action of diuron in algae and daphnids," *Aquat. Toxicol.*, vol. 97, no. 1, pp. 58–67, 2010, doi: https://doi.org/10.1016/j.aquatox.2009.12.005.

[16] B. I. Escher and K. Fenner, "Recent Advances in Environmental Risk Assessment of Transformation Products," *Environ. Sci. Technol.*, vol. 45, no. 9, pp. 3835–3847, May 2011, doi:

10.1021/es1030799.

[17] A. C. Belfroid, M. van Drunen, M. A. Beek, S. M. Schrap, C. A. M. van Gestel, and B. van Hattum, “Relative risks of transformation products of pesticides for aquatic ecosystems,” *Sci. Total Environ.*, vol. 222, no. 3, pp. 167–183, 1998, doi: https://doi.org/10.1016/S0048-9697(98)00298-8.

[18] E. L. Schymanski *et al.*, “Identifying small molecules via high resolution mass spectrometry: Communicating confidence,” *Environmental Science and Technology*. 2014, doi: 10.1021/es5002105.

[19] M. Krauss, H. Singer, and J. Hollender, “LC–high resolution MS in environmental analysis: from target screening to the identification of unknowns,” *Anal. Bioanal. Chem.*, vol. 397, no. 3, pp. 943–951, 2010, doi: 10.1007/s00216-010-3608-9.

CHAPTER 2 SPATIAL AND TEMPORAL VARIABILITY OF MICROPOLLUTANTS WITHIN A WASTEWATER CATCHMENT SYSTEM

Introduction

While the utility and benefits of anthropogenic chemicals are undeniable, it is also a fact that these compounds have infiltrated the natural environment [1], to the detriment of environmental and human health. One source of chemical pollution in the environment is from treated wastewater, as not all micropollutants are effectively removed during treatment. Those pharmaceuticals, personal care products, flame retardants, plasticizers, and even pesticides inevitably find their way down the drain and at the wastewater treatment plant [2]–[5].

An example of a single, highly-studied compound can be found in fipronil, a common spot-on flea and tick treatment for pets, which was found to be dislodged by bathing up to 28 days post-application [6]. Furthermore, fipronil and its degradates were found to disperse throughout the home presumably via dust and dander [7], which may lead to down-the-drain transport via laundering or showering. Especially in drier climates such as California, where the influence of wastewater effluent on receiving surface waters is largest, these contaminants can have significant effects on aquatic life [8].

Application of broad-scope screening methods such as suspect and nontarget analysis of high-resolution mass spectrometry (HRMS) data can be valuable in environmental monitoring, where changing consumer use patterns and the introduction of new compounds make conventional targeted screening challenging. These approaches have been used to isolate “fingerprints” of human activity, indicating whether a waterway is influenced by agricultural, industrial, or municipal wastewater pollution [9], [10]. Many studies have also trained these tools on understanding removal of compounds across treatment processes [11], [12], which may help to improve the treatment of wastewater before it enters the environment [13]–[15].

However, another option is to look further upstream, to the wastewater catchment system itself, to isolate the sources of these pollutants. Understanding patterns of contaminant loads in time and space may allow for improved management practices such as source control or pretreatment. Few studies have examined the patterns in contaminants within the wastewater catchment system [16]. In this study, wastewater treatment plant (WWTP) influent and effluent plus sites within the catchment system were sampled seven times over a 9-month period. These samples were screened against a library of water contaminants to find spectral matches, which were later confirmed with analytical standards or structure elucidation. Comparison of contaminant patterns between sampling months and sampling sites reflected the complexity of the system.

Experimental

Sampling

Detailed descriptions of the sample collection, preparation, and data acquisition methods applied to this sample set have been previously reported [17] and are summarized in Appendix 2. This includes Figure A2-1, which is a schematic of the connections within the sewer system: trunkline sites A, B, C, D, E, and G all connect separately to the influent of the WWTP. All samples were collected with 15-minute sampling intervals as 24-hour time weighted composite samples using ISCO (model) autosamplers, with the exception of the June 2016 samples which were collected at 30-minute intervals. In July and September, three additional "specialty" sites were sampled to capture wastewater from anticipated contributors of pesticides to wastewater: a laundromat, a pet groomer, and a pest control operation (PCO). These sewer laterals were sampled in such a way that the wastewater would be from the single targeted source.

Suspect Screening

To support subsequent processing in MS-DIAL, raw data files from GC– and LC–QTOF-MS were converted from the vendor format to the analysis base file format (Reifycs Analysis Base File Converter v. 4.0.0). All data were then deconvoluted and aligned using MS-DIAL (v. 3.90). Tentative identifications of aligned features were established by searching against the NIST17 database for GC-EI data, an NCI-specific pesticide database for GC-NCI, and combined library of the Agilent Water Contaminants, Pesticides, and Forensic Toxicology libraries LC-ESI+. Parameter selection and workflow performance evaluation are described in detail in the Supporting Information (Table A1-2 for MS-DIAL alignment parameters; Table A4-2 for detection performance of LC targets in standards and spikes; Table A3-1 for detection performance of GC targets in standards and spikes). For GC suspect screening, the use of retention-index dictionaries added an additional level of confidence, and additional identification steps were not taken.

LC-ESI+ data was also screened using the *Find by Formula* workflow in *MassHunter Qualitative Analysis* against the same library used in MS-DIAL, where a "qualified" identification required mass error less than 15 ppm, an intensity greater than 1000 counts, confirmation with at least one coeluting fragment ion (with a coelution score > 80%), an overall match score of >80% (weighted score of accurate mass, isotopic spacing and isotopic abundance). As in the MS-DIAL alignment, $[M + H]^+$, $[M + Na]^+$, and $[M + NH_4]^+$ adducts were searched. Qualified library hits were compared against library identifications made by MS-DIAL as separate lines of evidence. For each compound that was found by the *Qualitative Analysis* software, which does not perform alignment, there was a range of retention times (RT) and mass-to-charge ratios (m/z) if it was detected in multiple samples. The median, 25^{th} and 75^{th}

percentiles of RT and m/z were used to compare against MS-DIAL aligned features (as each feature is represented by an average RT and m/z). Some compounds identified in *Qualitative Analysis* had quite large interquartile ranges (IQR) of RT, large enough for these ions to be considered different features in the MS-DIAL alignment. Compounds that had a RT IQR greater than 0.7 minutes and were detected in fewer than five samples were omitted from the dataset. Those with RT IQR greater than 0.7 minutes but five or more detections were split apart based on RT. The filtered MS-DIAL alignment was searched for an aligned feature that was within 0.3 minutes of the median RT and ±10 ppm mass error (using median m/z) for each compound from the *Qualitative Analysis* set. Additionally, a Pearson correlation coefficient was computed using the peak height in samples as reported by *Qualitative Analysis* and MS-DIAL and was used to filter out features that did not show a significant correlation in sample abundance. Features were manually inspected in MS-DIAL for peak shape and library hits that were below the score threshold, which indicated that MS-DIAL's deconvolution had identified some qualifying fragments. Suspect identified compounds were selected for targeted MS/MS experiments based on peak height and detection frequency in wastewater samples (rather than spikes, standards, or blanks), compound class, and if there was a standard on-hand.

Quantification of Suspect Compounds

Compounds identified as probable structures by library spectrum match in LC samples that were on-hand as standards were included in a 13-point calibration curve ranging from 0.1 ng/mL to 1000 ng/mL. The calibration curve was run with the LC extracts so that RT and coeluting fragments could be used to confirm the identifications. Data analysis was carried out in *MassHunter Quantitative Analysis* software (v. 10.1), using the internal standard that was closest in retention time. Internal standards that had been added to the extracts were originally used for

target pesticide quantification (listed in Table A1-3). The volumes of the extracts had changed since the original processing, due to reinjection for multiple analyses, and as such, we did not want to add any additional spikes (such as matrix spikes), since the concentration would be unknown. Finally, concentrations were multiplied by the concentration factor for the samples: 1 mL extract/L sample for effluent and 5 mL extract/L sample for influent and trunkline.

Structure Confirmation

For library spectrum-matched LC compounds not currently in the lab inventory, targeted MS/MS experiments were used to gain further insight on the structure. Samples containing high abundances of these compounds were run with a list of precursors to isolate (exact masses and retention times) where collision cell voltages again cycled through 0, 10, and 40 eV. Instrumental parameters are included in Table A1-1. Again, the data were deconvoluted using MS-DIAL (parameters in Table A1-2), and results were exported to both MS-FINDER (v. 3.24) and SIRIUS CSI:FingerID for identification using *in silico* fragmentation approaches [18], [19]. Additionally, at the end of each targeted MS/MS run, a mix of RTI compounds was run in *All Ions* made for input into an RTI prediction platform (http://rti.chem.uoa.gr/) [20], which was then used to evaluate the top-ranked structure options for a suspect using experimental RT.

Computation of Mass Loads

Quantified concentrations in wastewater extracts for confirmed structures was both left- and right- censored, due to relative responses below the limit of quantification as well as above the highest calibration point. To create boxplots, the function ros(), from R package NADA (ver. 1.6-1.1) was used [21] to impute non-detect values. For points exceeding the calibration curve range, the highest calibration point was used. Censored values in mass load per capita box-and-whisker plots are differentiated by shape from un-censored values. Flow data was available for

trunkline sampling points, and the sum of these was used as an estimate of population for influent and effluent samples. To calculate the mass load (mg/d*person), the concentration of the sample (ng/L) was multiplied by the corresponding flow and divided by the population.

Statistical Analysis for Significant Difference

To determine if mass loads per capita were statistically significantly different between sampling months and sites, a pairwise Wilcox rank-sum test with a Benjamini-Hochberg correction was implemented for compounds with ≥50% un-censored data points. For annotated GC compounds, the raw peak height was divided by the peak height of an internal standard, 4,4'-dibromooctafluorobiphenyl (DBOFB), to obtain a scaled peak height. This was used in a similar pairwise Wilcox rank-sum test. A similar approach was used for the three annotated LC features, using instead the peak height of the internal standard, simazine-d10, for scaling.

Compound Correlation Test

Some compounds were observed following similar monthly or site-wise patterns, and so we obtained a correlation matrix, using function rcorr() from package Hmisc (v. 4.7-0) [22], consisting of correlation coefficients and p-values of the Spearman rank correlation of each compound against the other. A Spearman correlation was used rather than Pearson because relationships between compounds were not necessarily expected to be linear. Finally, p-values were adjusted for multiple tests to control the false discovery rate using p.adjust() with method "fdr".

Results and Discussion:

Quantification of micropollutants

In the LC data, there were 63 library hits corresponding between MS-DIAL and Qualitative Analysis. 14 of these were available in the lab inventory as standards and were quantified.

Additionally, the fungicide diethofencarb was identified by suspect screening, but when compared against an analytical standard, was not confirmed. This might be due perhaps to degradation of the already infrequently detected peaks in the original sample analysis (2016-2017), although others have found that a peak originally thought to be diethofencarb was in fact metoprolol acid, a metabolite of metoprolol and atenolol [23]. Additionally, a feature annotated as 8-hydroxyquinoline and one as benzotriazole were detected with moderate frequency (approximately 40% of samples) but were not confirmed when compared against standards. Benzotriazole is commonly detected in wastewater, owing to its application as a corrosion inhibitor in dishwashing machines [24], [25]. Table A3-2 presents the list of suspect hits, the frequency of feature detection, use class, and level of identification confidence (if confirmed) [26]. Table 2-1 summarizes the detection frequency of the compounds that were confirmed with analytical standards.

Table 2-1: Detection frequency in trunkline, influent, and effluent samples of quantified micropollutants

	Detection frequency		**Detection frequency**
Caffeine	87.5%	Metoprolol	7.14%
Carbamazepine	1.79%	O-Desmethytramadol	5.36%
DEET	92.9%	Oleamide	89.3%
DEHP	58.9%	Sulfamethoxazole	44.6%
DEP	75%	Tris(2-butoxyethyl) phosphate (TBEP)	92.9%
Fexofenadine	12.5%	Trimethoprim	14.3%
Iohexol	85.8%	Valsartan	58.9%

Among the list of compounds that were tentatively identified via suspect screening, many of the common use-classes of chemicals detected in wastewater were included, with the notable exception of any sweeteners. Other food-related compounds including caffeine, caffeine metabolites, and piperine were suspect-hits, with caffeine then being confirmed at a confidence

level 1, and piperine at 2a. In previous studies of wastewater treatment plants and surface water, sweeteners are detected with a ubiquity to even lend the artificial sweetener, acesulfame, the proposed role as indicator of anthropogenic load on surface waters [27].

Compounds detected at high frequencies and at high concentrations represent a range of use classes and potential down-the-drain routes. This group included caffeine, DEET, bis(2-ethylhexyl) phthalate (DEHP), diethyl phthalate (DEP), iohexol, oleamide, and tris(2-butoxyethyl) phosphate (TBEP). This is reflective of the high frequency of use of these compounds among the population, or in the case of iohexol, the dosage at which it is administered. Iodinated x-ray contrast media (ICM), such as iohexol, are consumed in large dosages, with one hospital studied by Weissbrodt et al. (2009) reporting iohexol as the ICM with the largest amount consumed per day. DEP and DEHP, although both phthalates, have different uses and thus may have different pathways to the wastewater system: DEP is used as a solvent and in multiple kinds of personal care products, whereas DEHP is primarily employed in soft plastics such as toys, food containers, and food packaging [29]. TBEP (also abbreviated as TBOEP) is a organophosphate ester flame retardant, a class that has seen an increase in use with the phase-out of brominated flame retardants [30]. A study of the San Francisco Bay, to which the WWTP of this study discharges, found a 100% detection frequency of TBEP in bay water samples [31]. TBEP and DEHP can enter the wastewater system via laundering of fabrics, which have been found to accumulate TBEP and similar semi-volatile compounds from air and dust [32]. Oleamide is a polymer lubricant used in plastics such as food and medicine containers, and has also been found to leach out of these plastics [33]. Sewer sampling that occurred at the sites of a groomer, laundry, and pest control operation (PCO) found a similar subset of compounds that were detected with high frequency, as detailed in Table 2-2.

Table 2-2: Detection frequency of quantifiable micropollutants in specialty sampling sites

Compound	Groomer (n = 4)	Laundry (n = 4)	PCO (n = 2)
Caffeine	100%	100%	100%
DEET		100%	100%
DEHP	25%	100%	100%
DEP	100%	100%	100%
Iohexol		75%	
O-Desmethyltramadol	50%		
Oleamide	25%		100%
TBEP	100%	100%	100%
Valsartan			50%

Compounds that were quantified less frequently or at lower concentrations were all pharmaceuticals or metabolites of pharmaceuticals (Table 2-3). Multiple classes of pharmaceuticals were represented: two antibiotics, sulfamethoxazole, and trimethoprim; one antihistamine, fexofenadine; a beta-blocker, metoprolol; an anti-seizure medication, carbamazepine; and the metabolite of an opioid painkiller, o-desmethyltramadol. Additionally, valsartan, an anti-hypertensive, was detected most frequently of the quantified pharmaceuticals. Valsartan and o-desmethyltramadol were the only pharmaceuticals detected at the specialty sites, reflecting the relatively small catchment served by these sampling locations. The higher frequency of detection of these compounds in WWTP effluent samples is most likely due to the higher sample volume and less-complex matrix. All pharmaceuticals quantified here have been documented in other studies of wastewater and surface water. A report of seven different WWTP in the San Francisco Bay area found valsartan to be among the top ten highest concentration pharmaceuticals in influent samples, with valsartan, metoprolol, carbamazepine, and sulfamethoxazole included in the top ten for effluent samples [34].

Table 2-3: Concentrations of infrequently detected quantifiable compounds

Month	Site	Sulfamethoxazole	Fexofenadine	Trimethoprim	Metoprolol	Carbamazepine	O-Desmethyltramadol
May	C	43.83					
May	Effluent	6.54	59.64				
June	D	28.95					
June	C	25.26					
June	A	28.98					
June	Effluent	6.62	52.79				
July	D	32.09					
July	C	51.61		102.00			
July	Influent	26.37					
July	Effluent	22.48	195.53		23.05		
Aug	D	25.38					
Aug	C	35.65					
Aug	Influent	25.47		68.06			
Aug	Effluent	79.25	> Cal	21.66	174.34	63.26	54.15
Sep	G						155.90
Sep	A	40.88		69.97			
Sep	Effluent	19.23	365.42	12.28	74.52		32.69
Nov	D	33.60					
Nov	C	132.40					
Nov	E	28.39					
Nov	A	43.47		60.34			
Nov	B		137.87				
Nov	Influent	31.81					
Nov	Effluent	15.47	117.86		42.28		
Jan	E	181.54		414.57			
Jan	B	27.32		66.12			
Jan	Effluent	5.37					

Detection frequency of LC annotated compounds

Of the suspect hits in the LC dataset, that were not quantified, 23 were selected for targeted MS/MS experiments due to peak height, sample detection frequency, and use class. However, only 3 structures were confirmed with tMS/MS experiments. These compounds were acetaminophen, mycophenolic acid, and piperine. In trunkline, influent, and effluent samples, corresponding MS-DIAL aligned features had detection frequencies of 57%, 54%, and 25%, respectively, where a detection was counted as a peak with height greater than 3000 counts. A study of seven different Bay Area WWTP found acetaminophen among the top-ten pharmaceutical compounds in WWTP influent [34]. Mycophenolic acid is an immunosuppressant drug developed for prevention of organ transplant rejection [35] and is also used in cancer treatment [36]. One study found mycophenolic acid in 6 out of 6 WWTP effluents [37]. Piperine is an alkaloid present in black pepper, is excreted in the feces, and thus has been found to be ubiquitous in wastewater [38].

The aligned EI dataset returned 1,470 annotated features. The subset considered herein was created by choosing a mix of use-classes and variable patterns within sampling dates and sites. Similarly, the NCI aligned dataset yielded 48 annotated features, most of which were pesticides, largely those covered by targeted analysis in Teerlink et al. [17]. Again, MS-DIAL aligned peaks with heights greater than 3000 counts were counted as detections, and the detection frequencies of a subset of suspect-identified compounds is included in Table A3-3. Of these, the most frequently detected compound in the trunkline, influent, and effluent samples was oxybenzone, a UV filter. Equally ubiquitous was 3-methyl phenol, a human urinary metabolite of toluene.

Comparison of LC compound loads across months and sites

Concentrations of quantified compounds were converted to mass loads per capita to gain a better understanding of contributions from different sections of the wastewater catchment system and throughout the year. Table 2-4 details the comparisons found to be significantly different ($p < 0.05$) using a Wilcox rank sum test.

Table 2-4: Per capita load (mg person^{-1} day^{-1}) comparisons found to be statistically significant using a Wilcox rank-sum test with a Benjamini-Hochberg test for multiple comparisons ($p < 0.05$)

Caffeine	May, Jun < Jul, Aug, Sep, Nov	Effluent < B, C, D, G
DEET	Jul, Aug, Sep > May, Jun, Nov, Jan	Jan > May
DEHP	May, Jun < Jul, Aug, Sep, Nov, Jan	
DEP	May, Jun < Nov, Jan < Jul, Aug, Sep	
Iohexol	May, Jun < Aug	C > D, E, Eff
Oleamide	Eff < Inf < A, B, C, D, E, G	
TBEP	May, Jun < Jul, Aug, Sep, Nov, Jan	

One interesting pattern that emerged was the significantly lower loads in the months of May and June for caffeine, DEET, DEHP, DEP, Iohexol, and TBEP. Alternatively, oleamide and valsartan do not show any significant monthly variation in load. In the case of caffeine, this difference in mass loads is unexpected, if one were to assume that caffeine consumption would remain consistent throughout the year (Figure 2-1). Although caffeine was proposed as a proxy for population, it is also susceptible to biodegradation by biofilms within the sewer system, a process which can vary depending on a number of variables [39]. Bis(2-ethylhexyl) phthalate and tris(2-butoxyethyl) phosphate have a similar pattern to caffeine, with May and June both lower than the other five months. The load per person of tris(2-butoxyethyl) phosphate measured

here is greater than that reported by O'Brien et al. [30], which was a cumulative organophosphate flame retardant load of 0.8 – 2.6 mg person^{-1} day^{-1}, with TBEP making up the greatest share, the quantifiable loads here varied from 0.01 mg person^{-1} day^{-1} to as high as 12.01 mg person^{-1} day^{-1}.

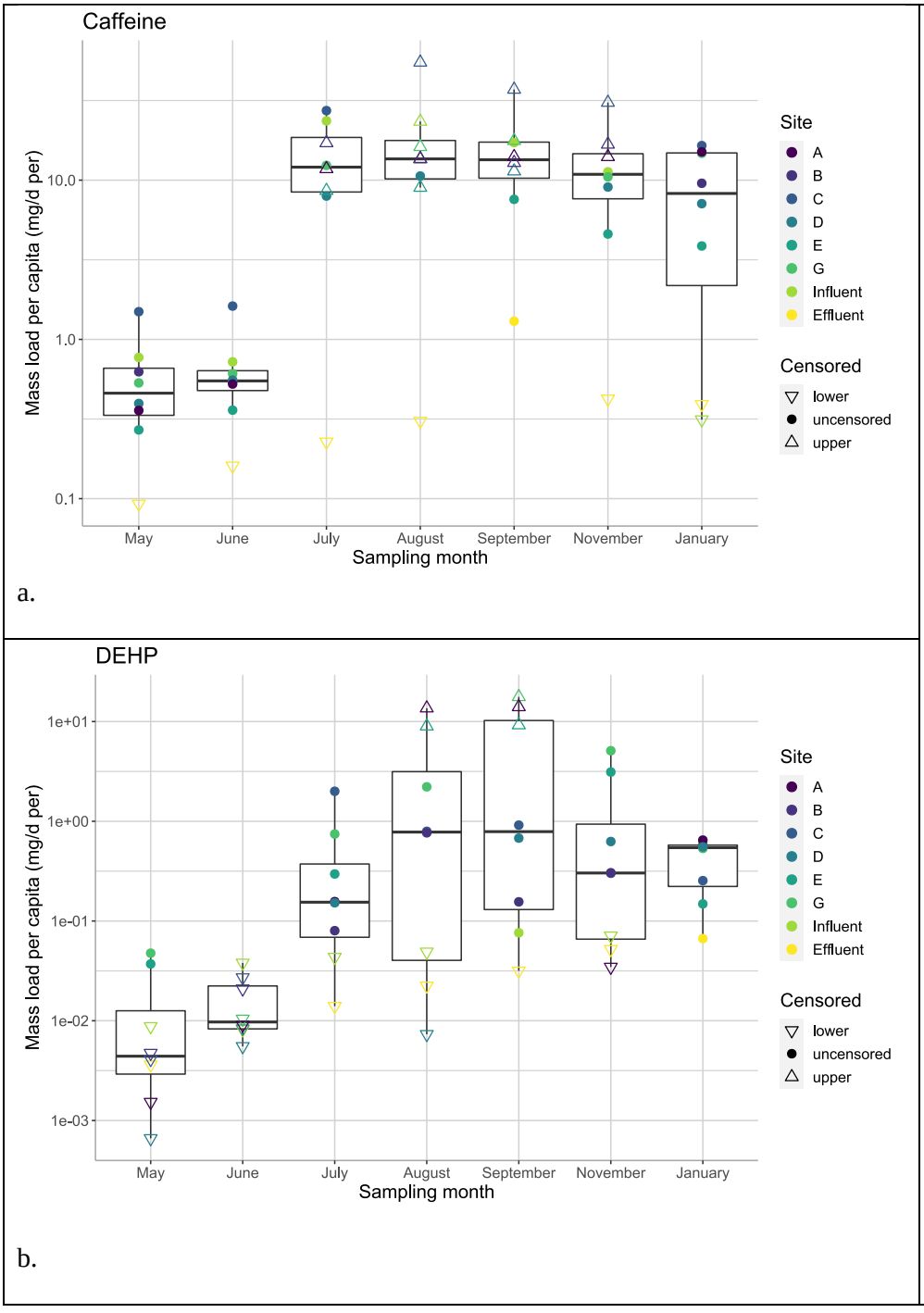

Figure 2-1. Mass load per capita of (a.) caffeine, (b.) bis(2-ethylhexyl) phthalate, and (c.) tris(2-butoxyethyl) phosphate across the sewer system, arranged by month, shows significantly lower amounts in the months of May and June.

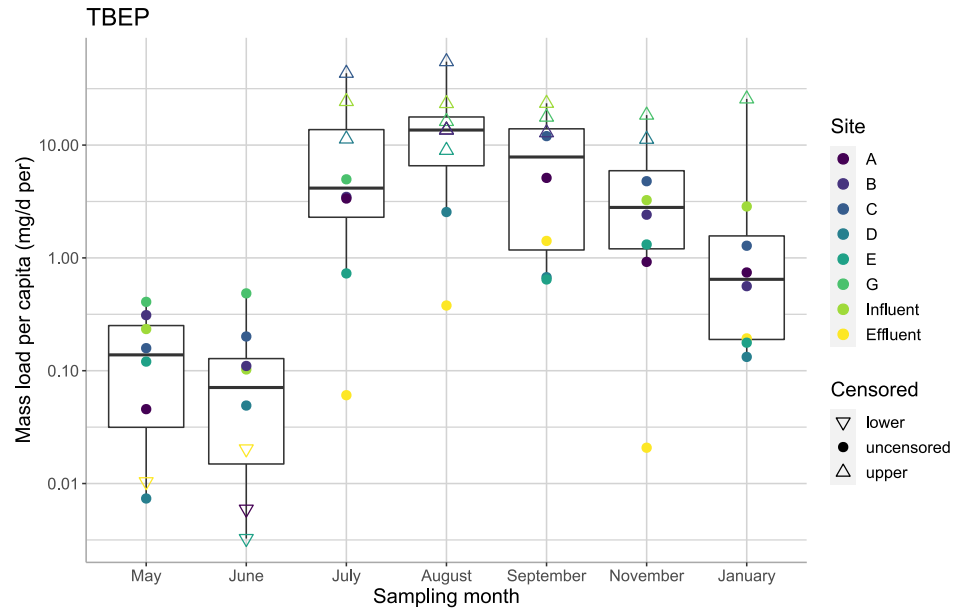

c.

For the X-ray contrast agent, iohexol, per capita loads in May and June are only significantly lower than the August load (Figure 2-2). The sampling site C had significantly higher loads than D, E, and WWTP effluent (Figure 2-2b).

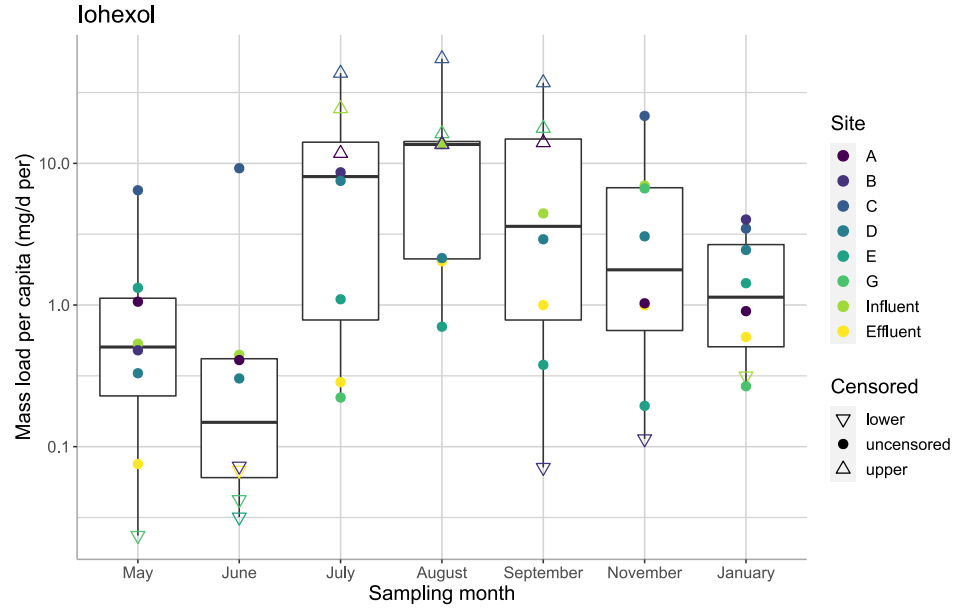

a.

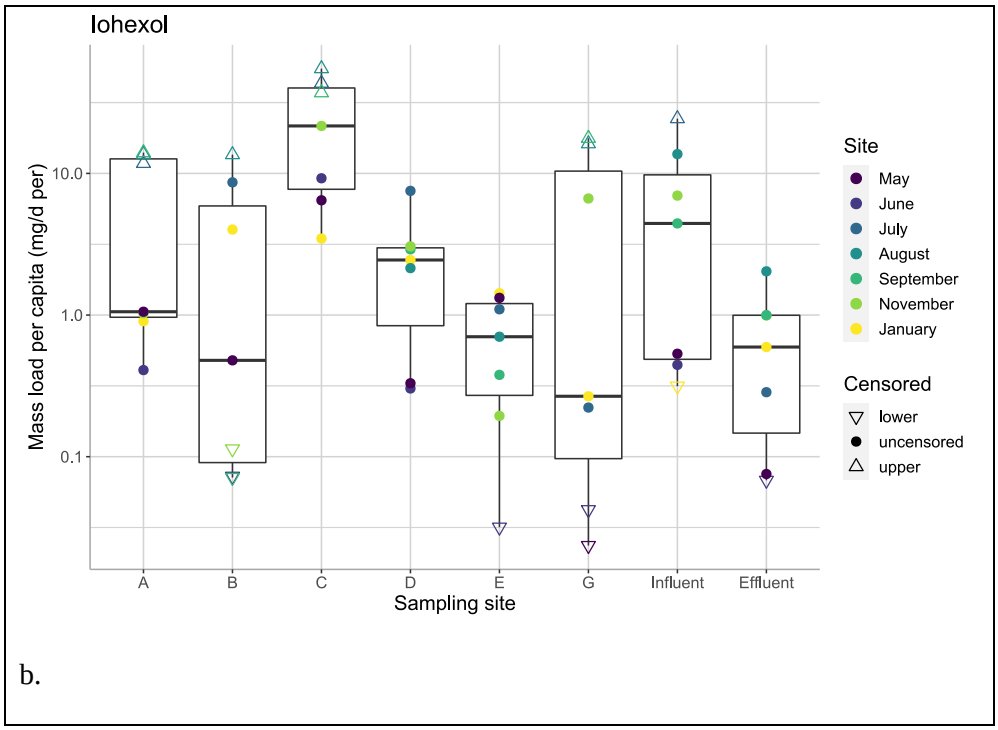

Figure 2-2. Mass load per capita of iohexol across the sewer system, arranged by (a.) month and (b.) site, shows that May, June are lower than August and site C is greater than D, E, and WWTP effluent.

However, in the case of DEET, the summer months of July, August, and September show significantly higher loads than all other months, which may correspond with times of mosquito prevalence (Figure 2-3a). Diethyl phthalate follows a similar pattern to DEET (Figure 2-3b): highest in July through September, with January and November greater than June and May. This similar pattern may be linked to the similar applications of products containing the two compounds.

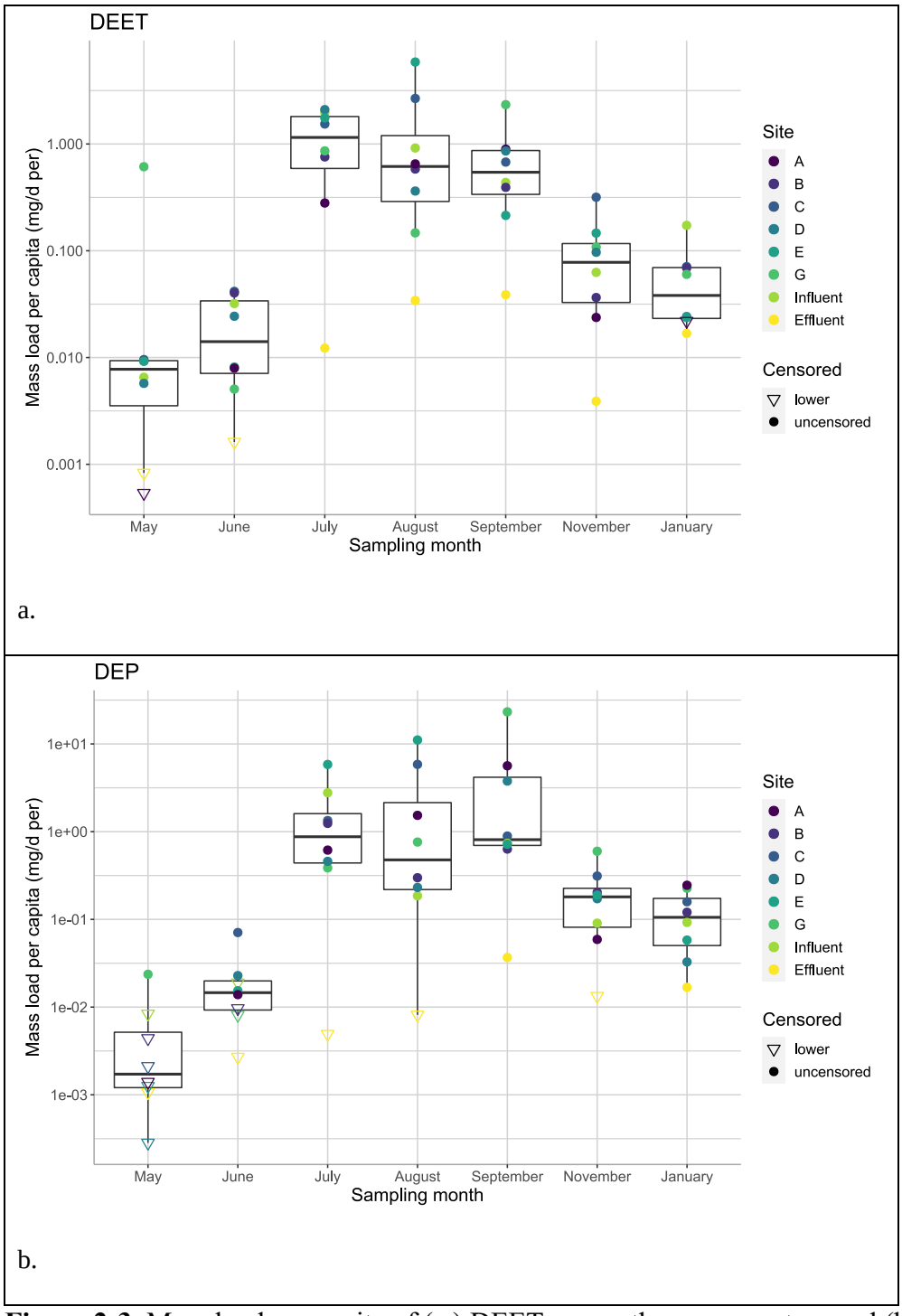

Figure 2-3. Mass load per capita of (a.) DEET across the sewer system and (b.) diethyl phthalate, arranged by month, shows significantly highest amounts in the summer months of July, August, and September.

Because the samples were collected as time-weighted composites, rather than flow-weighted, there is an associated uncertainty with the load patterns presented here [40]. Ort et al. [41] show that a pulse of anthropogenic gadolinium (an x-ray contrast agent) can occur over the span of 15 to 20 minutes at the influent of a WWTP; such pulses may be narrower upstream in the system at the sub-sewershed sampling sites. Samples were collected as 24-hour composites, with a sampling frequency of 15 minutes. Additionally, greater flows occurred in January, despite the fact that the system normally receives negligible inflows from non-sanitary sources [17].

Comparison of GC annotated compounds by month and site

For compounds annotated from the GC-EI and NCI datasets, absolute peak heights were scaled by the height of DBOFB internal standard in the sample before comparison. 2-Naphthalenol is a human xenobiotic metabolite (Phase 1) of naphthalene; the most likely routes human of exposure are through fuels, moth repellents, and cigarette smoke [42]. Phenol, 3-methyl (also known as m-cresol), is a urinary metabolite and used as a biomarker for human exposure to toluene, which may be found in fuels as well [43]. Presumably the general population could be exposed to naphthalene and toluene from vehicle exhaust. These two compounds show different patterns by month, with higher levels of 2-naphthalenol in May and June, and a majority of non-detects in later months (Figure 2-4). 3-methyl-phenol was detected consistently across the months, although January and November are significantly lower than May, June, August, and September.

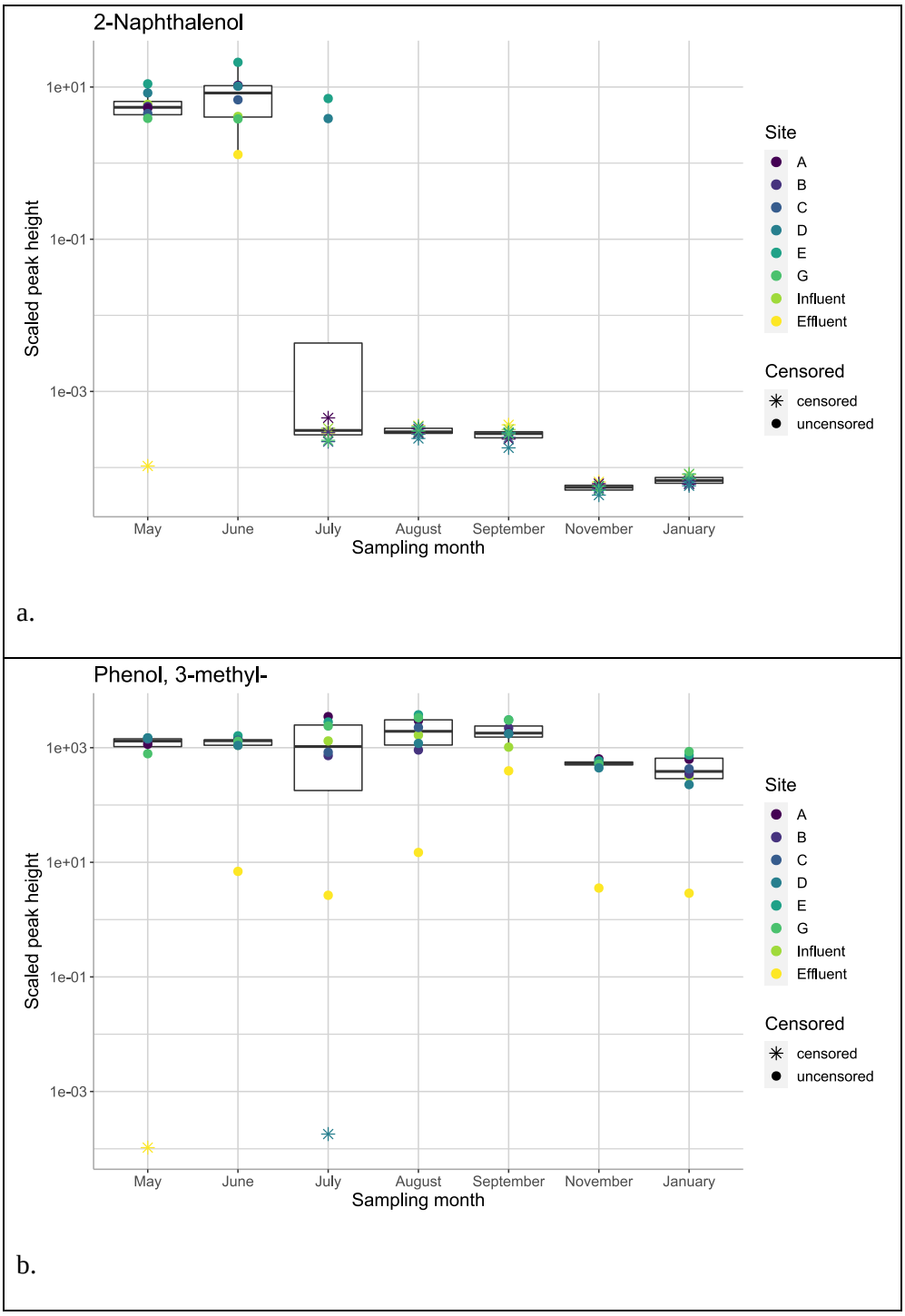

Figure 2-4. Different monthly patterns in two human biomarkers for exposure to xenobiotics (a.) 2-naphthalenol and (b.) phenol, 3-methyl- (m-cresol).

2-Propanol, 1-chloro-, phosphate (3:1) (TCPP) is a chlorinated organophosphate flame retardant that is now frequently used in flexible polyurethane foam products and can be found in

house dust [44]. The most probable down-the-drain route for this compound would be from laundry water [32], [45]. Compound abundance in September is significantly higher than in May, July, November, and January (Figure 2-5). January is also significantly lower than June and August, and November lower than May, June, and August.

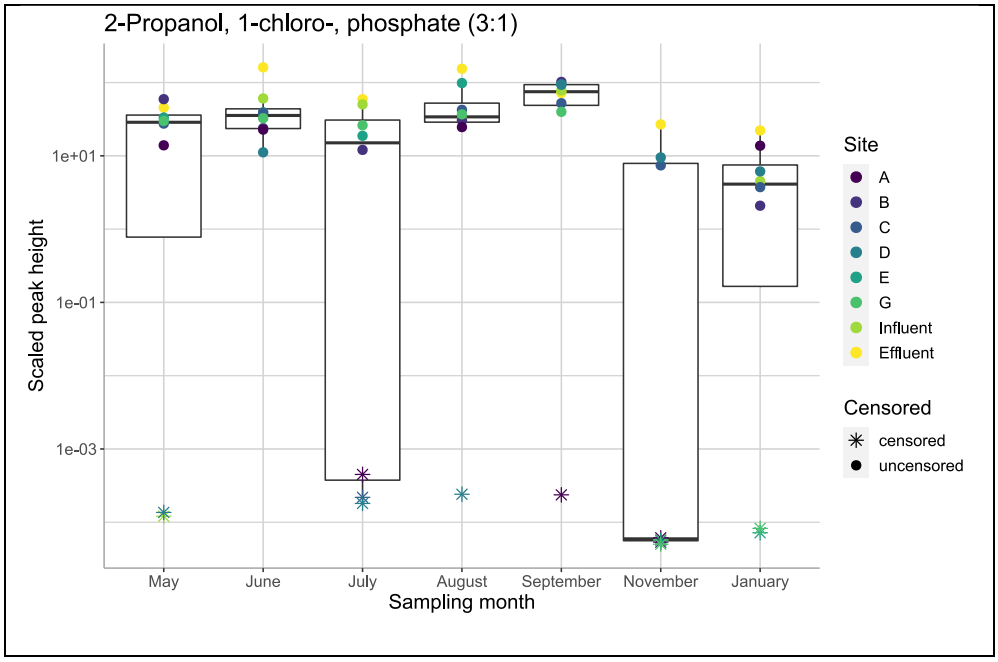

Figure 2-5. Scaled peak height of TCPP in sewershed, arranged by sampling month.

Correlations between micropollutants

Cholestan-3-ol, (3.beta.,5.beta.)[1] is a breakdown product of cholesterol by gut bacteria, and has been used as an indicator of fecal contamination of environmental waters [46]. The scaled peak abundance is higher in November and January with all other sampling months having detections below the 3000-count cut-off. This compound was found to be positively correlated with five other compounds and negatively correlated with two compounds, shown in Figure 2-6. The increased abundance in November and January is more intuitive for the expectorant, guaifenesin, which might see increased use during winter months, due to the seasonality of cold and flu-like

[1] Other names used in literature include 5β-coprostanol, 5β-cholestan-3β-ol. Cholestan-3-ol, (3.beta.,5.beta.) is the name used in the NIST spectral library.

illnesses. Two negatively correlated compounds are isobutyl 4-hydroxybenzoate (isobutyl paraben) and 2-naphthalenol.

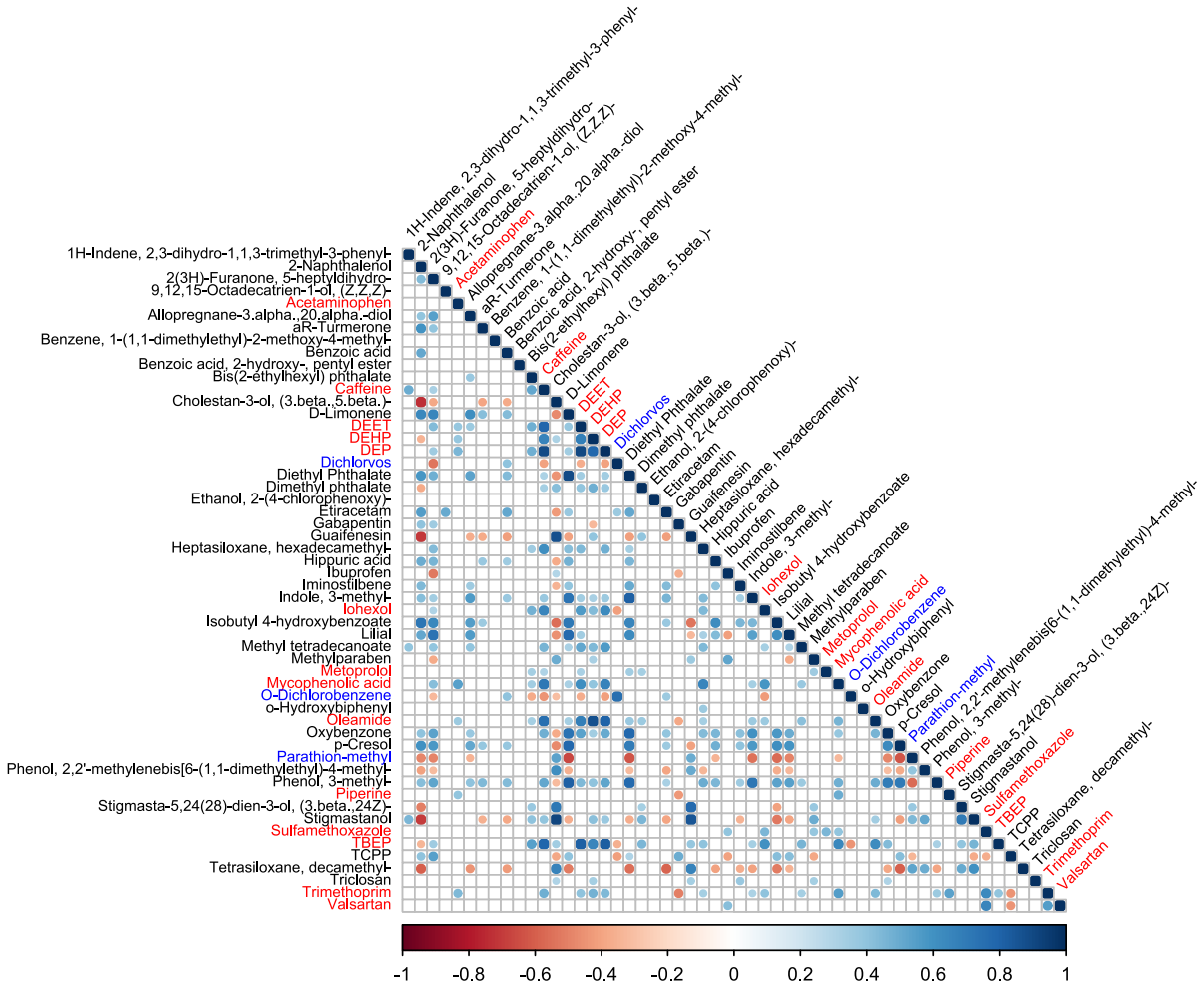

Figure 2-6. Correlation matrix showing statistically significant correlations between micropollutants identified in the sewer system. Compound names in black text were measured on the GC in EI mode, blue on the GC in NCI, and red on the LC in ESI positive.

Most correlations were observed between compounds measured with the same instrument. This could be due in part to the molecular properties of compounds that make them amenable to GC versus LC. For example, compounds that tend to sorb to suspended solids in the sewer system may vary in the same ways, depending on the TSS present. However, performing a Spearman's correlation with TSS and all annotated compounds in the GC data revealed that only hexadecamethyl heptasiloxane and 3-methyl phenol had a corrected p-value < 0.05, with $\rho =$

0.50 and 0.48, respectively. However, given the differences in physicochemical properties between LC- and GC- amenable compounds, this separation is not surprising. There are many parameters within the sewer system that might influence these groups of chemicals differently.

Conclusions

There have been many studies addressing the wide range of contaminants that find their way from the built environment, down the drain, and for some, into environmental waters. The dynamics of these compounds within the sewer system have been found in other studies to vary with physical, chemical, and biological parameters, not even considering the many anthropogenic processes that could drive variation. For these reasons, considering sub-sewershed contaminant patterns becomes even more complex. Ultimately, for the compounds considered here, all of which are fairly commonplace within wastewater, it does not seem that the geographical area captured by each trunkline sampling site is distinct. However, this may be because the sub-sewershed sites are quite similar in land-use patterns. Rather, seasonal variation in product use or within-sewer processes seems to be responsible for the overall system variation. However, there were many chemical features that went unidentified or undiscussed because the scope of chemicals within a sewer is so great.

Acknowledgments

Special thanks to Dr. Jennifer Teerlink at DPR for creating the sampling scheme. We would like to thank Karin North, James Stuart, Robert Hara, Dominic Hoang, Kyle Carbajal, and Samantha Engelage of Palo Alto Wastewater Treatment Plant for collecting samples and providing expert knowledge crucial to interpreting study findings. Many thanks to Chris Alaimo and Luann Wong of UC Davis for their hard work on sample processing and alignment.

References

[1] S. L. Klosterhaus, R. Grace, M. C. Hamilton, and D. Yee, "Method validation and reconnaissance of pharmaceuticals, personal care products, and alkylphenols in surface waters, sediments, and mussels in an urban estuary," *Environ. Int.*, vol. 54, pp. 92–99, 2013, doi: https://doi.org/10.1016/j.envint.2013.01.009.

[2] I. Shimabuku, D. Chen, Y. Wu, E. Miller, J. Sun, and R. Sutton, "Occurrence and risk assessment of organophosphate esters and bisphenols in San Francisco Bay, California, USA," *Sci. Total Environ.*, vol. 813, p. 152287, 2022, doi: https://doi.org/10.1016/j.scitotenv.2021.152287.

[3] A. S. Adeleye *et al.*, "Abundance, fate, and effects of pharmaceuticals and personal care products in aquatic environments," *J. Hazard. Mater.*, vol. 424, p. 127284, 2022, doi: https://doi.org/10.1016/j.jhazmat.2021.127284.

[4] R. Sutton, D. Chen, J. Sun, D. J. Greig, and Y. Wu, "Characterization of brominated, chlorinated, and phosphate flame retardants in San Francisco Bay, an urban estuary," *Sci. Total Environ.*, vol. 652, pp. 212–223, 2019, doi: https://doi.org/10.1016/j.scitotenv.2018.10.096.

[5] E. Archer, B. Petrie, B. Kasprzyk-Hordern, and G. M. Wolfaardt, "The fate of pharmaceuticals and personal care products (PPCPs), endocrine disrupting contaminants (EDCs), metabolites and illicit drugs in a WWTW and environmental waters," *Chemosphere*, vol. 174, pp. 437–446, 2017, doi: https://doi.org/10.1016/j.chemosphere.2017.01.101.

[6] J. Teerlink, J. Hernandez, and R. Budd, "Fipronil washoff to municipal wastewater from dogs treated with spot-on products," *Sci. Total Environ.*, vol. 599–600, pp. 960–966, 2017, doi: https://doi.org/10.1016/j.scitotenv.2017.04.219.

[7] M. B. Dyk, Y. Liu, Z. Chen, H. Vega, and R. I. Krieger, "Fate and distribution of fipronil on companion animals and in their indoor residences following spot-on flea treatments," *J. Environ. Sci. Heal. Part B*, vol. 47, no. 10, pp. 913–924, Nov. 2012, doi: 10.1080/03601234.2012.706548.

[8] R. G. Luthy, D. L. Sedlak, M. H. Plumlee, D. Austin, and V. H. Resh, "Wastewater-effluent-dominated streams as ecosystem-management tools in a drier climate," *Front. Ecol. Environ.*, vol. 13, no. 9, pp. 477–485, Nov. 2015, doi: https://doi.org/10.1890/150038.

[9] P. A. Lara-Martín, A. C. Chiaia-Hernández, M. Biel-Maeso, R. M. Baena-Nogueras, and J. Hollender, "Tracing Urban Wastewater Contaminants into the Atlantic Ocean by Nontarget Screening," *Environ. Sci. Technol.*, vol. 54, no. 7, pp. 3996–4005, 2020, doi: 10.1021/acs.est.9b06114.

[10] L. M. Beckers, W. Brack, J. P. Dann, M. Krauss, E. Müller, and T. Schulze, "Unraveling longitudinal pollution patterns of organic micropollutants in a river by non-target screening and cluster analysis," *Sci. Total Environ.*, vol. 727, p. 138388, 2020, doi: 10.1016/j.scitotenv.2020.138388.

[11] Y. Wang, W. Gao, Y. Wang, and G. Jiang, “Suspect screening analysis of the occurrence and removal of micropollutants by GC-QTOF MS during wastewater treatment processes,” *J. Hazard. Mater.*, vol. 376, pp. 153–159, 2019, doi: https://doi.org/10.1016/j.jhazmat.2019.05.031.

[12] J. E. Schollée, M. Bourgin, U. von Gunten, C. S. McArdell, and J. Hollender, “Non-target screening to trace ozonation transformation products in a wastewater treatment train including different post-treatments,” *Water Res.*, vol. 142, pp. 267–278, 2018, doi: https://doi.org/10.1016/j.watres.2018.05.045.

[13] G. Nürenberg, U. Kunkel, A. Wick, P. Falås, A. Joss, and T. A. Ternes, “Nontarget analysis: A new tool for the evaluation of wastewater processes,” *Water Res.*, vol. 163, p. 114842, 2019, doi: https://doi.org/10.1016/j.watres.2019.07.009.

[14] Y. Verkh, M. Rozman, and M. Petrovic, “A non-targeted high-resolution mass spectrometry data analysis of dissolved organic matter in wastewater treatment,” *Chemosphere*, vol. 200, pp. 397–404, Jun. 2018, doi: 10.1016/J.CHEMOSPHERE.2018.02.095.

[15] P. Gago-Ferrero, E. L. Schymanski, A. A. Bletsou, R. Aalizadeh, J. Hollender, and N. S. Thomaidis, “Extended Suspect and Non-Target Strategies to Characterize Emerging Polar Organic Contaminants in Raw Wastewater with LC-HRMS/MS,” *Environ. Sci. Technol.*, vol. 49, no. 20, pp. 12333–12341, Oct. 2015, doi: 10.1021/acs.est.5b03454.

[16] R. H. Lindberg, M. Östman, U. Olofsson, R. Grabic, and J. Fick, “Occurrence and behaviour of 105 active pharmaceutical ingredients in sewage waters of a municipal sewer collection system,” *Water Res.*, vol. 58, pp. 221–229, 2014, doi: https://doi.org/10.1016/j.watres.2014.03.076.

[17] J. Teerlink, R. Budd, C. Alaimo, L. Wong, and T. M. Young, “Sub-Sewershed Monitoring to Elucidate Down-the-Drain Pesticide Sources.”

[18] H. Tsugawa *et al.*, “Hydrogen Rearrangement Rules: Computational MS/MS Fragmentation and Structure Elucidation Using MS-FINDER Software,” *Anal. Chem.*, vol. 88, no. 16, pp. 7946–7958, Aug. 2016, doi: 10.1021/acs.analchem.6b00770.

[19] K. Dührkop *et al.*, “SIRIUS 4: a rapid tool for turning tandem mass spectra into metabolite structure information,” *Nat. Methods*, vol. 16, no. 4, pp. 299–302, 2019, doi: 10.1038/s41592-019-0344-8.

[20] R. Aalizadeh *et al.*, “Development and Application of Liquid Chromatographic Retention Time Indices in HRMS-Based Suspect and Nontarget Screening,” *Anal. Chem.*, vol. 93, no. 33, pp. 11601–11611, Aug. 2021, doi: 10.1021/acs.analchem.1c02348.

[21] P. Julian and D. Helsel, “NADA2: Data Analysis for Censored Environmental Data.” 2021, [Online]. Available: https://github.com/SwampThingPaul/NADA2.

[22] F. E. Harrell Jr, “Hmsic: Harrell Miscellaneous.” 2022, [Online]. Available: https://cran.r-project.org/package=Hmisc.

[23] V. Hinnenkamp, P. Balsaa, and T. C. Schmidt, “Target, suspect and non-target screening analysis from wastewater treatment plant effluents to drinking water using collision cross

section values as additional identification criterion," *Anal. Bioanal. Chem.*, vol. 414, no. 1, pp. 425–438, 2022, doi: 10.1007/s00216-021-03263-1.

[24] C. Ort, C. Schaffner, W. Giger, and W. Gujer, "Modeling stochastic load variations in sewer systems," *Water Sci. Technol.*, vol. 52, no. 5, pp. 113–122, Sep. 2005, doi: 10.2166/wst.2005.0122.

[25] H. Janna, M. D. Scrimshaw, R. J. Williams, J. Churchley, and J. P. Sumpter, "From Dishwasher to Tap? Xenobiotic Substances Benzotriazole and Tolyltriazole in the Environment," *Environ. Sci. Technol.*, vol. 45, no. 9, pp. 3858–3864, May 2011, doi: 10.1021/es103267g.

[26] E. L. Schymanski *et al.*, "Identifying small molecules via high resolution mass spectrometry: Communicating confidence," *Environmental Science and Technology*. 2014, doi: 10.1021/es5002105.

[27] K. Nödler, M. Tsakiri, M. Aloupi, G. Gatidou, A. S. Stasinakis, and T. Licha, "Evaluation of polar organic micropollutants as indicators for wastewater-related coastal water quality impairment," *Environ. Pollut.*, vol. 211, pp. 282–290, 2016, doi: https://doi.org/10.1016/j.envpol.2016.01.014.

[28] D. Weissbrodt *et al.*, "Mass Flows of X-ray Contrast Media and Cytostatics in Hospital Wastewater," *Environ. Sci. Technol.*, vol. 43, no. 13, pp. 4810–4817, Jul. 2009, doi: 10.1021/es8036725.

[29] "Phthalate Exposure Assessment in Humans," National Academies Press (US), Washington, D.C., 2008. [Online]. Available: https://www.ncbi.nlm.nih.gov/books/NBK215044/.

[30] J. W. O'Brien, P. K. Thai, S. H. Brandsma, P. E. G. Leonards, C. Ort, and J. F. Mueller, "Wastewater analysis of Census day samples to investigate per capita input of organophosphorus flame retardants and plasticizers into wastewater," *Chemosphere*, vol. 138, pp. 328–334, 2015, doi: https://doi.org/10.1016/j.chemosphere.2015.06.014.

[31] R. Sutton, Y. Xie, K. D. Moran, and J. Teerlink, "Occurrence and Sources of Pesticides to Urban Wastewater and the Environment," in *Pesticides in Surface Water: Monitoring, Modeling, Risk Assessment, and Management*, vol. 1308, American Chemical Society, 2019, pp. 5–63.

[32] A. Saini, C. Thaysen, L. Jantunen, R. H. McQueen, and M. L. Diamond, "From Clothing to Laundry Water: Investigating the Fate of Phthalates, Brominated Flame Retardants, and Organophosphate Esters," *Environ. Sci. Technol.*, vol. 50, no. 17, pp. 9289–9297, Sep. 2016, doi: 10.1021/acs.est.6b02038.

[33] K. Naumoska, U. Jug, V. Metličar, and I. Vovk, "Oleamide, a Bioactive Compound, Unwittingly Introduced into the Human Body through Some Plastic Food/Beverages and Medicine Containers," *Foods* , vol. 9, no. 5. 2020, doi: 10.3390/foods9050549.

[34] D. Lin, R. Sutton, J. Sun, and J. Ross, "Screening of Pharmaceuticals in San Francisco Bay Wastewater," 2018.

[35] J. O. Straub, R. Oldenkamp, T. Pfister, and A. Häner, "Environmental Risk Assessment

for the Active Pharmaceutical Ingredient Mycophenolic Acid in European Surface Waters," *Environ. Toxicol. Chem.*, vol. 38, no. 10, pp. 2259–2278, 2019, doi: https://doi.org/10.1002/etc.4524.

[36] H. Franquet-Griell, C. Gómez-Canela, F. Ventura, and S. Lacorte, "Predicting concentrations of cytostatic drugs in sewage effluents and surface waters of Catalonia (NE Spain)," *Environ. Res.*, vol. 138, pp. 161–172, 2015, doi: https://doi.org/10.1016/j.envres.2015.02.015.

[37] H. P. Singer, A. E. Wössner, C. S. McArdell, and K. Fenner, "Rapid Screening for Exposure to 'Non-Target' Pharmaceuticals from Wastewater Effluents by Combining HRMS-Based Suspect Screening and Exposure Modeling," *Environ. Sci. Technol.*, vol. 50, no. 13, pp. 6698–6707, Jul. 2016, doi: 10.1021/acs.est.5b03332.

[38] S. Wang *et al.*, "High-throughput wastewater analysis for substance use assessment in central New York during the COVID-19 pandemic," *Environ. Sci. Process. Impacts2*, vol. 22, pp. 2147–2161, 2020, doi: 10.1039/D0EM00377H.

[39] J. W. O'Brien *et al.*, "Impact of in-Sewer Degradation of Pharmaceutical and Personal Care Products (PPCPs) Population Markers on a Population Model," *Environ. Sci. Technol.*, vol. 51, no. 7, pp. 3816–3823, Apr. 2017, doi: 10.1021/acs.est.6b02755.

[40] C. Ort, M. G. Lawrence, J. Rieckermann, and A. Joss, "Sampling for Pharmaceuticals and Personal Care Products (PPCPs) and Illicit Drugs in Wastewater Systems: Are Your Conclusions Valid? A Critical Review," *Environ. Sci. Technol.*, vol. 44, no. 16, pp. 6024–6035, Aug. 2010, doi: 10.1021/es100779n.

[41] C. Ort, M. G. Lawrence, J. Reungoat, and J. F. Mueller, "Sampling for PPCPs in Wastewater Systems: Comparison of Different Sampling Modes and Optimization Strategies," *Environ. Sci. Technol.*, vol. 44, no. 16, pp. 6289–6296, Aug. 2010, doi: 10.1021/es100778d.

[42] "Toxicological profile for Naphthalene/1-Methylnaphthalene/2-Methylnaphthalene," 1995.

[43] "PubChem Annotation REcord for m-CRESOL, Source: Hazardous Substances Data Bank (HSDB)." National Center for Biotechnology Information, Bethesda, MD, [Online]. Available: https://pubchem.ncbi.nlm.nih.gov/source/hsdb/1815.

[44] H. M. Stapleton *et al.*, "Detection of Organophosphate Flame Retardants in Furniture Foam and U.S. House Dust," *Environ. Sci. Technol.*, vol. 43, no. 19, pp. 7490–7495, Oct. 2009, doi: 10.1021/es9014019.

[45] E. D. Schreder and M. J. La Guardia, "Flame Retardant Transfers from U.S. Households (Dust and Laundry Wastewater) to the Aquatic Environment," *Environ. Sci. Technol.*, vol. 48, no. 19, pp. 11575–11583, Oct. 2014, doi: 10.1021/es502227h.

[46] C. G. Seguel, S. M. Mudge, C. Salgado, and M. Toledo, "Tracing Sewage in the Marine Environment: altered signatures in Concepción Bay, Chile," *Water Res.*, vol. 35, no. 17, pp. 4166–4174, 2001, doi: https://doi.org/10.1016/S0043-1354(01)00146-4.

CHAPTER 3 BATCH CORRECTION METHODS FOR NONTARGET CHEMICAL ANALYSIS DATA: APPLICATION TO A MUNICIPAL WASTEWATER COLLECTION SYSTEM

Abstract

Nontarget chemical analysis using high resolution mass spectrometry has increasingly been used to discern spatial patterns and temporal trends in anthropogenic chemical abundance in natural and engineered systems. A critical experimental design consideration in such applications, especially those monitoring complex matrices over long time periods, is a choice between analyzing samples in multiple batches as they are collected, or in one batch after all samples have been processed. While datasets acquired in multiple analytical batches can include the effects of instrumental variability over time, datasets acquired in a single batch risk compound degradation during sample storage. To assess the influence of batch effects on the analysis and interpretation of nontarget data, this study examined a set of 56 samples collected from a municipal wastewater system over seven months. Each month's samples included 6 from sites within the collection system, one combined influent, and one treated effluent sample. Samples were analyzed using liquid chromatography high resolution mass spectrometry in positive electrospray ionization mode in multiple batches as the samples were collected and in a single batch at the conclusion of the study. Data were aligned and normalized using internal standard scaling and ComBat, an empirical Bayes method developed for estimating and removing batch effects in microarrays. As judged by multiple lines of evidence, including comparing principal variance component analysis between single and multi-batch datasets and through patterns in principal components and hierarchical clustering analyses, ComBat appeared to significantly reduce the influence of batch effects.

Introduction

High resolution mass spectrometry (HRMS) has been applied to an increasingly diverse set of environmental problems extending far beyond its well-known ability to establish the presence of previously unmonitored compounds via suspect screening against mass spectral databases. Even without database matches or confident structural annotations, ions of particular mass-to-charge ratio (m/z) and chromatographic retention time (RT) observed across numerous samples can provide critical information about environmental processes, and such approaches fall within the domain of nontarget chemical analysis. A number of such applications rely on the comparison of ion abundances of unidentified compounds between samples collected at different times, monitoring locations or points in a treatment process [1]–[5]. Most of these studies have used patterns in feature abundance across samples to group and prioritize features for further identification efforts (e.g., features that decrease or increase across a treatment process or are present at higher abundance in particular types of sources). When the inverse question is posed—how samples may be grouped according to abundance profiles of multiple features (i.e., a chemical fingerprint)—the temporal or spatial differences in chemical composition under investigation may be masked by "obscuring variability" [6], or unintentional variability added during analysis.

Obscuring variability can come from a variety of sources that cannot always be controlled, such as operator effects, variations in the ion source, recent instrument maintenance, and sample-specific matrix effects [6], [7]. Effects of these variables can become the major driving factor in separation of sample groups in a method such as principal components analysis (PCA), rendering it less informative about chemical similarities and differences among samples [8]. Furthermore, in environmental monitoring applications that span periods of months to years,

there will be batch effects regardless of whether samples are run in a single batch at the end of the study (due to differential degradation of compounds within extracts stored for varying periods) or in multiple batches as they are collected and processed (due mostly to instrumental variation). The ability to disentangle potential "batch effects" from the true chemical differences between samples is critical to drawing proper conclusions from the data.

While these challenges have already been addressed extensively in the fields of DNA microarrays, metabolomics, lipidomics, and others, environmental samples pose a unique set of challenges, delineated by Boysen et al. (2018). For example, complex and variable matrices can affect the ionization efficiency of compounds in inconsistent ways. In nontarget analysis of environmental samples, while there may be a group of constituents that are consistently detected, "contaminants of concern" may only appear sporadically or only at a specific site. This differs from a DNA microarray study, which employs a predetermined number of probes. The large proportion of sparse features in an environmental dataset can also make statistical analysis challenging. Environmental contaminants span a vast range of structural classes and are subject to significant fluctuation and alteration given changing consumption patterns and the advent of new compounds. Many environmental monitoring studies, mostly focusing on wastewater-impacted surface waters, have employed clustering methods on nontarget features to separate features into groups defined by spatial, temporal, or usage trends [2], [9]–[11]. Alternatively, studies aiming to identify new or site-specific contaminants focus on features with high intensity and low frequency [4], [12]. Of these six particular studies, only two reported employing intensity normalization to isotopically-labelled internal standards. Furthermore, an in-depth review of study reporting in eight nontarget papers found that despite the sensitivity of nontarget

analysis to analytical sequence, this aspect of data acquisition was “not adequately emphasized” [13].

Methods of correcting for batch effects have been categorized as quality-control (QC) based, isotopically-labelled, internal standard-based (ISTD), or sample-data driven [14]. QC-based methods rely on QC samples created from aliquots of all samples within a batch, which are injected multiple times throughout the course of a run. Then, models are used to find relationships between the QC peak intensities and injection order to separate batch effects from the biological/chemical differences [15], [16]. ISTD-based approaches employ a robust suite of isotopically labelled internal standards added to each sample, and feature peak intensities are scaled according to the corresponding ISTD. The method developed by Boysen et al. (2018) is a combination of both QC- and ISTD- methods, using replicate injections of pooled QC samples to determine the ISTD to best minimize the coefficient of variation for each feature. Compared to QC- or ISTD-based approaches, sample data-driven approaches have the benefit of avoiding the extra cost of internal standards and the need for additional instrument time [14]. One example of a sample data-driven method is ComBat, an empirical Bayes method that estimates the hyperparameters for the distribution of batch effects by pooling information across features within a batch, and then adjusts intensities accordingly [17]. Selection of the method of correction should be made based on the type of data collected and the nature of subsequent analyses to be performed. PCA, which performs a change of basis using variables explaining the greatest variation within the dataset, may become scrambled, whereas the results of a hierarchical cluster analysis, which considers the similarities between samples or features, may become clearer [18].

Because batch correction can introduce bias and variance, it is also necessary to identify measures of the "success" of batch correction approaches. These measures are borrowed from the 'omics fields that have addressed this issue previously, although they require special considerations when applied to environmental samples. For example, a visualization technique such as relative log abundance (RLA) plots, which centers features either by the within- or across-group median and uses boxplots to assess the "tightness" of features around zero must presume that metabolites will be present in every sample [19]. This method would not necessarily be applicable to sparse environmental datasets, especially ones geared towards the discovery of contaminants of concern unique to a site or sampling date. If we were to assume that (high quality) features that are detected in more than 85-90% of samples are part of a consistent background metabolome, then those features may be visualized via RLA plots for comparison between correction methods. Both De Livera et al. [19] and Drotleff & Lämmerhofer [20] recommend use of multiple methods to assess batch correction efficacy, combined with a holistic evaluation rather than quantitative thresholds. A method known as principal variability component analysis (PVCA) estimates the variability within the dataset that is associated with analytical batches by fitting a linear mixed model to the first few principal components [21], [22]. With this method, seeing a decrease in the variability associated with analytical batch from the uncorrected to the corrected data would suggest a successful correction.

Given the challenge posed by "obscuring variation" for nontarget studies that monitor complex environmental matrices over extended periods of time, this study aims to assess the applicability of batch-correction techniques and the measures of their success. While there is not a one-size-fits all approach for different datasets, this can still serve as a relevant example of the process. To this end, we used multiple datasets: 1) Wastewater treatment plant (WWTP) influent and effluent

samples plus sites within the catchment system collected 7 times over a 9-month period and analyzed in four different analytical batches as the samples were processed (multi-batch; MB), and 2) the same wastewater samples run in a single analytical batch (single batch; SB), after all the samples had been collected and processed (Table 3-1). ComBat correction, an empirical Bayes technique, was applied to the MB dataset and the results (MB-C) were compared to the uncorrected MB (MB-unC) and SB datasets using principal variation components analysis (PVCA), principal components analysis (PCA), and hierarchical clustering analysis (HCA). Additionally, a conventional approach of using sample median internal standard (ISTD) peak heights to scale raw peak heights of features was employed on the same MB dataset to obtain MB-IS, which was compared to MB-unC through PVCA and PCA.

Table 3-1: Description of datasets and processing applied to each

Sample description	Dataset name	Analytical batches	Analytical Run Date	Samples per analytical batch	Processes applied
– Sub-sewershed (n=42) – WWTP influent (n=7) – WWTP effluent (n=7)	SB	1	7/17/17	56	– Feature filtering – Log2 Transform – Quantile Normalization
	MB-unC	4	5/22/16 6/17/16 9/26/16 3/3/17	8 8 24 16	“”
	MB-IS	“”	“”	“”	– Feature filtering – Scaled by median ISTD peak height
	MB-C	“”	“”	“”	– Feature filtering – Log2 Transform – Quantile Normalization – ComBat correction

Experimental

This is the same sample set as described in the previous chapter. Detailed descriptions of the sample collection, preparation, data acquisition methods and quality assurance/quality control measures applied to this sample set are reported elsewhere [23] and are briefly described in Appendix 2.

Nontarget Alignment

First, raw data files were converted from instrument vendor format (Agilent .d files) to the analysis base file format (Reifycs Analysis Base File Converter v. 4.0.0). These files were then deconvoluted and aligned in MS-DIAL (v. 3.90) using internal standards for retention time correction. The data files included in the MB alignment were: 7 method blanks (one per month), 10 wastewater matrix spikes (one each month plus three extra), 4 100-ppb calibration standards (one per batch), 7 influent samples, 7 effluent samples, and 75 sub-sewershed samples. The data files included in the SB alignment were: 8 method blanks, 12 wastewater matrix spikes, 7-100 ppb calibration standards, 7 influent samples, 7 effluent samples, and 74 sub-sewershed samples. For SB, conventional LC-MS parameters were used, whereas for MB-unC/C, an All-Ions experiment file was included. Alignment parameters are detailed in the supporting information, Tables A4-1 and A1-3.

Data Pre-Processing

To remove low abundance background features, feature filtering rules were applied. A standard signal-to-noise cut-off of ten was used. Blank "subtraction" filters required that the maximum signal in wastewater samples be greater than ten times the average signal in the method blanks. Features with retention times below 4.5 minutes were excluded due to the poor

chromatographic quality of early-eluting peaks that results in unreliable alignment of these features.

To further reduce the number of features, Mass Spectral Feature List Optimizer (MS-FLO), which was designed as post-processing step to be used with MS-DIAL alignments [24], was implemented to join ammonium and sodium adducts to their matching molecular ion. Parameters used are included in Table A1-4. Next, features that were not detected at a height of 3,000 counts or more in at least one of the 56 WW samples were eliminated, as some features were only present in blank, standard, or spiked wastewater samples that were included in the alignment set for quality control purposes. The phenomenon of split features, which can occur during alignment despite the use of retention time correction from labelled internal standards, was handled by joining features that met the following three criteria: 1) retention times within ± 15 seconds, 2) m/z within 10 ppm, and 3) MS1 isotopic abundance ratios with coefficient of variation of 20% or less. Finally, features that occurred in 60% or more of samples from at least one month or site were retained, as the study goal was to find patterns of chemical profiles in space and time. After all feature filtering steps, the sample set was reduced to only include 56 wastewater samples: 7 influent, 7 effluent, and 42 trunkline samples, to enable better comparison between SB, MB, and the work done by Teerlink et al. [23].

To obtain the dataset MB-IS, every peak height was divided by the median ISTD peak height of the sample, using the labelled ISTDs that were also used for retention time correction in the MS-DIAL alignment (Table A1-3). This was used rather than a retention-time specific ISTD correction, because of the uneven distribution of ISTDs throughout the duration of the chromatographic run.

Additionally, raw height values were transformed by applying $y' = \log_2(y + 1)$, since ion abundances for over 90% of features in this data set range over more than six orders of magnitude. Then, for all datasets quantile normalization was applied to adjust the distributions of feature heights [25]. Quantile normalization was implemented in R using *normalize.quantiles* from the package *preprocessCore* (v. 1.54.0) [26].

Batch Correction

Briefly, ComBat assumes that the additive and multiplicative batch effects on each feature are part of a distribution of batch effects. These distributions are assumed to follow a Normal and Inverse Gamma distribution, respectively, when using the parametric version, as was used here. The hyperparameters of these two distributions (additive and multiplicative) are estimated empirically from the data for each batch, such that the method can pool information across features. These are then used to adjust intensities accordingly.

The parametric ComBat batch correction method [17] was applied to MB-unC to create MB-C. Covariates indicating experimental factors for site and sampling date were not applied. ComBat was applied in R using *ComBat*, part of the *sva* (v. 3.40.0) package [27].

Data Analysis (PCA, HCA, PVCA, and Differential Abundance)

The script for conducting PVCA was adapted from Boedigheimer et al. (2008). Experimental factors included in the model were: sampling location, sampling date, and analytical batch number (all variables as factors). The script first calculates the correlation matrix for the dataset, then uses *lme* (from package *lme4* v. 1.1.27.1) [28] to fit a linear mixed effects model using the experimental factors for each principal component, up to 60% of overall variance, where pc_n is the number of principal components required to account for 60% of overall variance. For the three multi-batch datasets, the model formula used was as follows:

$$pc_i \sim (1|\ Sampling\ month) + (1|Sampling\ location) + (1|Analytical\ batch) \quad \text{(Eq. 3-1)}$$

Where the mean of each sampling month, sampling location, and analytical batch was assumed to be randomly distributed with a center of zero and an unknown variance. For the single-batch dataset, the analytical batch term in Eq. 3-1 was omitted. For The mixed effects model pools information within each factor to compute an unbiased estimation of the variance. The weighted average of variance for each experimental factor is then computed using eigenvalue of each pc_i as the weight.

Matrices of the final 56 samples containing features that had been filtered, joined, quantile normalized, and (for MB-C only) ComBat corrected, were visualized using PCA. For hierarchical clustering, the same pc_n components used to account for 60% of the dataset variance used in PVCA were included, using Euclidean distance and the Ward's agglomeration algorithm [2], [10]. Number of clusters was selected after consideration of silhouette [29] and gap-statistic [30] plots, commonly used to determine optimal number of clusters.

Differential abundance of features compared across sampling months and sites was analyzed with the *limma* (v. 3.48.3) package [31] in R, using a similar approach to differential expression analysis for DNA microarrays [31], [32]. This method uses the function *lmFit* to compute a model for each feature according to experimental design groups. Modelling interactions between month and site was not possible since a single sample was taken for each month-site combination. Contrasts were defined to determine fold change and significance between experimental groupings of month, site, and cluster (as defined by HCA). For example, the contrast "Influent – Effluent" compares the abundances of features between influent and effluent samples. To compute statistical significance, the *eBayes* function was used, which employs an empirical Bayes approach to shrink standard errors of features toward a pooled estimate [33].

The Benjamini-Hochberg correction was used to control the false discovery rate , such that features with an adjusted p-value less than 0.05 were retained for analysis.

Results & Discussion

Feature filtering and joining

After applying filtering rules, the number of features decreased from 63,259 to 3,108 in SB and 136,938 to 25,822 in MB (Table A4-3).

One possible reason for this discrepancy may be the degradation of some features during sample storage before the acquisition of the single-batch data. The extent of this degradation may depend on the types of compounds present in samples, as it has been found that illicit drugs, pharmaceuticals, and their metabolites are stable when stored on SPE cartridges at -20°C [34], [35], whereas some antibiotics degrade in extracts at -20°C after four weeks [36]. Another possible explanation is that the SB dataset contains only MS1 information, whereas the MB dataset was acquired in *All-Ions* mode. This could lead to MS-DIAL misidentifying fragments as molecular ions. Finally, the use of multiple analytical batches could simply lead to more misalignment of features due to greater mass error and contamination from samples run between batches.

In addition to adducts making it through the alignment algorithm, “split features” are also often observed. These can take one of two forms: duplicate features and alternating features. Duplicate features have identical abundance values for most of the samples, but the algorithm missed the abundances for one of the features in a handful of samples so these are reported as two features (Table 3-2a). MS-FLO incorporates a duplicate feature joining tool, but duplicate features are not always consolidated by this application. The second form of split features, alternating features, result in abundances of the same magnitude being reported for every other feature across samples

(Table 3-2b). These "split features" are hypothesized to be artifacts from the retention time correction step in alignment, which should affect single-batch date less than multiple-batch data. The reduction in feature number after the process of joining split features was 6.7% (2,126 features) for SB and 5.5% (3,847 features) for MB.

Table 3-2. Example application of split feature joining algorithm

					Abundance					
	Alignment ID	Average m/z	Average RT	M:M+1 (or M+2)	Sample 1	Sample 2	Sample 3	Sample 4	Sample 5	Sample 6
(a)	141	83.0501	5.82	0.0607	119320	114649	166851	149155	108584	56291
	142	83.0502	5.7	0.0579	119320	114649	166851	149155	108584	56291
(b)	185	89.06	6.07	0.0457	0	938614	877930	0	0	699778
	187	89.0601	5.85	0.0501	141085	938614	568	715556	1375229	530

Ultimately, joined split-features made up 5.1% (about 1316 features) of MB and 24% (about 746 features) of SB. The existence of split features or similar alignment artifacts is a challenge that is not unique to our lab group or users of MS-DIAL. For example, Schollée et al. (2021) employed a similar algorithm of joining features when they faced the issue of peak tailing being identified as unique features when using *enviPick* for alignment.

Comparison of principal variance component analysis

PVCA allows for visualization of the contributions of experimental factors (sampling location, sampling date, and analytical batch) as well as the proportion of residual, or unexplained variance, to overall variance within the dataset (Figure 3-1). For SB, we included a simulated analytical batch, which assigned SB samples to the analytical batch number in which it was analyzed in the MB data sets. The weighted average proportion variance of 0.15 computed for batch is slightly higher than for sampling date, but lower than for sampling location or residual. With this sample set, it is difficult to separate the factors of sampling date and analytical batch, because samples from the same month are always in the same batch, and this collinearity is

likely the reason for the variability attributed to simulated analytical batch here. For MB-unC, analytical batch is associated with the greatest proportion of the variance, which then decreases after ISTD scaling is applied (MB-IS) and goes away completely with the application of ComBat correction (MB-C). Instead, for MB-C, much of the variability in the dataset is "residual", meaning it cannot be attributed to sample date or location alone.

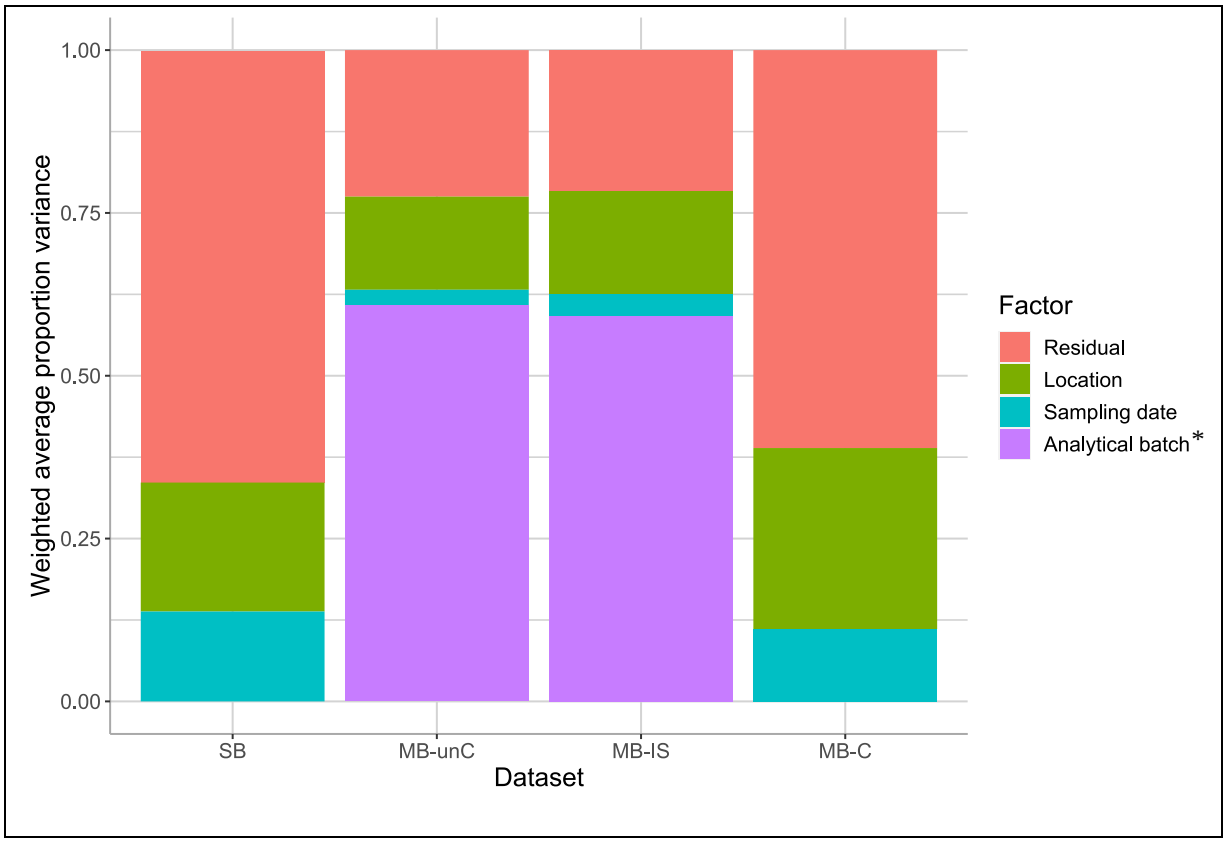

Figure 3-1. PVCA plots show contributions to the overall variance for three experimental factors plus unexplained (residual) variance for single-batch (SB), uncorrected multi-batch (MB-unC), ISTD-scaled multi-batch (MB-IS), and ComBat corrected multi-batch (MB-C). * The analytical batch factor was omitted for SB.

Comparison of principal components analysis and hierarchical clustering analysis

The change seen in the PVCA plots is consistent with the way that samples rearrange after PCA and HCA. For set SB, the plot of the first two principal components (Figure A4-2a) shows effective separation of effluent samples from influent and trunkline samples in PC1. Further inspection via HCA (pc_n = 16) reveals separation of six effluent samples plus July influent from

the rest of the sample set (Figure A4-2b) in clusters one and two, while the July effluent sample is found in cluster four. Mixing of months is observed in all clusters. There is some grouping by sampling site, for example in cluster three, there are five samples from site E and four from site G grouped together. Examination of principal component pair plots of PCs one through five (Figure A4-4a) shows a consistent mix of samples from different sampling dates and analytical batches (where a simulated analytical batch variable is included for the sake of comparison).

For the MB-unC PCA plot, apart from a cluster of effluent samples, there is clear evidence of separation of samples by batch (Figure 3-2a): samples from batches 1 and 3 group in the top-left corner, batch 2 in the bottom-left, batch 4 in the top-right, and effluent samples in the lower middle. Although they do form a relatively distinct cluster, the effluent samples are not clearly distinguished from influent/trunkline samples along either the first or second principal component axes, which account for the greatest percentage of overall variance. This indicates that before batch correction, analytical batch differentiates samples more than whether they were treated or untreated. November and January, the fourth analytical batch, group together, making up the entirety of cluster one in the HCA (Figure 3-2b). June, the second analytical batch, is also on its own, comprising the entirety of cluster five in Figure 3-2b. Interestingly, the third batch, consisting of months July, August, and September, groups close with the first batch (May), forming clusters two, three, and four. While cluster two is comprised entirely of May samples, two May lateral sites, E and G, mix with E and G samples from August, July, and September in cluster four. Higher-order principal components show the separation of May samples from other months, in Figure A4-4b. The only variation from the batch-wise segregation of samples can be seen in the clustering of September D, November G/E, and January D/G trunkline samples with

June effluent (Figure 3-2b, cluster six), and a group of May, July, August and September samples of only sites E and G (Figure 3-2b, cluster four).

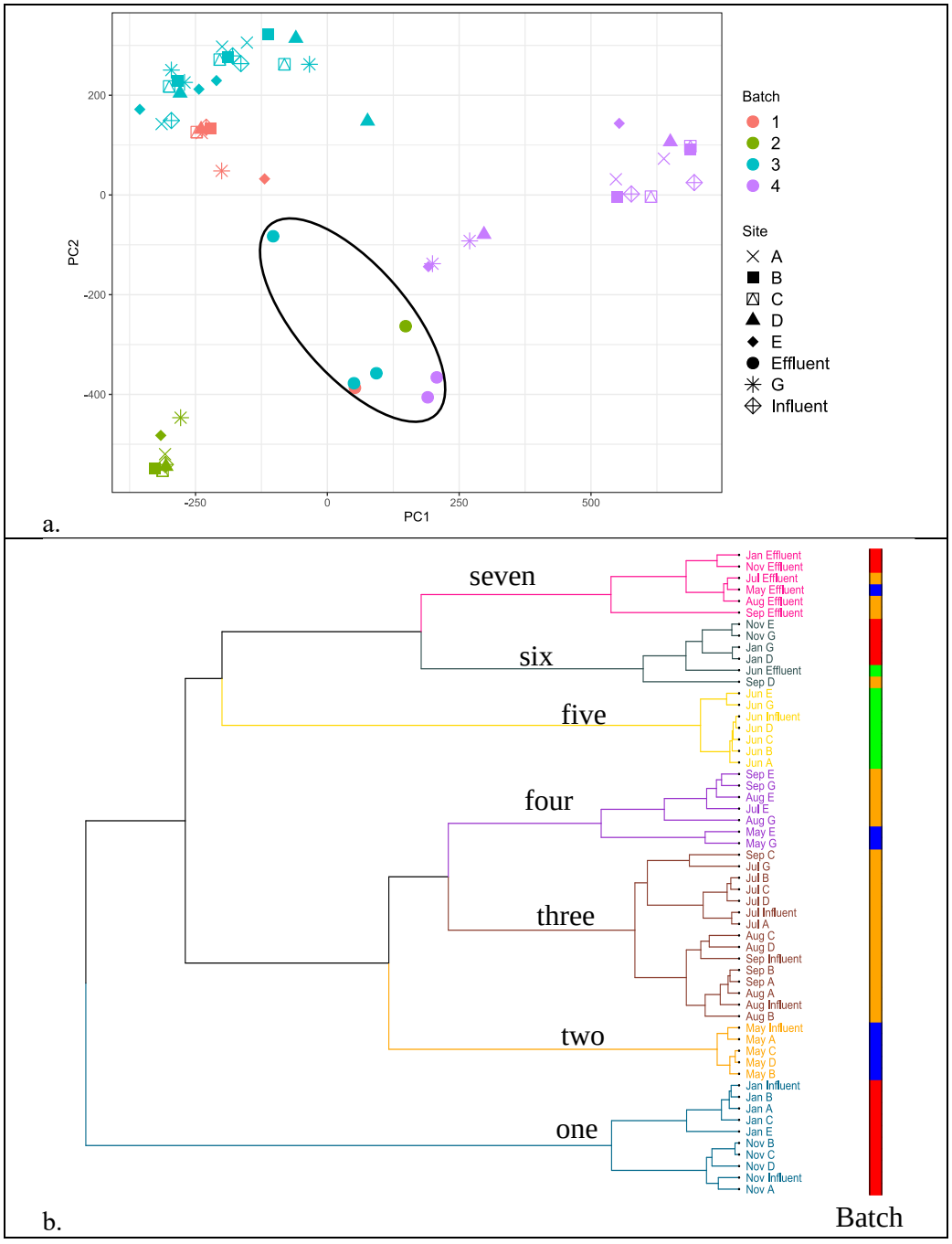

Figure 3-2. For MB-unC, a) plotting of first two principal components revealed clustering was driven by analytical batch, with effluent samples delineated by the drawn black oval, and b) HCA ($pc_n = 4$), divided into seven clusters, numbered one through seven for ease of discussion. The colored bar to the right of the dendrogram is colored according to analytical batch of each sample: blue for batch 1, green for 2, orange for 3 and red for 4. Cluster one is entirely batch 4

samples, two 100% batch 1, three is 100% batch 3, four a mix of 1 and 3, five 100% batch 2, six is combination of batches, and seven is all effluents except June (batch 2).

In the MB-IS dataset, feature peak-heights were scaled by the median internal standard peak height in each sample. The resulting plot of the first two principal components (Figure A4-3a) shows that the influent and trunkline samples are grouped again by batch, with batch 3 on the left, batch 1 in the middle, batch 4 in the upper right corner and batch 1 in the lower right corner. On the first principal component axis, the treated effluent samples are in line with the untreated samples from batches 1 and 4. This is also seen in Figure A4-3b, where only 2 clusters, six and seven, contain samples from different batches. For this dataset, the conventional remedy for batch effects, scaling by internal standards, is not enough.

After applying the ComBat batch effect correction method to MB-unC, the grouping of samples through PCA and HCA changed (Figure 3-3a and 3-3b). In the graph of the first three principal components, now most samples group together, although the group of effluent samples is clearly separated primarily by PC1. Additionally, the clustering of analytical batches that was observed previously in HCA is less apparent: cluster one has a mix of previously separated batches 3 and 4 and cluster two has a mix of batch 2 and 3, where batch 2 was previously very different from other samples. The same September D, November G/E, and January D/G trunkline samples that made up cluster six in Figure 3-2b are still grouped close to the effluent samples (clusters six and seven, Figure 3-3b). Cluster two now only contains the E trunkline samples that were previously with G trunkline samples in cluster four for MB-unC. Additional principal components bear out this increased mixing of samples between months, in Figure A4-5d. Interestingly, when a non-linear dimensionality reduction method, t-SNE, was used to visualize the MB-unC and MB-C datasets, a shift from organized clusters organized by treatment status (raw vs. treated effluent) and analytical batch (Figure A4-4a) to a complete absence of clusters

(Figure A4-4b) demonstrates the diverging effects on interpretation that occur after ComBat is applied.

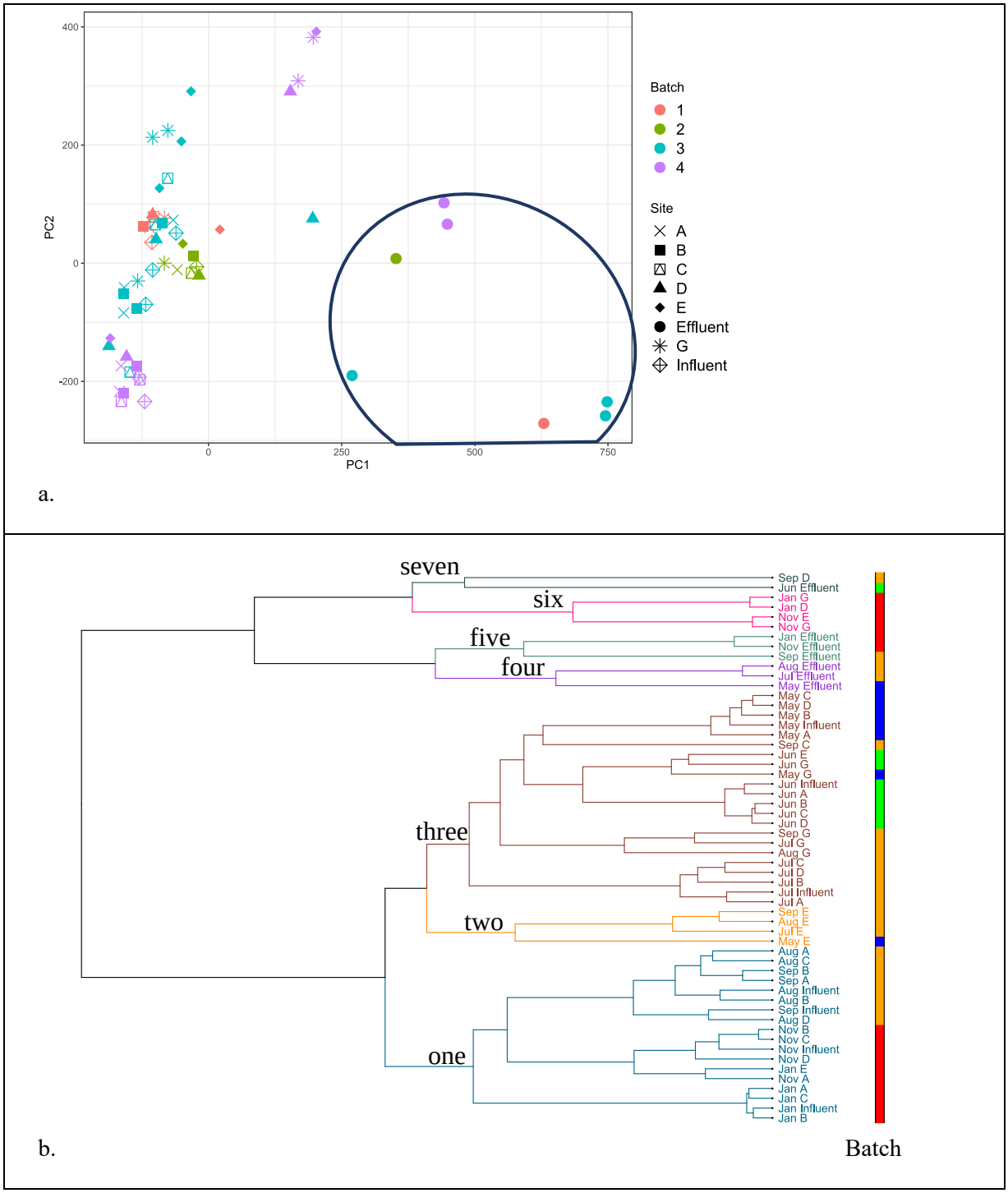

Figure 3-3. For MB-C (ComBat corrected MB-unC), a) plotting the first three PCs shows absence of batch-wise separation observed in Figure 2b (again with effluent samples circled) and b) HCA (pc_n = 13) shows more mixing of samples of different batches in the same cluster:

cluster three contains samples from batches 1, 2, and 3. Analytical batch is indicated by colored bar to the right of the dendrogram as in Figure 3-2.

As a final point of comparison, the same sample set was clustered according to concentrations of target pesticides as reported by Teerlink et al. (in review) [23]. While the dataset of quantified target pesticides considers a significantly smaller subset of compounds (nineteen pesticides) than the nontarget features, this data has been matrix corrected, which is difficult to achieve with nontarget data. Only two of the target compounds can be measured via LC-MS (fipronil and imidacloprid), while the rest were measured via GC-MS. However, we hypothesized that the adjuvants used in commercial formulations could create an LC-detectable source signature of the pesticide.

From this analysis, August G, November A and E, and January B and D all were differentiated from the bulk of the samples (Figure A4-6). Clearly the August G sample is unique, because it is the only sample with a quantifiable amount of chlorothalonil. November A is the only sample in the set with quantifiable esfenvalerate, while November E is unique for the significantly higher concentrations of the pyrethroids, cypermethrin, deltamethrin, and permethrin, which were frequently detected across sites and months. January D contained a higher concentration of cyfluthrin, also frequently detected across sites and months, and January B and D both had much higher concentrations of fipronil amide.

Similarly, in the nontarget MB-unC/C analyses, November E and January D were distinguished in HCA, which would suggest that the nontarget approach is also able to pick out unique samples despite the higher background noise of nontarget features. Recall that for both MB-unC/C, November G, and January G samples were included in a distinct cluster with November E and January D, perhaps indicating an additional chemical similarity between these

samples. For SB, there was some correspondence with the target data with some separation of "distinctive" samples, with the distinctive groups made up of five E (including November) and four G samples (including August, November, and January). A different grouping of four E samples was observed in both the MB-unC (cluster 4) and MB-C (cluster 2) datasets. The site E catchment area has a much higher percentage of high-density residential zoning than other sites, which Teerlink et al. (in review) [23] connected with this site's significantly higher loadings of pyrethroids. Presumably the higher density of people could lead to a distinct nontarget signature from associated with higher loadings of pharmaceutical and personal care products as well.

However, other samples that were unique in their target pesticide concentrations were not found to be as unique when considering nontarget features. January B was grouped near January influent, A, and C in HCA for SB, MB-unC and MB-C, perhaps indicating that the bulk of the nontarget features for this sample outweighed whatever differences result from the high concentrations of target pesticides. This may be true for November A and August G as well, which were distinguished from the target data as the single quantifiable detections of esfenvalerate and chlorothalonil, respectively, do not show consistent separation in the nontarget datasets.

Comparison of differential abundance

Evaluation of features found to be significantly different between sampling dates or sampling sites was carried out for MB-unC and MB-C. There was a total of 21 contrasts for comparing abundance by month, and 28 by site. Additionally, 21 contrasts were created by dividing samples according to clusters determined using HCA (Figure 3-2b and 3-3b). Using the within-cluster sum of squares and gap-statistic methods, the optimal number of clusters was between 7 and 10, so the number of 7 clusters was selected (Figures A4-8 through A4-11). It is important to note

that the “one-two” contrast for MB-unC does not consist of the same samples as the “one-two” contrast for MB-C (and so on) because of different HCA results.

In set MB-unC, features with an adjusted p-value < 0.05 were found for all 21 contrasts comparing months. Only 5 comparisons of months had significantly different features for MB-C: August – July, September – July, January – November, September – August, and January – July. Table A4-4 summarizes the number of significantly different features found for each dataset and contrast. As illustrated in Figures A4-12 and A4-15, p-value distribution shapes differed considerably between MB-unC and MB-C. The sharp drop-off from the left to right in many of the contrasts in the MB-unC set indicates a higher number of significantly different features. A small subset of features was found to be significant before and after ComBat correction: 14 features for January – November, 4 for September – August, 127 for August – July, 2 for January – July, and 79 for September – July.

While 23 out of the 28 site-wise contrasts returned significantly different features for MB-unC, only 2 had significant results for MB-C: 1 feature for In – G and 5 for G – Eff. The 1 feature for In – G and 4 features for G – Eff were also significant in MB-unC. While some studies have found that a drawback of applying ComBat is the generation of false positive data [37], [38], we found that applying ComBat in this study may have actually lessened differences between samples. Indeed, others have found that applying ComBat with an unbalanced experimental design can deflate significance [39], but in an environmental monitoring application, the relationship between sampling date and run date is intractable. Furthermore, the assumption of the algorithm itself that “phenomena resulting in batch effects often affect many genes in similar ways (i.e. increased expression, higher variability, etc),” [17] may be appropriate for DNA microarrays, but not for the behavior of compounds with unknown physicochemical properties

analyzed by the LC-QTOF-MS. It is also possible that many of the features that collectively constitute the "wastewater metabolome" simply do not vary much between months and sampling sites.

Comparison of the HCA clusters for the ComBat corrected dataset was slightly more successful than comparison by month or site. Indeed, in the analysis of target pesticides, it is evidenced that there can be considerable variation within sampling dates and sampling locations. For example, there were many significantly different features within the effluent samples, contained in clusters four, five, and seven. Creating an m/z vs RT plot of features significant to each cluster (Figures A4-20 and A4-21) revealed a large swath of features that could be composed of homologous series that were significant to cluster seven (July Effluent and September D). No features were found to be significant to the largest cluster, three, perhaps because there was still too much variability between the samples (22 out of the 56 samples). As was the case with comparison by site and by month, many more features were found to be significant for MB-unC clusters. The swath of (possible) homologous series in the effluent samples was present in this dataset as well (Figures A4-18 and A4-19).

Recommendations

We have shown with these datasets that batch effects from multiple analytical runs can be examined through PVCA, PCA, and HCA, and the novel application of ComBat can reduce the obscuring effect on the overall spatial and temporal differences in the data. Given the choice between analyzing samples in multiple analytical batches or a single analytical batch over the course of a long-term environmental monitoring study, we would recommend the use of multiple batches with the application of a method such as the one demonstrated here. Further recommendations would include additional QA/QC measures that we did not have at the time of

data acquisition for this study, such as replicate injections of pooled matrix spikes for each class of matrix (for example, the trunkline/influent would be a separate matrix spike from the effluent). Furthermore, a more robust standard mix of labelled internal standards with improved coverage of the range of retention times and physicochemical properties could enable ISTD-based batch correction approaches, which may be more appropriate for MS data. Finally, a controlled study using synthetic wastewater and surface water matrices spiked with a suite of compounds covering a range of physicochemical properties would be useful to compare effects of ComBat on samples with matrices of differing complexity.

Acknowledgments

Research reported in this publication was supported by the National Institute of Environmental Health Science of the National Institutes of Health under award number P42 ES004699 and by the California Department of Pesticide Regulation under contract numbers 14-C0103 and 18-C0041. The content is solely the responsibility of the authors and does not necessarily represent the official views of the National Institutes of Health or the California Department of Pesticide Regulation. Special thanks to Dr. Jennifer Teerlink at DPR for creating the sampling scheme. We would like to thank Karin North, James Stuart, Robert Hara, Dominic Hoang, Kyle Carbajal, and Samantha Engelage of Palo Alto Wastewater Treatment Plant for collecting samples and providing expert knowledge crucial to interpreting study findings. Special thanks to Dr. Blythe Durbin-Johnson, Principal Statistician with the UC Davis Department of Biostatistics, for statistics advising. Special thanks as well to Dr. Daniel Cuthbertson of Agilent, for suggesting the use of ComBat for this application. Many thanks to Chris Alaimo and Luann Wong of UC Davis for their hard work on sample processing.

References

[1] J. E. Schollée, J. Hollender, and C. S. McArdell, “Characterization of advanced wastewater treatment with ozone and activated carbon using LC-HRMS based non-target screening with automated trend assignment,” *Water Res.*, vol. 200, 2021, doi: 10.1016/j.watres.2021.117209.

[2] C. M. G. Carpenter, L. Y. J. Wong, C. A. Johnson, and D. E. Helbling, “Fall Creek Monitoring Station: Highly Resolved Temporal Sampling to Prioritize the Identification of Nontarget Micropollutants in a Small Stream,” *Environ. Sci. Technol.*, vol. 53, no. 1, pp. 77–87, 2019, doi: 10.1021/acs.est.8b05320.

[3] N. A. Alygizakis, P. Gago-Ferrero, J. Hollender, and N. S. Thomaidis, “Untargeted time-pattern analysis of LC-HRMS data to detect spills and compounds with high fluctuation in influent wastewater,” *J. Hazard. Mater.*, vol. 361, no. August 2018, pp. 19–29, 2019, doi:

10.1016/j.jhazmat.2018.08.073.

[4] M. Krauss, C. Hug, R. Bloch, T. Schulze, and W. Brack, “Prioritising site-specific micropollutants in surface water from LC-HRMS non-target screening data using a rarity score,” *Environ. Sci. Eur.*, vol. 31, no. 1, p. 45, 2019, doi: 10.1186/s12302-019-0231-z.

[5] J. E. Schollée, M. Bourgin, U. von Gunten, C. S. McArdell, and J. Hollender, “Non-target screening to trace ozonation transformation products in a wastewater treatment train including different post-treatments,” *Water Res.*, vol. 142, pp. 267–278, 2018, doi: https://doi.org/10.1016/j.watres.2018.05.045.

[6] M. Sysi-Aho, M. Katajamaa, L. Yetukuri, and M. Orešič, “Normalization method for metabolomics data using optimal selection of multiple internal standards,” *BMC Bioinformatics*, vol. 8, pp. 1–17, 2007, doi: 10.1186/1471-2105-8-93.

[7] A. K. Boysen, K. R. Heal, L. T. Carlson, and A. E. Ingalls, “Best-Matched Internal Standard Normalization in Liquid Chromatography-Mass Spectrometry Metabolomics Applied to Environmental Samples,” *Anal. Chem.*, vol. 90, no. 2, pp. 1363–1369, 2018, doi: 10.1021/acs.analchem.7b04400.

[8] J. Boccard, D. Tonoli, P. Strajhar, F. Jeanneret, A. Odermatt, and S. Rudaz, “Removal of batch effects using stratified subsampling of metabolomic data for in vitro endocrine disruptors screening,” *Talanta*, vol. 195, pp. 77–86, 2019, doi: https://doi.org/10.1016/j.talanta.2018.11.019.

[9] P. A. Lara-Martín, A. C. Chiaia-Hernández, M. Biel-Maeso, R. M. Baena-Nogueras, and J. Hollender, “Tracing Urban Wastewater Contaminants into the Atlantic Ocean by Nontarget Screening,” *Environ. Sci. Technol.*, vol. 54, no. 7, pp. 3996–4005, 2020, doi: 10.1021/acs.est.9b06114.

[10] V. Albergamo *et al.*, “Nontarget Screening Reveals Time Trends of Polar Micropollutants in a Riverbank Filtration,” *Environ. Sci. Technol.*, vol. 53, no. 13, pp. 7584–7594, Jul. 2019, doi: 10.1021/acs.est.9b01750.

[11] L. M. Beckers, W. Brack, J. P. Dann, M. Krauss, E. Müller, and T. Schulze, “Unraveling longitudinal pollution patterns of organic micropollutants in a river by non-target screening and cluster analysis,” *Sci. Total Environ.*, vol. 727, p. 138388, 2020, doi: 10.1016/j.scitotenv.2020.138388.

[12] T. Bader, W. Schulz, T. Lucke, W. Seitz, and R. Winzenbacher, “Application of Non-Target Analysis with LC-HRMS for the Monitoring of Raw and Potable Water: Strategy and Results,” in *Assessing Transformation Products of Chemicals by Non-Target and Suspect Screening − Strategies and Workflows Volume 2*, vol. 1242, American Chemical Society, 2016, pp. 3–49.

[13] K. T. Peter *et al.*, “Nontargeted Analysis Study Reporting Tool: A Framework to Improve Research Transparency and Reproducibility,” *Anal. Chem.*, vol. 93, no. 41, pp. 13870–13879, Oct. 2021, doi: 10.1021/acs.analchem.1c02621.

[14] W. Han and L. Li, “Evaluating and minimizing batch effects in metabolomics,” *Mass Spectrom. Rev.*, vol. n/a, no. n/a, Nov. 2020, doi: https://doi.org/10.1002/mas.21672.

[15] Z. Rong *et al.*, "NormAE: Deep Adversarial Learning Model to Remove Batch Effects in Liquid Chromatography Mass Spectrometry-Based Metabolomics Data," *Anal. Chem.*, vol. 92, no. 7, pp. 5082–5090, Apr. 2020, doi: 10.1021/acs.analchem.9b05460.

[16] J. Kuligowski, Á. Sánchez-Illana, D. Sanjuán-Herráez, M. Vento, and G. Quintás, "Intra-batch effect correction in liquid chromatography-mass spectrometry using quality control samples and support vector regression (QC-SVRC)," *Analyst*, vol. 140, no. 22, pp. 7810–7817, 2015, doi: 10.1039/C5AN01638J.

[17] W. E. Johnson, C. Li, and A. Rabinovic, "Adjusting batch effects in microarray expression data using empirical Bayes methods," *Biostatistics*, vol. 8, no. 1, pp. 118–127, Jan. 2007, doi: 10.1093/biostatistics/kxj037.

[18] R. A. van den Berg, H. C. J. Hoefsloot, J. A. Westerhuis, A. K. Smilde, and M. J. van der Werf, "Centering, scaling, and transformations: Improving the biological information content of metabolomics data," *BMC Genomics*, vol. 7, pp. 1–15, 2006, doi: 10.1186/1471-2164-7-142.

[19] A. M. De Livera *et al.*, "Normalizing and Integrating Metabolomics Data," *Anal. Chem.*, vol. 84, no. 24, pp. 10768–10776, Dec. 2012, doi: 10.1021/ac302748b.

[20] B. Drotleff and M. Lämmerhofer, "Guidelines for Selection of Internal Standard-Based Normalization Strategies in Untargeted Lipidomic Profiling by LC-HR-MS/MS," *Anal. Chem.*, vol. 91, no. 15, pp. 9836–9843, Aug. 2019, doi: 10.1021/acs.analchem.9b01505.

[21] G. Nyamundanda, P. Poudel, Y. Patil, and A. Sadanandam, "A Novel Statistical Method to Diagnose, Quantify and Correct Batch Effects in Genomic Studies," *Sci. Rep.*, vol. 7, no. 1, pp. 1–10, 2017, doi: 10.1038/s41598-017-11110-6.

[22] M. J. Boedigheimer *et al.*, "Sources of variation in baseline gene expression levels from toxicogenomics study control animals across multiple laboratories," *BMC Genomics*, vol. 9, no. 1, p. 285, 2008, doi: 10.1186/1471-2164-9-285.

[23] J. Teerlink, R. Budd, C. Alaimo, L. Wong, and T. M. Young, "Sub-Sewershed Monitoring to Elucidate Down-the-Drain Pesticide Sources."

[24] B. C. DeFelice *et al.*, "Mass Spectral Feature List Optimizer (MS-FLO): A Tool To Minimize False Positive Peak Reports in Untargeted Liquid Chromatography–Mass Spectroscopy (LC-MS) Data Processing," *Anal. Chem.*, vol. 89, no. 6, pp. 3250–3255, Mar. 2017, doi: 10.1021/acs.analchem.6b04372.

[25] C. Müller *et al.*, "Removing Batch Effects from Longitudinal Gene Expression - Quantile Normalization Plus ComBat as Best Approach for Microarray Transcriptome Data," *PLoS One*, vol. 11, no. 6, p. e0156594, Jun. 2016, [Online]. Available: https://doi.org/10.1371/journal.pone.0156594.

[26] B. Bolstad, "preprocesCore: A collection of pre-processing functions," 2021. https://github.com/bmbolstad/preprocessCore (accessed Mar. 03, 2021).

[27] J. T. Leek *et al.*, "sva: Surrogate Variable Analysis." 2021.

[28] D. Bates, M. Machler, B. Bolker, and S. Walker, "Fitting Linear Mixed-Effects Models

Using {lme4},” *J. Stat. Softw.*, vol. 67, no. 1, pp. 1–48, 2015, doi: 10.18637/jss.v067.i01.

[29] P. J. Rousseeuw, “Silhouettes: A graphical aid to the interpretation and validation of cluster analysis,” *J. Comput. Appl. Math.*, vol. 20, pp. 53–65, 1987, doi: https://doi.org/10.1016/0377-0427(87)90125-7.

[30] R. Tibshirani, G. Walther, and T. Hastie, “Estimating the number of clusters in a data set via the gap statistic,” *J. R. Stat. Soc. Ser. B (Statistical Methodol.*, vol. 63, no. 2, pp. 411–423, Jan. 2001, doi: https://doi.org/10.1111/1467-9868.00293.

[31] M. E. Ritchie *et al.*, “limma powers differential expression analyses for RNA-sequencing and microarray studies,” *Nucleic Acids Res.*, vol. 43, no. 7, pp. e47–e47, Apr. 2015, doi: 10.1093/nar/gkv007.

[32] B. Phipson, S. Lee, I. J. Majewski, W. S. Alexander, and G. K. Smyth, “ROBUST HYPERPARAMETER ESTIMATION PROTECTS AGAINST HYPERVARIABLE GENES AND IMPROVES POWER TO DETECT DIFFERENTIAL EXPRESSION,” *Ann. Appl. Stat.*, vol. 10, no. 2, pp. 946–963, Jun. 2016, doi: 10.1214/16-AOAS920.

[33] G. K. Smyth, “Linear Models and Empirical Bayes Methods for Assessing Differential Expression in Microarray Experiments,” *Stat. Appl. Genet. Mol. Biol.*, vol. 3, no. 1, 2004, doi: doi:10.2202/1544-6115.1027.

[34] D. R. Baker and B. Kasprzyk-Hordern, “Critical evaluation of methodology commonly used in sample collection, storage and preparation for the analysis of pharmaceuticals and illicit drugs in surface water and wastewater by solid phase extraction and liquid chromatography–mass spectrometry,” *J. Chromatogr. A*, vol. 1218, no. 44, pp. 8036–8059, 2011, doi: https://doi.org/10.1016/j.chroma.2011.09.012.

[35] I. González-Mariño, J. B. Quintana, I. Rodríguez, and R. Cela, “Determination of drugs of abuse in water by solid-phase extraction, derivatisation and gas chromatography–ion trap-tandem mass spectrometry,” *J. Chromatogr. A*, vol. 1217, no. 11, pp. 1748–1760, 2010, doi: https://doi.org/10.1016/j.chroma.2010.01.046.

[36] S. Riediker, A. Rytz, and R. H. Stadler, “Cold-temperature stability of five β-lactam antibiotics in bovine milk and milk extracts prepared for liquid chromatography–electrospray ionization tandem mass spectrometry analysis,” *J. Chromatogr. A*, vol. 1054, no. 1, pp. 359–363, 2004, doi: https://doi.org/10.1016/j.chroma.2004.07.085.

[37] T. Zindler, H. Frieling, A. Neyazi, S. Bleich, and E. Friedel, “Simulating ComBat: How batch correction can lead to the systematic introduction of false positive results in DNA methylation microarray studies,” *BMC Bioinformatics*, vol. 21, no. 1, pp. 1–15, 2020, doi: 10.1186/s12859-020-03559-6.

[38] V. Nygaard, E. A. Rødland, and E. Hovig, “Methods that remove batch effects while retaining group differences may lead to exaggerated confidence in downstream analyses,” *Biostatistics*, vol. 17, no. 1, pp. 29–39, Jan. 2016, doi: 10.1093/biostatistics/kxv027.

[39] T. Li, Y. Zhang, P. Patil, and W. E. Johnson, “Overcoming the impacts of two-step batch effect correction on gene expression estimation and inference,” *Biostatistics*, p. kxab039, Dec. 2021, doi: 10.1093/biostatistics/kxab039.

CHAPTER 4 IDENTIFICATION OF SUSPECTED AGROCHEMICALS AND TEMPORAL PATTERNS OF NONTARGET FEATURES IN BATCH-SCALE WOODCHIP BIOREACTORS

Introduction

Woodchip bioreactors have shown promise as a potential best management practice to mitigate the harmful effects of agricultural run-off on environmental waters [1]. The primary function of these bioreactors is to leverage the microbial reduction of nitrate (NO_3^-) to nitrogen gas while the microbial community uses the woodchips as a carbon source, thus reducing the nutrient load that is released to the environment [2]. One added benefit may also be the removal of pesticides [3]. However, in such a complex reaction system, the exact mechanism and extent to which the parent compounds are mineralized is unknown. Of the pesticides that adsorb to woodchips, some fraction will be irreversibly bound, while another portion could desorb, some of which may be available for biodegradation by the resident microbial community into transformation products (TPs). Even in a simplified microcosm of the system, variables such as redox conditions, composition of the microbial community, and unidentified organic matter create a complex interplay of processes. Understanding the relative contributions of abiotic and biotic processes and the importance of particular removal processes is essential for confident application of these systems in the field.

When pesticides were spiked into batch microcosms of these woodchip bioreactors, sorption was found to be the main pathway for removal from the aqueous phase, occurring mostly within the first 24 hours, although desorption from the woodchips also occurred in a bench-scale flow-through system when there was a greater mass of imidacloprid already sorbed to the woodchips [4]. This does not rule out the possibility of microbial degradation, which may only be observed from measuring the woodchip-sorbed fraction or by extending the duration of the trial. Indeed,

the half-life of imidacloprid in a sediment-water system was found to be 27 days, with the formation of bound residues of metabolite desnitro-imidacloprid [5], while diuron was found to be completely degraded by an anaerobic sediment culture after about 20 days [6].

Nontarget analysis of high-resolution mass spectral (HRMS) data from these systems can be used to untangle the many processes at play, given its broad scope approach which can capture a diverse set of parent compounds and TPs. Furthermore, application of statistics with time-series data can elucidate the significant patterns of chemical changes within the system. For example, application of multivariate statistics to nontarget features in a riverbank filtration system uncovered different classes of contaminants defined by their travel throughout the system [7]. Screening can be focused by comparing the aligned MS1 data against a curated, open source list of known agrochemicals [8] and their associated environmental transformation products predicted by a program such as Envipath, which uses functional group-specific biotransformation rules to predict TPs [9].

The purpose of this work was to gain a greater insight into the varied physicochemical and biological processes at work within a woodchip bioreactor system through the application of HRMS methods. We hypothesized that temporal trends of nontarget features within the biologically active and control microcosms would arise, depending on the dominant process at play, and that a curated suspect list of agrochemicals combined with a pathway prediction model would improve identification of environmentally relevant compounds. The nontarget dataset used here is aligned from three separate trials that examined the kinetics of imidacloprid and diuron removal from the water phase in a simplified batch-scale woodchip bioreactor system. Although only a single pesticide (imidacloprid or diuron) was intentionally spiked into the systems, the woodchips were collected from an operational field bioreactor that is exposed to a

variety of agrochemicals. Evidence obtained from different pesticides and TPs offers a window into the complexity of these systems and their potential for use as a best management practice.

Experimental

Preparation of small-scale batch woodchip reactors

Three trials were conducted with the same experimental structure, with differing variables noted in Table 4-1. Three treatment conditions were applied: an unmodified woodchip treatment batch (TB), an microbially-suppressed woodchip control (MC), and a no-woodchip control (NWC). Synthetic tile drainage was formulated with $MgSO_4$, KNO_3, NaCl, and $NaHCO_3$ to maintain electrical conductivity [4]. This was added to a 40 mL Teflon tube, and woodchip-containing groups (TB and MC) had 3 or 5 g of woodchips, depending on the experiment. Tubes were filled completely to eliminate headspace. Woodchips had been obtained from the multichannel bioreactor located in the central coast region of California, such that they were already "aged", and were stored at 4 °C airtight buckets. Woodchips for all three trials were from different collection batches. Both control groups (NWC and MC) were dosed with NaN_3 to suppress microbial activity. All groups were dosed with the same starting concentration of 40 ng/mL of imidacloprid or diuron. Samples were made in triplicate for 6 time points. The reactors were tumbled until sacrificed and analyzed.

Table 4-1: Structure of batch-scale woodchip bioreactor experiments

Experiment	Mass of woodchips (g)	Woodchip collection batch	Days until near-complete NO_3^- removal (d)
Imidacloprid-1 (I-1)	3	1	Not reached
Diuron (D)	5	2	2
Imidacloprid-2 (I-2)	5	2	8

Sample extraction

All water samples were extracted within 24 hours of collection. Extraction and analysis of water samples for pesticide content were carried out following Moschet et al. (2016), with some modifications: the filtration step was omitted due to the small sample volumes. Instead, the tubes containing synthetic tile drainage water and woodchips were centrifuged, then the supernatant was pipetted directly onto Oasis HLB SPE cartridges (Waters, Massachusetts, USA) that had been preconditioned with ethyl acetate, methanol, and ultrapure H_2O. Cartridges were dried and then eluted with ethyl acetate and methanol, which were evaporated under gentle N_2, combined, and evaporated to 0.2 mL. Extracts were then brought up to 1 mL with ultrapure H_2O, and 200 ng/mL of labelled internal standards were added to every extract. Extracts were stored at -20°C until acquisition. Water samples from the field bioreactors were extracted as described in Appendix 2 and Wrightwood et al. [4].

LC-QTOF-MS analysis

Extracts were analyzed by Agilent 1260 Infinity HPLC coupled to an Agilent 6530 QTOF-MS with a Zorbax Eclipse Plus C18 column (100 mm, 2.5 mm, 1.8 μm, Agilent Technologies, Inc.). Briefly, 20 μL of extract was injected with the following mobile phases used in a 23 min run at a flow rate of 0.35 mL/min in electrospray ionization (ESI) positive mode: (A) deionized water plus 0.1% formic acid, (B) acetonitrile plus 0.1% formic acid. For initial data independent acquisition (DIA), All-Ions fragmentation mode was used, meaning all ions with m/z 50−1050 were fragmented in the collision cell with collision energies (CE) of 0, 10, 20, and 40 eV. CE = 0 means no fragmentation and is equivalent to a full MS scan. The standard mix of LC-amenable compounds included 13 positively ionizing compounds. LC-QTOF-MS parameters for All Ions acquisition are included in Table A1-1. Extracts from experiments I-1 and D were run in a single

batch, and I-2 in a separate batch, with randomized sample order and blank and QC injection every 10 to 15 sample injections.

Data dependent acquisition (DDA) of prioritized features was then run using targeted MS/MS (tMS/MS) methods with a list of exact mass targets and retention times where collision cell voltages again cycled through 0, 10, and 40 eV once a precursor was isolated. Full scan data (CE 0 eV) were acquired at a rate of 4 spectra s^{-1} and high energy scans at 6 spectra s^{-1}. Additional parameters are included in Table A1-1. A 100 ng/mL mix of the ESI+ retention time index (RTI) calibrants for RTI prediction of candidate structures [10] after the tMS/MS experiments were run.

Nontarget alignment and feature filtering

MSDIAL (v. 3.66) alignment software was used for nontarget feature alignment because it is open source, works with data acquired in All-Ions mode, and allows aligned feature sets to be exported in formats that are amenable to subsequent statistical analysis [11]. This program has the added benefit of executing a retention time correction using the retention times of internal standards, which makes it possible to align samples that were acquired during different runs, as exact retention times can vary across runs on the LC. A list of labelled internal standards used for this correction can be found in Table A1-3, along with other alignment parameters in Table A1-2.

Due to the large number of features generated during alignment, multiple feature filtering parameters were applied. A standard signal-to-noise cut-off of ten was used. To further reduce the number of features, Mass Spectral Feature List Optimizer (MS-FLO), which was designed as a post-processing step to be used with MS-DIAL alignments [12], was implemented to join ammonium and sodium adducts to their matching molecular ion. Parameters used are included in

Table A1-4. The phenomenon of split features, which can occur during alignment despite the use of retention time correction from labelled internal standards, was handled by joining features that met the following three criteria: 1) retention times within ± 15 seconds, 2) m/z within 10 ppm, and 3) MS1 isotopic abundance ratios with coefficient of variation of 20% or less. Blank "subtraction" filters required that the maximum signal in reactor samples be greater than ten times the average signal in the blanks. Features with retention times below 4.5 minutes were excluded due to the poor chromatographic quality of early-eluting peaks that results in unreliable alignment of these features. Finally, any feature that did not appear in two out of three of at least one set of replicates was eliminated.

Suspect screening and feature prioritization

Figure 4-1 outlines the workflow of the feature prioritization process. This relied on the suspect screening that occurs simultaneously with nontarget alignment in MSDIAL and was used to generate a list of possible "parent" compounds from the Agilent Pesticide and Water Contaminants and the Massbank of North America (MoNA) libraries. Suspect hits that appeared in multiple sets of replicates and were agriculturally relevant were prioritized, and parent compounds were input to the Envipath pathway prediction model. Additionally, the suspect list PubChemLite (October 31, 2020) was filtered for compounds with agrochemical information (a category in the PubChem Compound Table of Contents and metadata column within PubChemLite) and was used to find exact-mass matches within the filtered feature set (neutral mass within +/- 10ppm). As with the suspect hits, any matched parent compounds were input to Envipath to generate a list of possible transformation product structures [9]. Exact masses of Envipath-predicted TPs were then searched for within the features (neutral mass within +/- 10ppm).

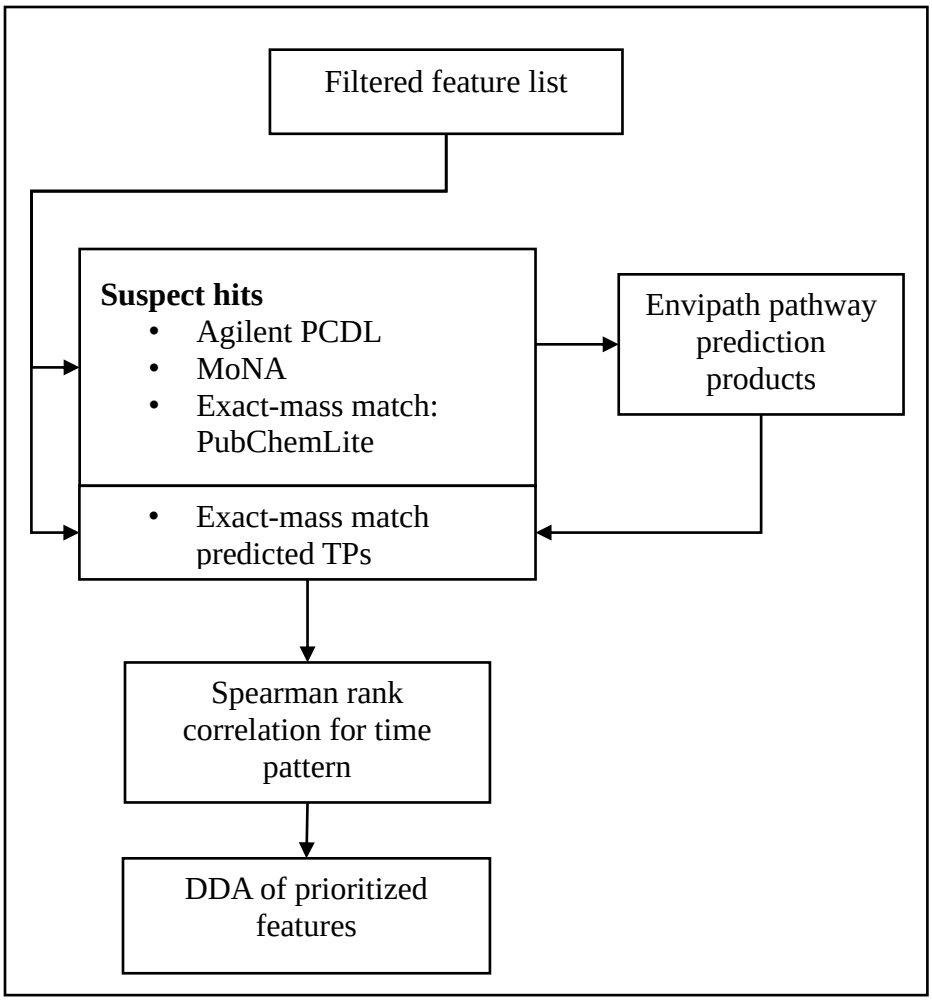

Figure 4-1. Flow diagram of feature prioritization process, beginning from filtered feature list, for identification of agrochemicals and transformation products. Suspect hits of parent pesticides from the Agilent PCDL and PubChemLite were run through Envipath to generate possible environmental TPs, which were searched for in the filtered feature list.

After the suspect screening step, a statistical test was used to categorize the time pattern observed for the matched features. For each treatment group (TB, MC, and NWC) within each batch (D, I-1, and I-2), a Spearman rank correlation test with a Benjamini-Hochberg correction was applied to determine if the feature abundance showed a significant relationship with time. For every feature, this resulted in 9 correlation coefficients (rho) values and 9 p-values. Theoretically, if a feature showed a significant decrease with time in both the MC and the TB treatment groups, it could plausibly be adsorbing, whereas if it showed a significant decrease

with time in only the TB batch, it may be degraded microbially. Table 4-2 outlines the definition for each time pattern. One unexpected pattern that was found by investigating some suspect-identified compounds was an evolution of a compound over time in only MC treatment set, since it was presumed that increasing abundance of a feature would indicate production via metabolism. However, this pattern indicates that there may be compounds desorbing from the woodchips that are rapidly degraded in the microbially-active treatment group (TB) and thus are only observed in the microbially inactive group (MC).

Features that were a suspect hit or exact-mass match as a "parent" agrochemical and showed a significant pattern with time and features that were an exact-mass match with a predicted TP of a parent agrochemical were considered for tMS/MS experiments. Features that had a maximum peak height less than 50,000 counts were discarded, because the potential for successfully acquiring good MS/MS results is lower for low-abundance peaks. This shortened the list from 171 features to 29 features.

Table 4-2: Spearman rank correlation conditions for inclusion in feature prioritization lists

	Correlation in MC	**Correlation in NWC**	**Correlation in TB**
Microbially degraded (deg)	$p > 0.05$	$p > 0.05$	$rho < 0$ & $p < 0.05$
Microbially formed (met)	$p > 0.05$	$p > 0.05$	$rho > 0$ & $p < 0.05$
Adsorbed to woodchips (ads)	$rho < 0$ & $p < 0.05$	$p > 0.05$	$rho < 0$ & $p < 0.05$
Desorbed from woodchips (des)	$rho > 0$ & $p < 0.05$	$p > 0.05$	$rho > 0$ & $p < 0.05$
Evolution in microbial control (MC)	$rho > 0$ & $p < 0.05$	$p > 0.05$	$p > 0.05$

Structure determination from DDA spectra

Acquisition of spectra from prioritized precursor ions was impaired by changes in retention times, which occurred because of the time elapsed between initial DIA and subsequent DDA analyses. For those that were acquired, multiple lines of evidence were employed to determine molecular formula and structure when possible. First, raw instrument data files from tMS/MS experiments (Agilent .d format) were converted to .abf files and aligned in MS-DIAL (parameters available in Table A1-2). Most aligned features were considered "high-quality"- that is, the apex of the peak was within the window of fragmentation and the peak itself was of good quality. However, some "low-quality" features were also aligned, seen in poorly shaped and noisy peaks or a peak with only the tail in the window of fragmentation.

All aligned features were exported to MSFINDER and SIRIUS/CSI:FingerID, two open-source formula and structure generation software programs. MSFINDER relies on MS1 isotopic spacing and abundance to generate formula candidates, and then scores the known structures based on whether the measured mass spectral peaks can be explained by fragmentation rules [13]. Parameters used are included in Table A4-5. Alternatively, SIRIUS/CSI:FingerID takes a "ground-up" approach by generating fragmentation trees for calculated molecular formulas, which are then used to construct a "molecular fingerprint" [14], [15] The molecular fingerprint predicts the presence of functional groups, bonds, and heteroatoms that may be present in the compound of interest. Structural candidates are scored on their similarity to the predicted molecular fingerprint.

The resulting lists of candidate structures from MSFINDER and SIRIUS/CSI:FingerID were merged for each feature to find the common compounds. Compounds were ranked according to a

combination of the scores provided by the two software programs, as described in Appendix 5, Equation A1-A3.

Suspect structures were run through a retention time index prediction model available at http://rti.chem.uoa.gr/ to confirm that the structure was plausible, given the experimental retention time [10]. When the suspect structure was the highest scoring and had a plausible RT, that was reported. When the highest scoring structure was not the suspect compound, this was no longer investigated, being outside the scope of the study. For some features, where there was no overlap between the two programs and/or structures returned had very low scores (<5 for MSFINDER and <-100 for CSI:FingerID), if the structure was plausible given the RT, experimental spectra were compared against library spectra of the suspect. If there was no available spectrum for the suspect, it was generated using CFM-ID. CFM-ID is an *in silico* fragmentation tool that used machine learning from collision induced dissociation datasets to score potential fragment probabilities [16].

Results & Discussion

Overview of targeted MS/MS experiment results

Of the 29 features that were chosen for tMS/MS experiments, 21 were exact-mass matches from PubChemLite, including 7 known transformation products. One feature was a suspect hit from the MoNA library. The other 7 features were exact mass matches with Envipath-predicted TP's generated from the parent suspect hits and exact mass matches. Suspected parent compounds that were input to Envipath for TP prediction are listed in Table 4-3. However, not all parent compounds could be confirmed: 5 were omitted from tMS/MS experiments due to low peak intensity. Additionally, some TPs of parents that were not suspect hits in the system were included in the tMS/MS list due to documentation on PubChem, and thus PubChemLite.

Interestingly, there were no exact-mass matches to any TPs predicted from imidacloprid or diuron, despite these compounds being used in the fields that drain to the woodchip bioreactor system and being spiked during the bench-scale experiments. The results of the Spearman correlation test with time for exact-mass hits are included in the appendix: Table A4-1 for the first imidacloprid batch, Table A4-2 for the diuron batch, and Table A4-3 for the second imidacloprid batch.

Table 4-3: Inputs to Envipath pathway prediction program

Parent compound	**Matched via**	**tMS/MS inclusion****	**InChIKey**
Aldimorph	Exact mass	1	SBUKOHLFHYSZNG-UHFFFAOYSA-N
Antimycin A1	Exact mass	1	UIFFUZWRFRDZJC-UHFFFAOYSA-N
Atrazine	Library*	0	MXWJVTOOROXGIU-UHFFFAOYSA-N
Butopyronoxyl	Exact mass	0	OKIJSNGRQAOIGZ-UHFFFAOYSA-N
Chlorantraniliprole	Exact mass	1	PSOVNZZNOMJUBI-UHFFFAOYSA-N
Cyantraniliprole	Exact mass	1	DVBUIBGJRQBEDP-UHFFFAOYSA-N
DEET	Exact mass; Library	1	MMOXZBCLCQITDF-UHFFFAOYSA-N
Diuron	Target		XMTQQYYKAHVGBJ-UHFFFAOYSA-N
(Z,Z)-Gossyplure	Exact mass	0	BXJHOKLLMOYSRQ-QOXWLJPHSA-N
Imidacloprid	Target		YWTYJOPNNQFBPC-UHFFFAOYSA-N
MCPA-2-ethylhexyl	Exact mass	0	IDGRPSMONFWWEK-UHFFFAOYSA-N
MCPA-isooctyl	Exact mass	0	PDIYKJRLQHHRAG-UHFFFAOYSA-N
Prallethrin	Exact mass	1	SMKRKQBMYOFFMU-UHFFFAOYSA-N

* Suspect screening in MS-DIAL found TP's of atrazine, so atrazine was input to Envipath
** 1: indicates inclusion in tMS/MS list; 0: indicates exclusion from tMS/MS list due to low abundance (<50,000)

After the tMS/MS experiments, 21 of the annotated features were successfully captured within the retention time window and had a well-shaped extracted ion chromatogram (EIC), 2

were measured within the RT window but had a noisy EIC, 3 were missed due to changed RT, and 3 were missed due to RT shift and had a poor EIC peak shape. From the 21 acquired targeted mass spectra, an unequivocal formula was generated for 17. Of the 4 spectra without clear formulae, one was not aligned by MSDIAL and could not be processed by MSFINDER and SIRIUS CSI:FingerID, while the other three did not show clear agreement. Six compounds were then identified with confidence level 2a, included 3 parent pesticides, 2 pesticide TPs, and indole-3-carboxylic acid. Additionally, there were two spectra for which the molecular formula matched the suspected identity, but a level 2a identification could not be reached. These results are explained in the following sections and are summarized in Table A5-4.

Level 2a: Parent Pesticides

Three parent pesticides were confirmed against library spectra (level 2a confidence): chlorantraniliprole, cyantraniliprole, and DEET. Chlorantraniliprole and cyantraniliprole are both synthetic anthranilic diamines (or "ryanoid") insecticides, derived from the naturally occurring alkaloid ryanodine, much in the way that pyrethroid insecticides were derived from the natural product, pyrethrin [17]. The application of the three main synthetic ryanoids, which includes these two, has been steadily increasing since 2008 [17], and inspection of the California Department of Pesticide Regulation (CDPR) Pesticide Use Reporting (PUR) from 2016-2018 shows their use in the areas draining to the multichannel woodchip bioreactor [18].

Cyantraniliprole showed contrasting patterns with time in the two imidacloprid-spiked experiments. The first imidacloprid experiment showed the feature decreasing with time in the microbially-active woodchips only, with low abundance in both the control groups (Figure 4-2a), suggesting microbial degradation as a potential removal mechanism (Table A5-1). The second imidacloprid batch showed an increase with time in both the microbially-active woodchips and

microbially-suppressed woodchip groups (Figure 4-2b), indicating both sorption and microbial removal mechanisms (Table A5-3). These experiments differed both in the mass of woodchips used, as well as the date the woodchips were collected from the field, which was reflected in the differing rates of nitrate removal (Table 4-1). While we did not take sulfate or ORP measurements, it is not unreasonable that redox conditions within these two experiments might have been different as well. Cyantraniliprole was found to have high K_d values in an anaerobic water-sediment system with sediment residues increasing initially due to sorption, then decreasing due to microbial breakdown or formation of nonextractable residues [19]. Cyantraniliprole was not present above the intensity cut-off in the samples from the diuron-spiked experiment.

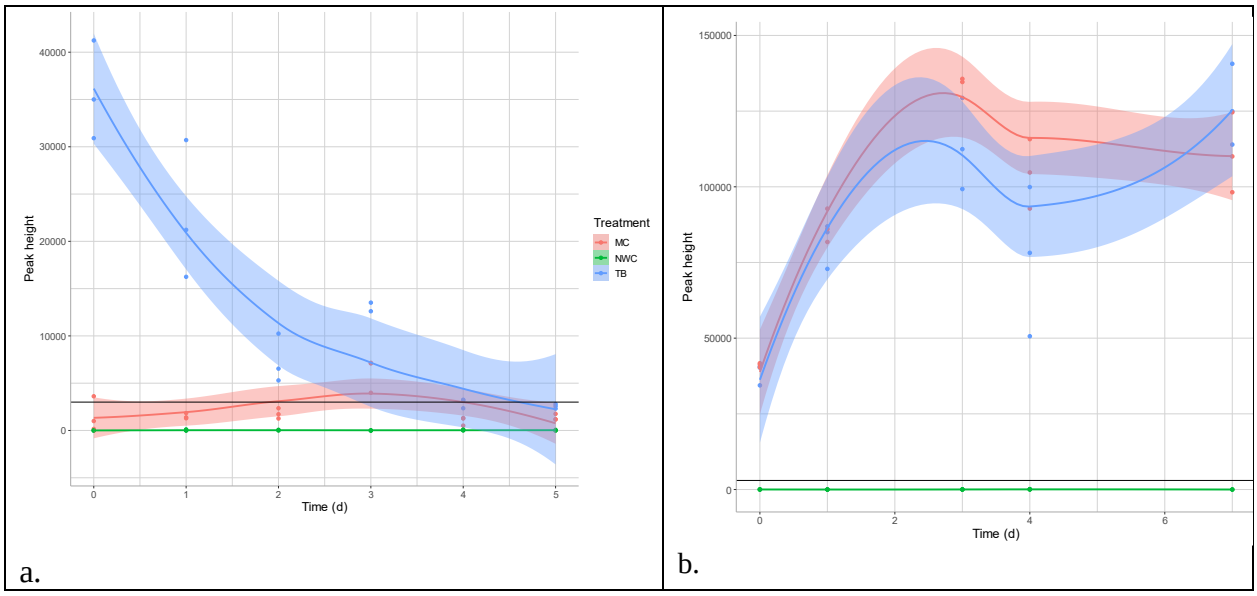

Figure 4-2. Patterns in batch-scale reactors with time for the feature identified as cyantraniliprole in a) first and b) second imidacloprid spiked batches.

The feature identified as chlorantraniliprole demonstrated less striking temporal patterns: seen in Figure 4-3, the majority of peaks are below 3000 counts in all treatment groups, with one outlier sample from the second imidacloprid-spiked batch in the TB group at the day 0 time point having a peak of about 80,000 counts. Although the results of the Spearman test determined that

this feature had the pattern of increasing through time only in the MC samples in the second imidacloprid spiked test (Table A5-3), the peak heights are rather low, and not that different from the other two treatment groups. This shows the limitations of this screening method, as some results can be spurious.

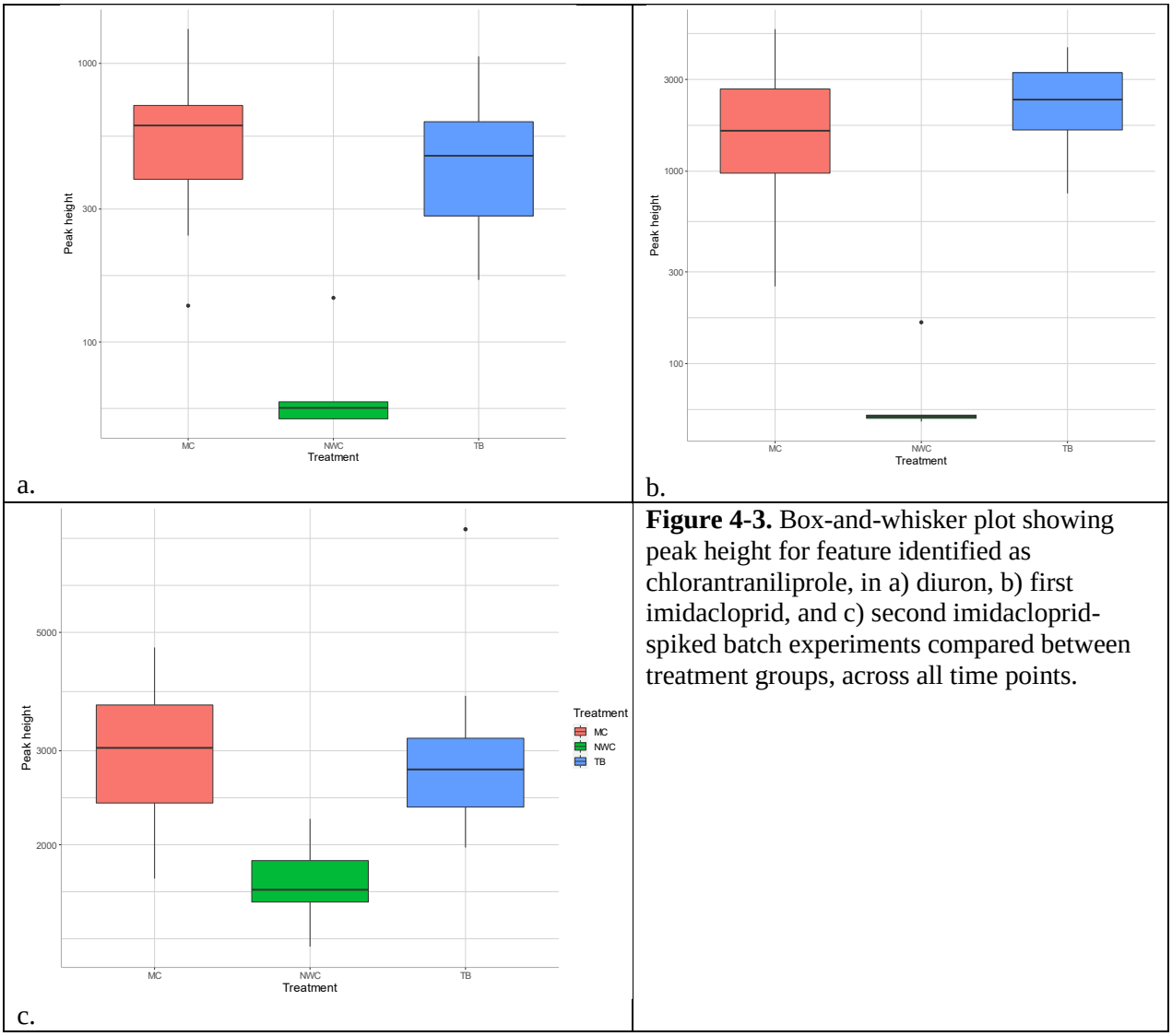

Figure 4-3. Box-and-whisker plot showing peak height for feature identified as chlorantraniliprole, in a) diuron, b) first imidacloprid, and c) second imidacloprid-spiked batch experiments compared between treatment groups, across all time points.

The presence of DEET in the woodchip samples was unexpected. DEET is not typically used in agriculture, rather it is used as an insect repellant applied on the skin of humans or animals. However, DEET is ubiquitous in surface water and groundwater in the U.S. and other countries,

so it could have been present in the irrigation water [20]. As with chlorantraniliprole, the results of the Spearman test determined that this feature had the pattern of increasing through time only in the MC samples in the diuron spiked test, which alone suggests desorption from the woodchips that would be microbially degraded (Table A5-2). However, the peak heights are rather low, and not that different from the other two treatment groups, as seen in Figure 4-4.

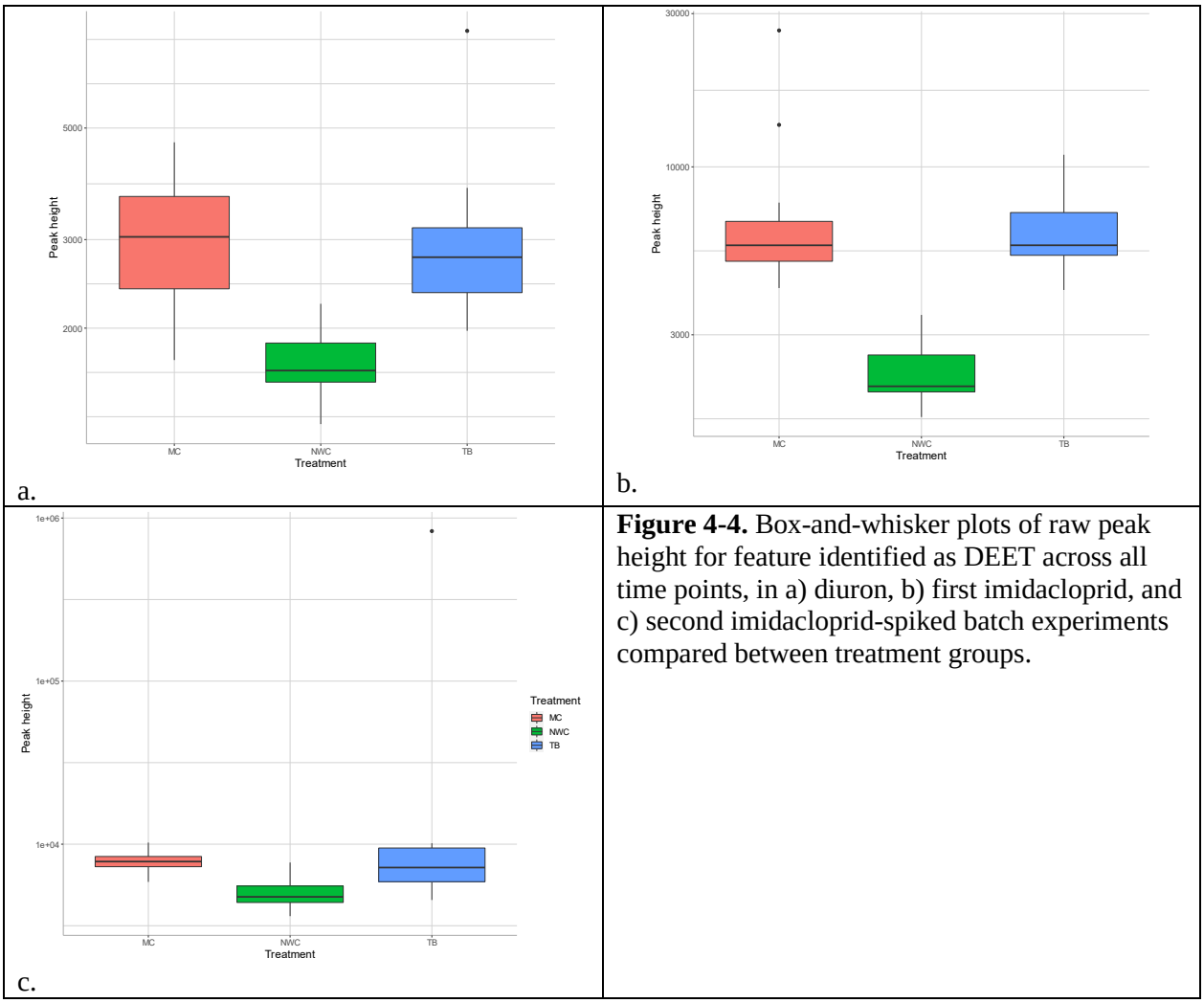

Figure 4-4. Box-and-whisker plots of raw peak height for feature identified as DEET across all time points, in a) diuron, b) first imidacloprid, and c) second imidacloprid-spiked batch experiments compared between treatment groups.

Level 2b-2a: Pesticide TPs

Azoxystrobin acid was one of the pesticide TPs identified, at a level 2a, which is defined as a library spectrum match [21]. Greater detail on the match is included in the appendices: Figure

A5-6 for the MS2 and Table A5-8 for the fragment masses. As seen in Figure 4-5, this feature shows in increasing pattern with time in the TB and MC treatments during all three trials, but only was labelled with the “desorption” pattern for the second imidacloprid-spiked experiment, in which it is present at much higher abundance (Table A5-3). Azoxystrobin is a strobilurin fungicide with documented use in the PUR [18] and was measured in quantifiable amounts in the influent and treated effluent of the field bioreactors (Figure 4-6) [4]. Azoxystrobin acid is a major but nonspecific microbial degradation product of azoxystrobin, as it can be formed in both anaerobic and aerobic soils, as well as water and water-sediment systems [22], any of which would have been possible in this case. Additionally, it is subject to leaching, at variable rates depending on soil properties [23].

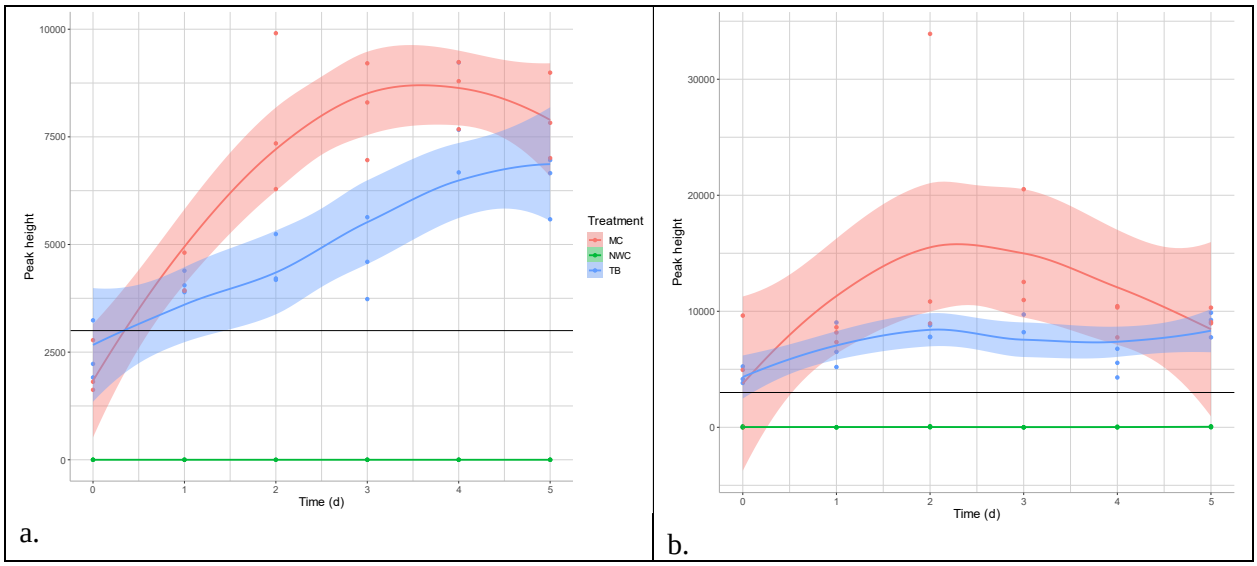

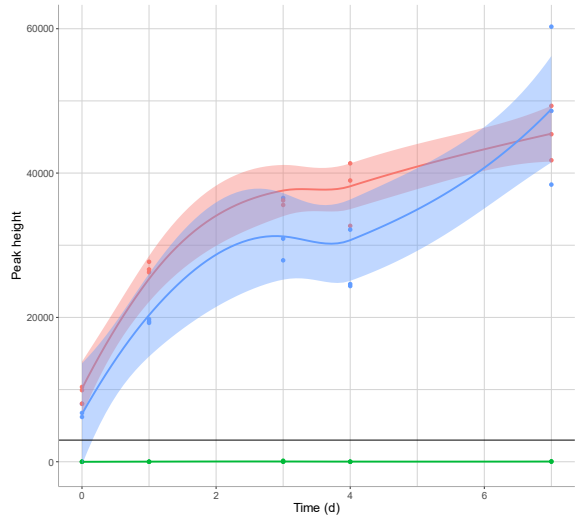

c.

Figure 4-5. Raw peak height for feature identified as azoxystrobin acid, in a) diuron, b) first imidacloprid, and c) second imidacloprid-spiked batch experiments compared between treatment groups shows increasing pattern with time in both MC and TB groups.

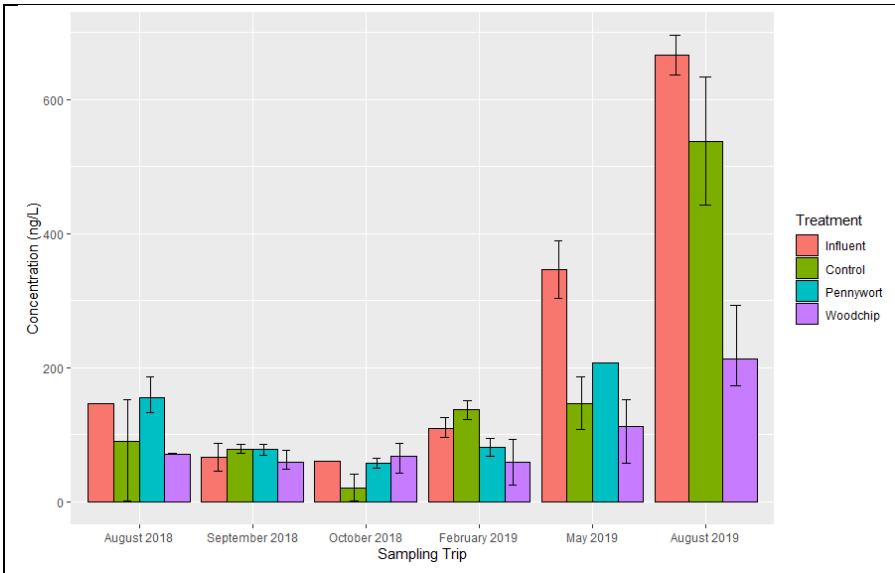

Figure 4-6. Measurements of azoxystrobin concentrations in influent and treated effluent (no-woodchip control, pennywort, and woodchip) from field bioreactors.

Additionally, the m/z = 455.0034 was identified at a 2a confidence level as IN-J9Z38, a documented transformation product of cyantraniliprole. While other identifications were accomplished through structure generation and scoring in both MSFINDER and SIRIUS-CSI:FingerID, that was not possible for m/z = 455.0034. This might have been due to the many molecular formulae possible at such a high m/z, combined with lack of fragmentation at the

lower two collision energies. However, comparison of the fragments seen at higher collision energies (Figure 4-8a) with a spectrum acquired by Huynh et al. [24] (Figure 4-8b) showed similar fragments with an average mass error less than 15 ppm (Table 4-4) and the RTI prediction model accepted the structure given the measured RT. Furthermore, the formula is supported by the MS1, with relative abundance of M-2 = 73%; M = 100%; M+2 = 22%. The combination of halogens this most closely corresponds to is a single Cl and Br, seen in Figure 4-7.

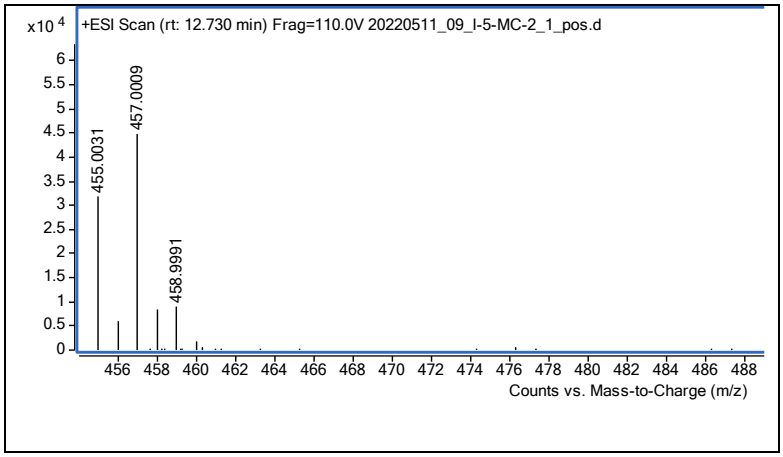

Figure 4-7. MS1 isotopic abundance patterns for m/z = 455.0023 corresponds to with a single Cl and Br.

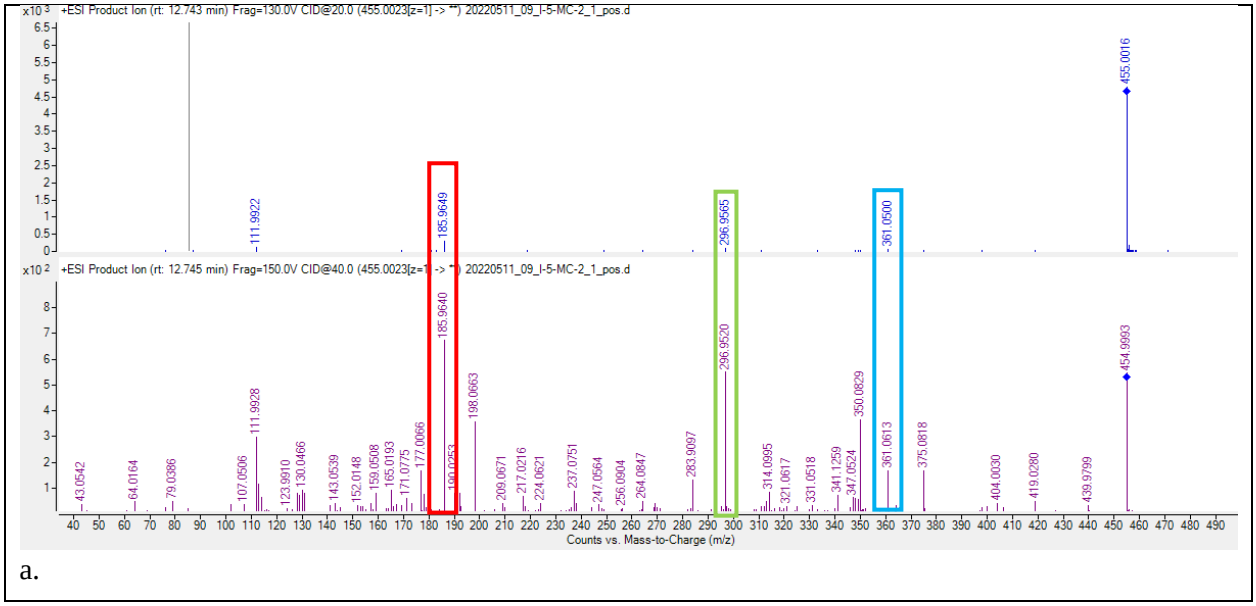

a.

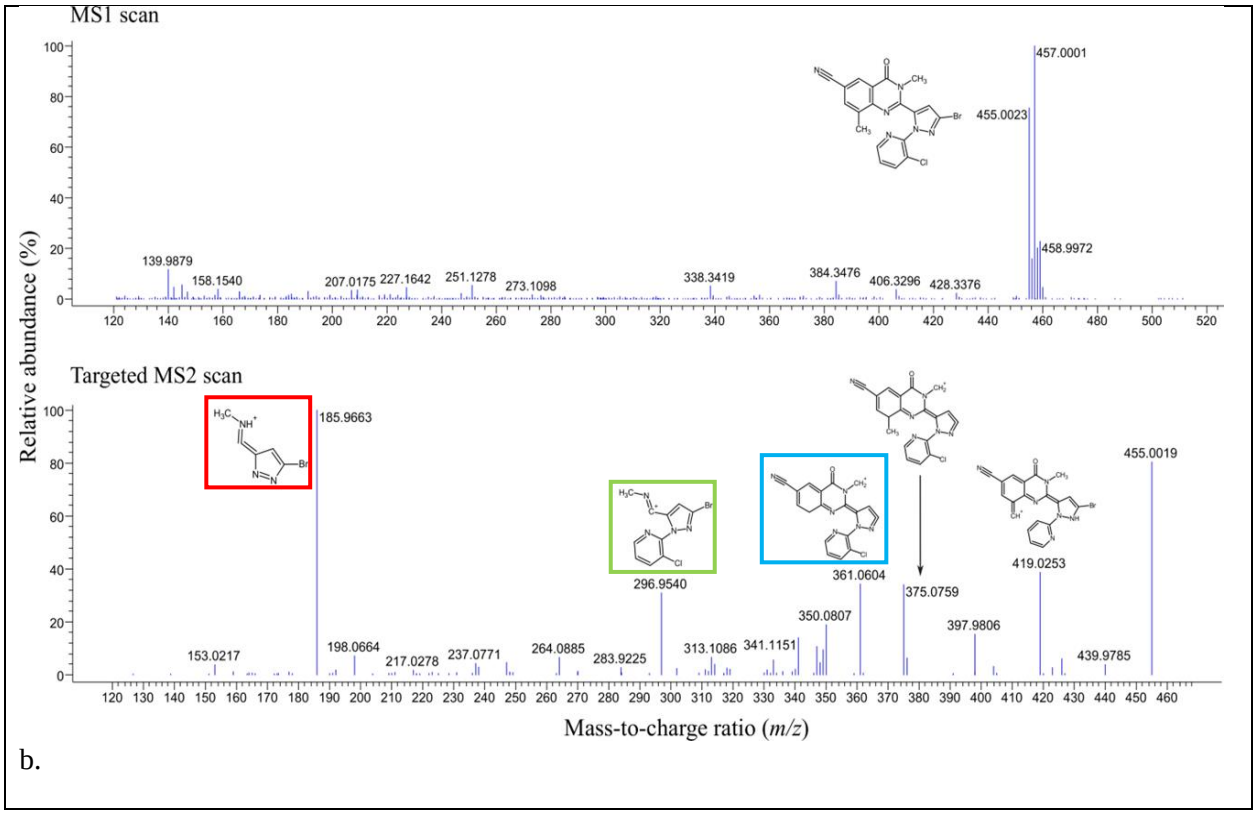

Figure 4-8. a) MS2 at 20 and 40 eV for m/z = 455.0023 measured in present study, compared to b) MS1 and MS2 measured by Huynh et al. for IN-J9Z38 [24]

Table 4-4: Fragment mass errors calculated from 20 and 40 eV collision energies for IN-J9Z38

Fragment molecular formula	Fragment exact mass	Average mass error (ppm)
$C_5H_5N_3Br$	185.9666	-11.56
$C_{10}H_7BrClN_4$	296.9542	0.17
$C_{18}H_{10}N_6OCl$	361.0604	-13.16
$C_{19}H_{12}BrClN_6O$	455.0023	-3.96

Like azoxystrobin acid, IN-J9Z38 is similarly nonspecific, as it can be formed from cyantraniliprole in aerobic and anaerobic soil and sediment, during hydrolysis, and as a plant metabolite [25]. Evaluation by the European Food Safety Authorization categorized cyantraniliprole as moderately to highly mobile in soil and IN-J9Z38 as immobile [25], thus it is likely that this TP formed somewhere in the field bioreactor system. The increasing peak heights with time in both the MC and TB treatments suggests desorption from the woodchips (Figure 4-

9), rather than formation during the trial. Other bench-scale studies using woodchips from this system have been influenced by the presence of pesticides sorbed to the woodchips: Wrightwood et al. [4] found that a batch of woodchips with particularly high sorbed imidacloprid led to higher effluent concentrations of imidacloprid.

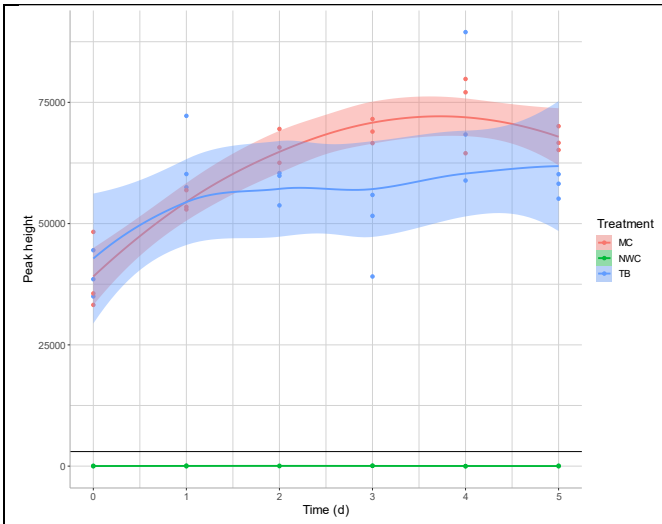

a.

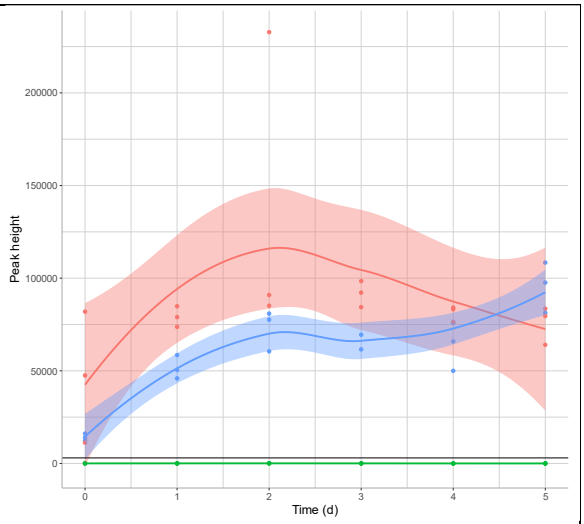

b.

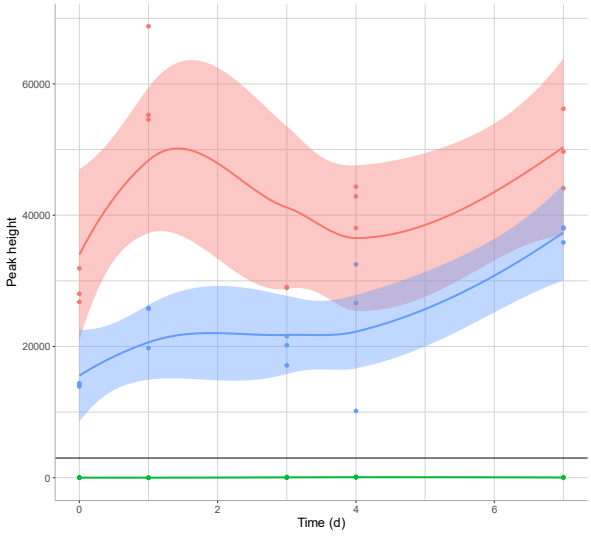

c.

Figure 4-9. Peak height of feature identified as IN-J9Z38 in a) diuron, b) first imidacloprid, and c) second imidacloprid-spiked batch scale experiments over time, compared between treatment groups.

M/z = 208.0992 was prioritized as an exact mass match to metabolite CGA 50720 of S-Metolachlor, and while the formula generated from the targeted mass spectrum is consistent with this, and although the structure was predicted to match with the measured retention time, the

structure was not among the highest scoring in SIRIUS CSI:FingerID or MSFINDER. By inspecting the individual collision energies in Qualitative Navigator (B.08.00), more fragments were observed than were included in MSFINDER. Because there was no available library spectrum for this structure and very little literature regarding it, CFM-ID was used to generate an *in-silico* spectrum. Using this diagnostic evidence (Figure A5-5, Table A5-7), this identification is classified with a 2b level of confidence [21].

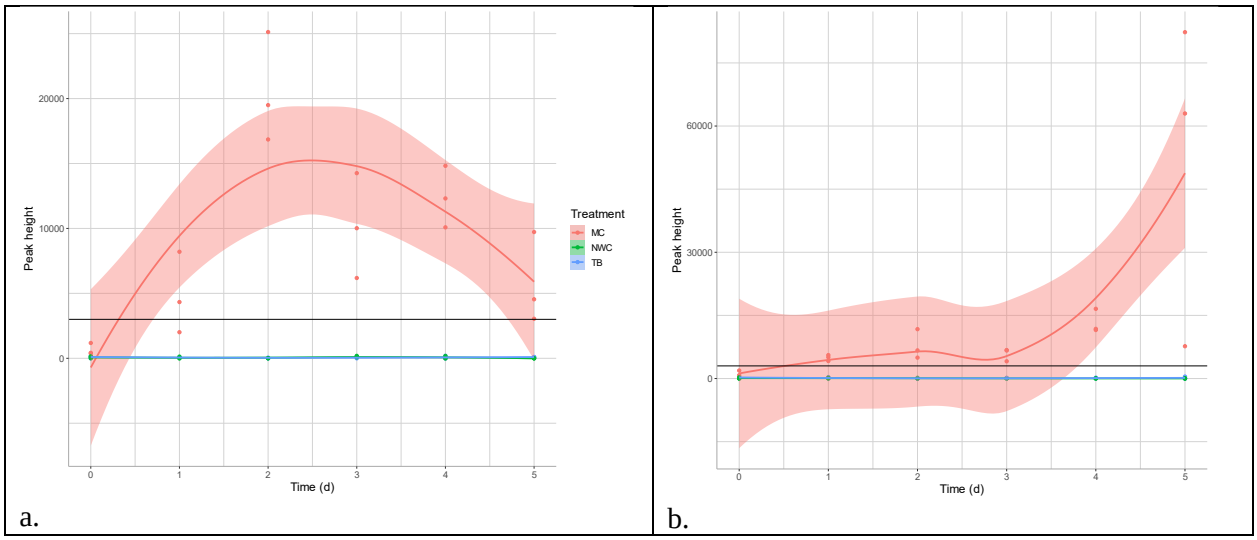

Figure 4-10. Peak height of feature identified tentatively as metochlor metabolite CGA 50720 in a) diuron and b) first imidacloprid spiked experiments.

This feature showed a significant correlation with time in the MC samples of the first imidacloprid-spiked experiment, and an increase-then-decrease pattern with time in the MC samples of the diuron-spiked experiment (Figure 4-10). Again, there is not much literature on this metabolite, so information such as its mobility and persistence in soil or water. It was included in the suspect list used by Reemtsma et al. [26], but was not identified. This metabolite can form from metolachlor by aqueous photolysis, metabolism in aerobic and anaerobic soil, and metabolism in aerobic and anaerobic aquatic systems [27], [28]. Metolachlor is a broad-spectrum herbicide and PUR from 2017 indicates a single application in the area near the bioreactors [18].

Level 3-2a: Indole Compounds

The feature with m/z = 162.055 was identified as indole-3-carboxylic acid (ICA), with a 2a confidence level. An additional indole-containing compound may be the feature with m/z = 176.0705, but the precise structure cannot be determined. For this feature, the highest scoring structure in MSFINDER and SIRIUS-CSI:FingerID was indole-3-acetic acid (IAA), but the RTI prediction for this structure returned "Predicted/Expected retention times are not reliable (Box 3)". However, another structural isomer is methyl indole-3-carboxylate, which scored lower in the structure generating programs, but returned an acceptable RTI prediction result (Box 2). For these reasons, it is difficult to choose either structure without an analytical standard, resulting in a confidence level of 3.

Both features were striking examples of the "MC" time pattern, seen in plots of peak height over time for ICA (Figure 4-11) and m/z = 176.0705 (Figure 4-12). IAA, one of the candidate structures of m/z = 176.0705, has agrochemical information on its PubChem entry due to its activity as a plant growth hormone. IAA, ICA, and other indole compounds can also be formed by rhizobacteria [29] (although this specific study did not measure methyl indole-3-carboxylic acid) under anaerobic to micro-aerobic conditions [30]. Sodium azide was the agent used in the microbial control samples to suppress microbial activity, as it disrupts the function of the electron transport chain. Generation of these compounds in the microbial control but not in the microbially active batches suggests that these compounds desorb from the woodchips and are degraded in microbially active bioreactors.

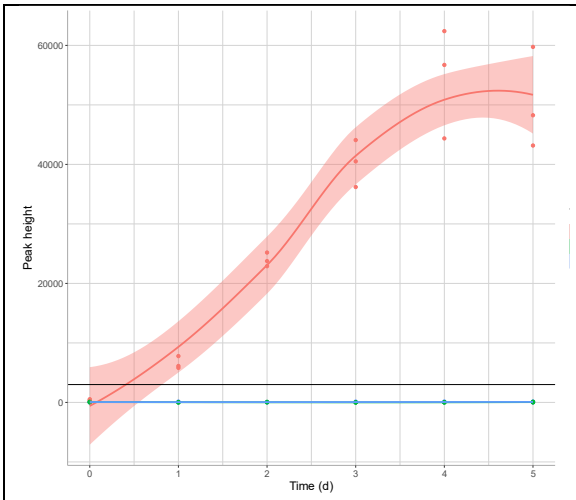

a.

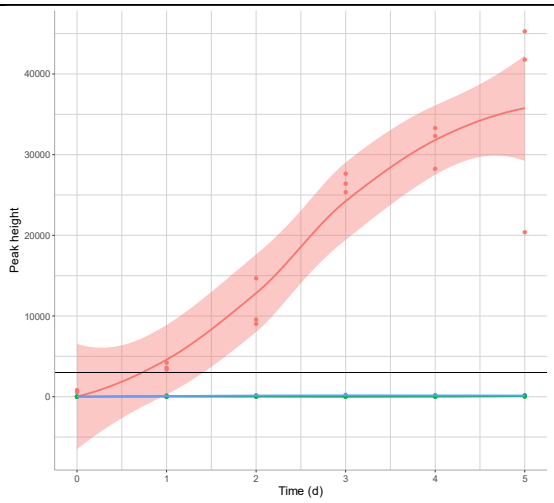

b.

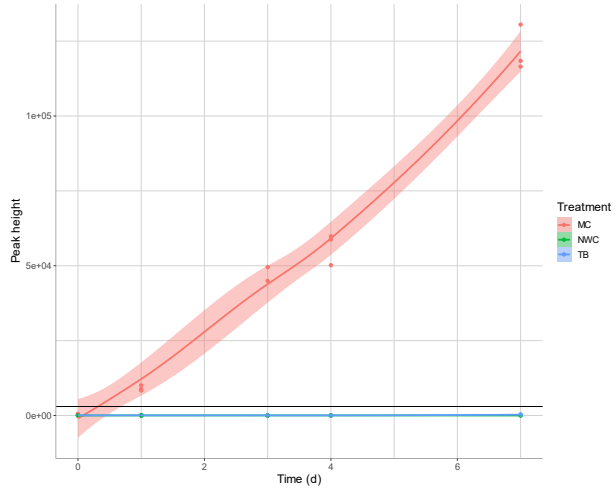

c.

Figure 4-11. Peak height of feature identified as ICA in a) diuron, b) first imidacloprid, and c) second imidacloprid-spiked batch scale experiments over time (days), compared between treatment groups.

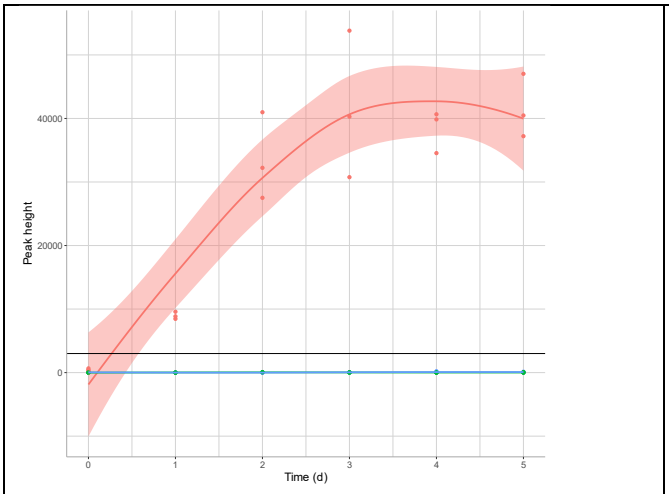

a.

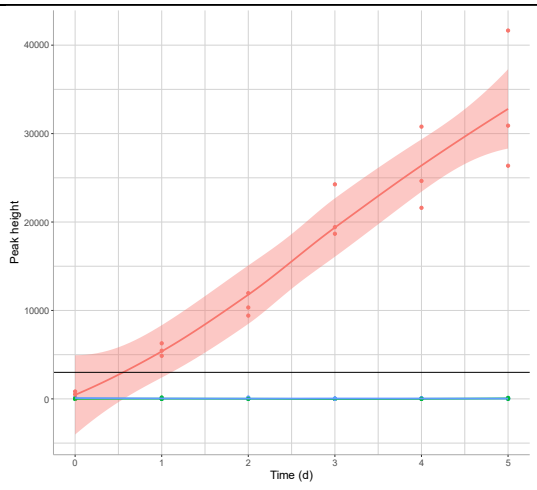

b.

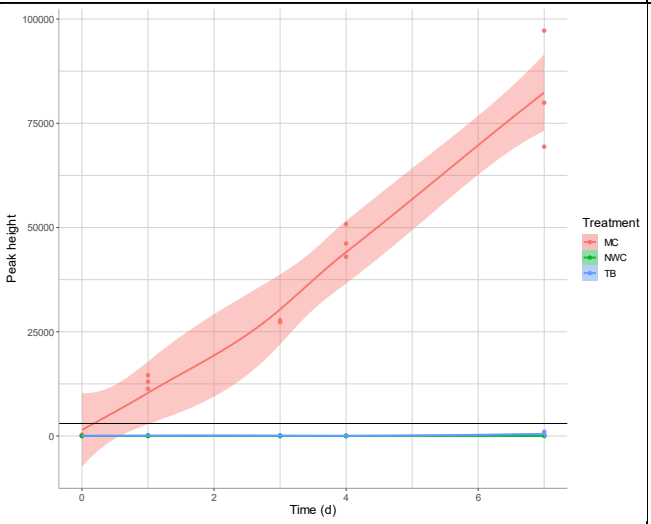

c.

Figure 4-12. Peak height of feature m/z = 176.0705 in a) diuron, b) first imidacloprid, and c) second imidacloprid-spiked batch scale experiments over time (days), compared between treatment groups.

Conclusions

One important component of predicting the efficacy of woodchip bioreactors in the treatment of pesticide-contaminated agricultural run-off is understanding the contributions of physicochemical versus biological processes to removal of pesticides. By using woodchips collected from field bioreactors in a more controlled study, it was observed that adsorbed compounds could pose a risk for desorption, while compounds that get removed by degradation shift the concern to transformation products. Of course, this will depend on a range of variables, including the lignin and cellulose content of the woodchips themselves [31], the molecular

structures of the pesticides in the system [32], as well as the microbial community and other environmental factors. Future studies could gather woodchip samples from multiple bioreactor sites and compare the effects of lignin/cellulose content and microbial community composition on degradation processes. Even a small-scale, controlled study such as this comprises a surprisingly complex system. Compounds such as cyantraniliprole, its metabolite IN-J9Z38, and azoxystrobin acid appear to be re-mobilizable from the woodchips and not subject to microbial degradation under these conditions. In a flow-through reactor such as those in the field system, this may pose a risk to receiving waters [33], or it may indicate that compounds are becoming bioavailable again for further breakdown [34].

References:

[1] L. Christianson, J. Tyndall, and M. Helmers, "Financial comparison of seven nitrate reduction strategies for Midwestern agricultural drainage," *Water Resour. Econ.*, vol. 2–3, pp. 30–56, 2013, doi: https://doi.org/10.1016/j.wre.2013.09.001.

[2] L. E. Christianson, A. Bhandari, and M. J. Helmers, "A practice-oriented review of woodchip bioreactors for subsurface agricultural drainage," *Applied Engineering in Agriculture*. 2012.

[3] Z. Mortensen *et al.*, "Isolation of Microbial Populations with the Ability To Use Pesticides as a Sole Carbon Source in Multichannel Woodchip Bioreactors under a Controlled Environment," 2019.

[4] O. M. Wrightwood, M. E. Hattaway, T. M. Young, and H. N. Bischel, "Assessment of Woodchip Bioreactor Characteristics and Their Influences on Joint Nitrate and Pesticide Removal," *ACS ES&T Water*, vol. 2, no. 1, pp. 106–116, Jan. 2022, doi: 10.1021/acsestwater.1c00277.

[5] S. E. Koshlukova, "Imidacloprid: Risk Characterization Document Dietary and Drinking Water Exposure," *Assessment*, no. 2, pp. 1–2, 2006, [Online]. Available: https://www.cdpr.ca.gov/docs/risk/rcd/imidacloprid.pdf.

[6] H. H. Attaway, N. D. Camper, and M. J. B. Paynter, "Anaerobic microbial degradation of diuron by pond sediment," *Pestic. Biochem. Physiol.*, vol. 17, no. 1, pp. 96–101, 1982, doi: https://doi.org/10.1016/0048-3575(82)90130-4.

[7] V. Albergamo *et al.*, "Nontarget Screening Reveals Time Trends of Polar Micropollutants in a Riverbank Filtration," *Environ. Sci. Technol.*, vol. 53, no. 13, pp. 7584–7594, Jul. 2019, doi: 10.1021/acs.est.9b01750.

[8] E. L. Schymanski, T. Kondić, S. Neumann, P. A. Thiessen, J. Zhang, and E. E. Bolton, "Empowering large chemical knowledge bases for exposomics: PubChemLite meets MetFrag," *J. Cheminform.*, vol. 13, no. 1, p. 19, 2021, doi: 10.1186/s13321-021-00489-0.

[9] J. Wicker *et al.*, "enviPath--The environmental contaminant biotransformation pathway resource," *Nucleic Acids Res.*, vol. 44, no. D1, pp. D502–D508, Jan. 2016, doi: 10.1093/nar/gkv1229.

[10] R. Aalizadeh *et al.*, "Development and Application of Liquid Chromatographic Retention Time Indices in HRMS-Based Suspect and Nontarget Screening," *Anal. Chem.*, vol. 93, no. 33, pp. 11601–11611, Aug. 2021, doi: 10.1021/acs.analchem.1c02348.

[11] H. Tsugawa *et al.*, "MS-DIAL: data-independent MS/MS deconvolution for comprehensive metabolome analysis," *Nat. Methods*, vol. 12, no. 6, pp. 523–526, Jun. 2015, doi: 10.1038/nmeth.3393.

[12] B. C. DeFelice *et al.*, "Mass Spectral Feature List Optimizer (MS-FLO): A Tool To Minimize False Positive Peak Reports in Untargeted Liquid Chromatography–Mass Spectroscopy (LC-MS) Data Processing," *Anal. Chem.*, vol. 89, no. 6, pp. 3250–3255, Mar. 2017, doi: 10.1021/acs.analchem.6b04372.

[13] H. Tsugawa *et al.*, “Hydrogen Rearrangement Rules: Computational MS/MS Fragmentation and Structure Elucidation Using MS-FINDER Software,” *Anal. Chem.*, vol. 88, no. 16, pp. 7946–7958, Aug. 2016, doi: 10.1021/acs.analchem.6b00770.

[14] K. Dührkop *et al.*, “SIRIUS 4: a rapid tool for turning tandem mass spectra into metabolite structure information,” *Nat. Methods*, vol. 16, no. 4, pp. 299–302, 2019, doi: 10.1038/s41592-019-0344-8.

[15] M. Ludwig, K. Dührkop, and S. Böcker, “Bayesian networks for mass spectrometric metabolite identification via molecular fingerprints,” *Bioinformatics*, vol. 34, no. 13, pp. i333–i340, Jul. 2018, doi: 10.1093/bioinformatics/bty245.

[16] F. Wang, J. Liigand, S. Tian, D. Arndt, R. Greiner, and D. S. Wishart, “CFM-ID 4.0: More Accurate ESI-MS/MS Spectral Prediction and Compound Identification,” *Anal. Chem.*, vol. 93, no. 34, pp. 11692–11700, Aug. 2021, doi: 10.1021/acs.analchem.1c01465.

[17] M. L. Grieneisen and M. B. Isman, “Recent Developments in the Registration and Usage of Botanical Pesticides in California,” in *Managing and Analyzing Pesticide Use Data for Pest Management, Environmental Monitoring, Public Health, and Public Policy*, vol. 1283, American Chemical Society, 2018, pp. 149-169 SE–8.

[18] “Pesticide Use Reporting, Annual 2016-2018.” .

[19] C. Zhang *et al.*, “Uptake, translocation and distribution of cyantraniliprole in rice planting system,” *J. Hazard. Mater.*, vol. 436, p. 129125, 2022, doi: https://doi.org/10.1016/j.jhazmat.2022.129125.

[20] S. Merel and S. A. Snyder, “Critical assessment of the ubiquitous occurrence and fate of the insect repellent N,N-diethyl-m-toluamide in water,” *Environ. Int.*, vol. 96, pp. 98–117, 2016, doi: https://doi.org/10.1016/j.envint.2016.09.004.

[21] E. L. Schymanski *et al.*, “Identifying small molecules via high resolution mass spectrometry: Communicating confidence,” *Environmental Science and Technology*. 2014, doi: 10.1021/es5002105.

[22] E. T. Rodrigues, I. Lopes, and M. Â. Pardal, “Occurrence, fate and effects of azoxystrobin in aquatic ecosystems: A review,” *Environ. Int.*, vol. 53, pp. 18–28, 2013, doi: https://doi.org/10.1016/j.envint.2012.12.005.

[23] L. F. Jørgensen, J. Kjær, P. Olsen, and A. E. Rosenbom, “Leaching of azoxystrobin and its degradation product R234886 from Danish agricultural field sites,” *Chemosphere*, vol. 88, no. 5, pp. 554–562, 2012.

[24] K. Huynh, L. Corkidi, E. Leonard, C. Palmer, J. Bethke, and N. Tharayil, “Dissipation and transformation of the diamide insecticide cyantraniliprole in ornamental snapdragon (Antirrhinum majus),” *Chemosphere*, vol. 281, p. 130753, 2021, doi: https://doi.org/10.1016/j.chemosphere.2021.130753.

[25] “Conclusion on the peer review of the pesticide risk assessment of the active substance cyantraniliprole,” John Wiley & Sons, Ltd, Sep. 2014. doi: https://doi.org/10.2903/j.efsa.2014.3814.

[26] T. Reemtsma, L. Alder, and U. Banasiak, “A multimethod for the determination of 150 pesticide metabolites in surface water and groundwater using direct injection liquid chromatography–mass spectrometry,” *J. Chromatogr. A*, vol. 1271, no. 1, pp. 95–104, 2013, doi: https://doi.org/10.1016/j.chroma.2012.11.023.

[27] US Environmental Protection Agency, “Reregistration Eligibility Decision (RED) Metolachlor,” 1995. [Online]. Available: https://archive.epa.gov/pesticides/reregistration/web/pdf/0001.pdf.

[28] D. Liu, R. J. Maguire, and G. J. Pacepavicius, “Microbial transformation of metolachlor,” *Environ. Toxicol. Water Qual.*, vol. 10, no. 4, pp. 249–258, 1995.

[29] M. Mujahid, C. Sasikala, and C. V Ramana, “Production of indole-3-acetic acid and related indole derivatives from L-tryptophan by Rubrivivax benzoatilyticus JA2,” *Appl. Microbiol. Biotechnol.*, vol. 89, no. 4, pp. 1001–1008, 2011, doi: 10.1007/s00253-010-2951-2.

[30] O. Ona, J. Van Impe, E. Prinsen, and J. Vanderleyden, “Growth and indole-3-acetic acid biosynthesis of Azospirillum brasilense Sp245 is environmentally controlled,” *FEMS Microbiol. Lett.*, vol. 246, no. 1, pp. 125–132, May 2005, doi: 10.1016/j.femsle.2005.03.048.

[31] Z. E. Ilhan, S. K. Ong, and T. B. Moorman, “Herbicide and Antibiotic Removal by Woodchip Denitrification Filters: Sorption Processes,” *Water, Air, Soil Pollut.*, vol. 223, no. 5, pp. 2651–2662, Jun. 2012, doi: 10.1007/s11270-011-1057-5.

[32] E. Barriuso, P. Benoit, and I. G. Dubus, “Formation of Pesticide Nonextractable (Bound) Residues in Soil: Magnitude, Controlling Factors and Reversibility,” *Environ. Sci. Technol.*, vol. 42, no. 6, pp. 1845–1854, Mar. 2008, doi: 10.1021/es7021736.

[33] ECHA (European Chemicals Agency), “Guidance on information requirements and chemical safety assessment.” p. Chapter R, 2017, [Online]. Available: https://echa.europa.eu/documents/10162/17224/information_requirements_r11_en.pdf/a8cce23f-a65a-46d2-ac68-92fee1f9e54f?t=1498475968629.

[34] J. Dec and J.-M. Bollag, “Microbial Release and Degradation of Catechol and Chlorophenols Bound to Synthetic Humic Acid,” *Soil Sci. Soc. Am. J.*, vol. 52, no. 5, pp. 1366–1371, 1988, doi: https://doi.org/10.2136/sssaj1988.03615995005200050030x.

CHAPTER 5 DISCUSSION AND CONCLUSION

While the main conclusions have been stated in Chapters 2-4, this final chapter is intended to integrate conclusions from all three chapters, discuss regulatory applicability and outline potential directions for future research.

Conclusions

Chapter 2 used suspect screening to explore a wastewater catchment system across space and time. Suspect-identified anthropogenic contaminants that were then quantified did not reveal much spatial variability. This may be because land use between the catchment areas sampled does not vary greatly, except that site E has a greater percentage of high-density residential zoning. Instead, greater variability was observed between the sampling months for a selection of the identified compounds: DEET showed a pattern consistent with presence of mosquitoes outdoors; caffeine unexpectedly showed significantly lower levels in May and June. Compounds measured by the GC-QTOF-MS included human metabolites of xenobiotics, which indicate exposure to compounds found in cigarette smoke and vehicle exhaust. This is illustrative of the wealth of information to be gleaned from wastewater data; biomarkers such as these could be used as proxies to compare exposures to air pollution, an important variable in public health applications. However, exposures could not be accurately back calculated without knowing that the compounds wouldn't arise in the system from other sources or are not degraded in the sewer system.

Chapter 3 focused on the challenges associated with nontarget analysis of the same wastewater dataset, because samples had been collected many months apart and LC-MS data was acquired in multiple analytical batches. An empirical Bayes method (ComBat) for estimation and subtraction of analytical batch effects was applied to the dataset, which was then compared to

three common alternatives: the same data acquired in a single analytical batch (with varying holding times), the multi-batch dataset before application of ComBat, and the multi-batch dataset scaled by the median internal standard peak height. When using principal variance component analysis, there was a clear removal of variance associated with analytical batch after the application of ComBat, which was not seen with internal standard scaling. Additionally, PCA of the corrected dataset grouped samples according to treatment status (treated effluent versus raw wastewater) along the first principal component, rather than according to the analytical batch as in the uncorrected data. Furthermore, fewer features were found to be significantly different between sample sites and dates after the application of ComBat, compared to the uncorrected dataset. This was especially true of the site-wise comparisons: almost no features were found to be significantly different between the group of all seven effluent samples and the raw wastewater, except for the group of all seven samples from site G. The lack of differentiation between sites was similar to that seen with the suspect-identified compounds in Chapter 2.

Chapter 4 demonstrated how to leverage time-series data for pattern identification of nontarget features. Like wastewater treatment systems, woodchip bioreactors are the sites of many biological and physicochemical processes, occurring in series or parallel. By identifying features displaying trends indicative of microbial degradation or adsorption, we can get a better understanding of the treatment efficacy of the bioreactors. For example, multiple compounds were observed to desorb from the woodchips, including cyantraniliprole and its transformation product, IN-J9Z38. This means that desorption of pesticides and TPs into bioreactor effluent could also happen in the field reactors, although the specific conditions that cause this are unclear. Suspect screening in woodchip bioreactors can be more focused than in wastewater, because only chemicals used in agriculture are of concern, and curation efforts of chemical

metadata enables this, as in the creation of the PubChemLite database. Using a curated suspect list has been found to yield more accurate identifications [1].

The lens through which a system is viewed (i.e., target, suspect, and nontarget) has an effect on our understanding of that system, due to the advantages and disadvantages of each approach. For example, there was greater spatial variability observed within the wastewater dataset when specific target pesticides were considered [2] than when a broad scope nontarget method was used in Chapter 2. In wastewater, nontarget screening may make it difficult to pull out low-level contaminants of concern, unless toxicity can be used as an orthogonal data source, due to the much greater abundance of endogenous metabolites and commonly used components of consumer products. However, the ability to isolate chemical features with a pattern of interest, without having to know their identity, can afford greater levels of insight into the processes occurring within complex treatment systems.

Discussion

It has been argued that anthropogenic chemicals should also be considered "agents of global change", along with CO2 emissions, nutrient pollution, and biodiversity loss, because of their rate of proliferation, utilization, and diversification [3], [4]. This growth is not likely to slow with a growing population, a changing climate, and improved chemical discovery pipelines. As we continue to discover these chemicals and their transformation products in environmental water and other matrices, and observe the toxic outcomes, it will be important to implement treatment systems at the interfaces of the built and natural environments. For example, N-(1,3-Dimethylbutyl)-N′-phenyl-p-phenylenediamine-quinone (6PPD-quinone) was determined to be the culprit of acute mortality events in coho salmon after storm events; this highly toxic ozonation product of 6PPD in tire wear particles was washed from roads into urban streams [5].

However, bioretention beds were found to eliminate the toxicity of urban stormwater, and represent a low-cost and scalable solution that effectively removes a variety of toxic components of stormwater runoff [6].

When it comes to measuring the efficacy of treatment systems, whether they are large, centralized wastewater treatment plants or low-tech bioreactors, monitoring for single or a handful of compounds will no longer be sufficient. Suspect screening and nontarget analysis should be implemented as a key first step, to establish the presence of important compounds, which could then be measured in exact quantities by target screening [7]. However, successful nontarget studies begin with thoughtful experimental design.

Every decision node in an un-targeted study represents a trade-off. First, as noted in Chapter 2, collecting flow-weighted wastewater samples provides the most accurate measurement of contaminant loads. In Chapter 4, by measuring only the aqueous phase of the reactors, time and materials were saved, but the exact mechanism of diuron or imidacloprid removal could not be determined. Next, sample clean up can affect what chemicals are ultimately detected: solid phase extraction was found to affect to recovery of source-specific feature fingerprints, especially with increasing dilution and matrix complexity [8]. However, forgoing SPE with raw wastewater samples would not be an option, thus the extraction medium will define the “chemical space” that can be assessed [9]. This chemical space will be further narrowed by the choice of instrument and ionization method used. Consider the lack of correlation between compounds measured on the GC with those measured on the LC in chapter 3: completely different conclusions about the nature of the system might be reached if only one or the other was used. Other choices that come with data acquisition include whether to run in a single batch or in multiple batches when samples are received and processed over a long span of time, as seen in

chapter 2. The choice to collect in data-dependent (DDA) versus data-independent acquisition (DIA) mode will also affect the features that are ultimately identified: DDA is appropriate if only high-abundance features are to be considered and eliminates the need for reacquisition of MS/MS later, but DIA fragments all ions, retaining a broader scope but making it necessary to rerun samples in targeted MS/MS mode to determine structures.

These are just a handful of decisions that must be made in these studies, not even considering the data-processing steps. Fortunately, there has been a great deal of work done to create guidelines for replicability and making studies supportive of regulatory action [10]–[12]. On the front of identifying pesticide transformation products, there are two main roadblocks: first, while studies of parent and transformation products are required for pesticide reregistration, this information exists in "gray literature" that is not readily available, and second, reference material and library spectra of transformation products are frequently not commercially available. While tools such as the EnviPath pathway prediction model and CFM-ID have been developed to fill these gaps, an alternative is the European Crop Protection Association (ECPA), which is committed to providing reference materials for transformation products of the chemicals it produces [7]. Additionally, information on chemical usage should be made available by regulatory agencies for improved suspect screening; for example, the California Department of Pesticide Regulation's Pesticide Use Reporting database is extremely valuable in documenting agricultural pesticide applications, but currently the most recent year available is 2018. A proactive approach would be to require chemical manufacturers to be able to publicly produce chemical data such as risk assessments and reference material as a condition of market access.

References

[1] E. L. Schymanski, T. Kondić, S. Neumann, P. A. Thiessen, J. Zhang, and E. E. Bolton,

"Empowering large chemical knowledge bases for exposomics: PubChemLite meets MetFrag," *J. Cheminform.*, vol. 13, no. 1, p. 19, 2021, doi: 10.1186/s13321-021-00489-0.

[2] J. Teerlink, R. Budd, C. Alaimo, L. Wong, and T. M. Young, "Sub-Sewershed Monitoring to Elucidate Down-the-Drain Pesticide Sources."

[3] E. S. Bernhardt, E. J. Rosi, and M. O. Gessner, "Synthetic chemicals as agents of global change," *Front. Ecol. Environ.*, vol. 15, no. 2, pp. 84–90, 2017, doi: 10.1002/fee.1450.

[4] W. Brack *et al.*, "One planet: one health. A call to support the initiative on a global science–policy body on chemicals and waste," *Environ. Sci. Eur.*, vol. 34, no. 1, p. 21, 2022, doi: 10.1186/s12302-022-00602-6.

[5] Z. Tian *et al.*, "A ubiquitous tire rubber–derived chemical induces acute mortality in coho salmon," *Science (80-.).*, p. eabd6951, Dec. 2020, doi: 10.1126/science.abd6951.

[6] J. K. McIntyre *et al.*, "Soil bioretention protects juvenile salmon and their prey from the toxic impacts of urban stormwater runoff," *Chemosphere*, vol. 132, pp. 213–219, 2015, doi: https://doi.org/10.1016/j.chemosphere.2014.12.052.

[7] J. Hollender *et al.*, "High resolution mass spectrometry-based non-target screening can support regulatory environmental monitoring and chemicals management," *Environ. Sci. Eur.*, vol. 31, no. 1, p. 42, 2019, doi: 10.1186/s12302-019-0225-x.

[8] K. T. Peter, E. P. Kolodziej, and J. R. Kucklick, "Assessing Reliability of Non-targeted High-Resolution Mass Spectrometry Fingerprints for Quantitative Source Apportionment in Complex Matrices," *Anal. Chem.*, vol. 94, no. 6, pp. 2723–2731, Feb. 2022, doi: 10.1021/acs.analchem.1c03202.

[9] B. L. Milman and I. K. Zhurkovich, "The chemical space for non-target analysis," *TrAC Trends Anal. Chem.*, vol. 97, pp. 179–187, 2017, doi: https://doi.org/10.1016/j.trac.2017.09.013.

[10] K. T. Peter *et al.*, "Nontargeted Analysis Study Reporting Tool: A Framework to Improve Research Transparency and Reproducibility," *Anal. Chem.*, vol. 93, no. 41, pp. 13870–13879, Oct. 2021, doi: 10.1021/acs.analchem.1c02621.

[11] W. Schulz and T. Lucke, "Non-Target Screening in Water Analysis - Guideline for the application of LC-ESI-HRMS for screening." 2019, [Online]. Available: http://www.wasserchemische-gesellschaft.de.

[12] B. Ng, N. Quinete, and P. R. Gardinali, "Assessing accuracy, precision and selectivity using quality controls for non-targeted analysis," *Sci. Total Environ.*, vol. 713, p. 136568, 2020, doi: https://doi.org/10.1016/j.scitotenv.2020.136568.

APPENDIX 1 GENERAL SUPPLEMENTARY EXPERIMENTAL

Table A1-1: LC-QTOF-MS parameters for All Ions acquisition and targeted MS/MS (tMS/MS) acquisition

Agilent 6530 QTOF	
Injection volume (µL)	20
LC settings	
Mobile phase	
A (pos)	milliQ water + 0.1% formic acid
B (pos)	Acetonitrile + 0.1% formic acid
Solvent flow (µL/min)	350
Gradient	
	2% B for 1.5 min
	2-100% B for 15 min
	100% B for 5 min
	Equilibration to initial conditions for 3 min
Column	Zorbax Eclipse Plus (2.5 mm ID, 1.8 µm particle size)
Guard-column	Zorbax Eclipse Plus (2.5 mm ID, 1.8 µm particle size)
Column temperature (°C)	30
Source parameters	
Gas temperature (°C)	300
Gas flow rate (L/min)	12
Nebulizer (psi)	25
Sheath gas temperature (°C)	350
Sheath gas flow rate (L/min)	11
Capillary (V)	3000
Nozzle voltage (V)	1500
Fragmentor (V)	110
Skimmer (V)	65
Cell RF (eV)	0,10, 20, 40
Octopole RF (V)	750
MS Settings	
Gas temperature (°C)	300
Drying gas flow rate (L/min)	12
Nebulizer (psig)	25
Sheath gas temperature (°C)	350
Sheath gas flow rate (L/min)	11
Vcap	3500
Fragmentor (V)	110
Reference mass correction	121.0509, 922.0098
All Ions Data independent acquisition (DIA)	
Scan range	50-1050 m/z
Scan speed	4 spectra/s
Collision energies (eV)	0, 10, 20, 40
Targeted MS/MS Data dependent acquisition (DDA)	
MS1	

Scan range	30-1050 m/z
Scan speed	4 spectra/s
Collision energies (eV)	0
Maximum time between MS (s)	3
MS2	
Scan range MS2	30-1050 M/Z
Scan speed	6 spectra/s
Collision energies (eV)	0, 10, 20, 40
Retention time window (min)	0.8
Isotopic width	Narrow (1.3 m/z)
Z	1

Table A1-2: General MS-DIAL alignment parameters for tMS/MS and All Ions data

	tMS/MS	**All Ions**
Project		
MS1 Data type	Profile	Profile
MS2 Data type	Centroid	Profile
Ion mode	Positive	Positive
Target	Metabolomics	Metabolomics
Mode	ddMSMS	diMSMS
Data collection parameters		
Retention time begin	4	0
Retention time end	100	100
Mass range begin	0	0
Mass range end	2000	5000
MS2 mass range begin	0	0
MS2 mass range end	2000	0
Centroid parameters		
MS1 tolerance	0.01	0.01
MS2 tolerance	0.025	0.025
Isotope recognition		
Maximum charged number	2	2
Data processing		
Number of threads	5	5
Peak detection parameters		
Smoothing	LinearWeightedMovingAverage	LinearWeightedMovingAverage

method		
Smoothing level	3	3
Minimum peak width	5	5
Minimum peak height	3000	3000
Peak spotting parameters		
Mass slice width	0.1	0.1
Exclusion mass list	(mass & tolerance)	
Deconvolution parameters		
Sigma window value	0.5	0.5
MS2Dec amplitude cut off	0	0
Exclude after precursor	TRUE	TRUE
Keep isotope until	0.5	0.5
Keep original precursor isotopes	FALSE	FALSE
MSP file and MS/MS identification setting		
MSP file	MergedPCDL_AllSpectra_Positive.msp	MergedPCDL_AllSpectra_Positive.msp
Retention time tolerance	100	100
Accurate mass tolerance (MS1)	0.01	0.01
Accurate mass tolerance (MS2)	0.05	0.05
Identification score cut off	80	80
Using retention time for scoring	FALSE	TRUE
Using retention time for filtering	FALSE	FALSE
Text file and post identification (retention time and accurate mass based) setting		
Text file		
Retention time tolerance	0.1	0.1

Accurate mass tolerance	0.01	0.01
Identification score cut off	85	85
Advanced setting for identification		
Relative abundance cut off	0	0
Top candidate report	FALSE	TRUE
Adduct ion setting		
[M+H]+ [M+NH4]+ [M+Na]+		
Alignment parameters setting		
Reference file	(varies for alignment)	(varies for alignment)
Retention time tolerance	0.05	0.05
MS1 tolerance	0.015	0.015
Retention time factor	0.5	0.5
MS1 factor	0.5	0.5
Peak count filter	0	0
N% detected in at least one group	0	0
Remove feature based on peak height fold-change	FALSE	FALSE
Sample max / blank average	5	5
Sample average / blank average	5	5
Keep identified and annotated metabolites	TRUE	TRUE
Keep removable features and assign the tag for checking	TRUE	TRUE
Gap filling by compulsion	FALSE	TRUE
Tracking of isotope labels		
Tracking of	FALSE	FALSE

isotopic labels		
Ion mobility		
Ion mobility data	FALSE	FALSE

Table A1-3: Labelled internal standards used for retention time alignment in MS-DIAL

Compound	Rt (min)	Rt tol. (min)	m/z	m/z tol. (Da)	Min. Height	Use
Methomyl-D3	6.65	0.2	166.0721	0.025	5000	T
Simazine-D5	9.5	0.2	207.1163	0.025	5000	T
Dimethoate-D6	8.16	0.2	236.0443	0.025	5000	T
Diuron-D6	10.89	0.2	239.0618	0.025	5000	T
Imidacloprid-D4	8.01	0.2	260.0858	0.025	5000	T
Pendimeth-D5	15.9	0.2	287.1775	0.025	5000	T
Boscalid-D4	12.69	0.2	347.0651	0.025	5000	T

Table A1-4: Parameters used for MS-FLO for adduct feature joining

Sodium adduct joining	Ammonium adduct joining
[0. Global Parameters]	**[0. Global Parameters]**
row merging delimiter = _	row merging delimiter = _
[1. Contaminant Ion Removal]	**[1. Contaminant Ion Removal]**
enabled = False	enabled = False
[2. Duplicate Removal]	**[2. Duplicate Removal]**
enabled = True	enabled = True
mz tolerance = 0.01	mz tolerance = 0.01
retention time tolerance = 0.1	retention time tolerance = 0.1
peak height tolerance = 1.0	peak height tolerance = 1.0
minimum peak match ratio = 0.85	minimum peak match ratio = 0.85
[3. Isotope Detection]	**[3. Isotope Detection]**
enabled = True	enabled = True
mz tolerance = 0.01	mz tolerance = 0.01
retention time tolerance = 0.02	retention time tolerance = 0.02
minimum r^2 to match = 0.0	minimum r^2 to match = 0.0
mass shift = 1.003355	mass shift = 1.003355
[4. Adduct Joiner]	**[4. Adduct Joiner]**
enabled = True	enabled = True
mz tolerance = 0.01	mz tolerance = 0.01
retention time tolerance = 0.02	retention time tolerance = 0.02
adduct = ['M+H', 'M+Na', 21.98187, 0.0, 0.8]	adduct = ['M+H', 'M+NH4', 17.026547, 0.0, 0.8]

Table A1-5: MSFINDER Settings

Formula finder parameters	
LEWIS and SENIOR CHECK	Yes
Ms1 Tolerance	10
Isotopic Abundance Tolerance	20
Mass tolerance type	ppm
Element Ratio Check	Common Range
Extended Range	FALSE
Extreme Range	FALSE
Element Probability Check	Yes
Element selection	O, N, P, S, F, Cl, Br, I
Structure finder parameters	
TreeDepth	2
MS2 tolerance	20
Relative Abundance Cut Off	5%
Data source	
MINEs (Metabolic In Silico Network Expansions) setting	Never use it
PubChem Online setting	Only use when there is no query in local databases
Local Databases	
HMDB (Human)	
YMDB (Yeast)	
PubChem	
SMPDB (Human)	
UNPD (Natural Product)	
ChEBI (Biomolecules)	
PlantCyc (Plant)	
KNApSAcK (Natural Product)	
BMDB (Bovine)	
FooDB (Food)	
ECMDB (E.coli)	
DrugBank (Drug)	
T3DB (Toxin)	
STOFF (Environment)	
NANPDB (Natural Product)	
LipidMAPS (Lipids)	
Urine (Human)	
Saliva (Human)	
Feces (Human)	
Serum (Human)	
CSF (Human)	
User Defined DB: PubChemLite	

APPENDIX 2 ADDITIONAL EXPERIMENTAL (CHAPTERS 2 AND 3)

Sample Collection

Briefly, samples were collected as twenty-four-hour time-weighted composites at the wastewater treatment plant influent, effluent, and six sub-catchment locations before the treatment plant.

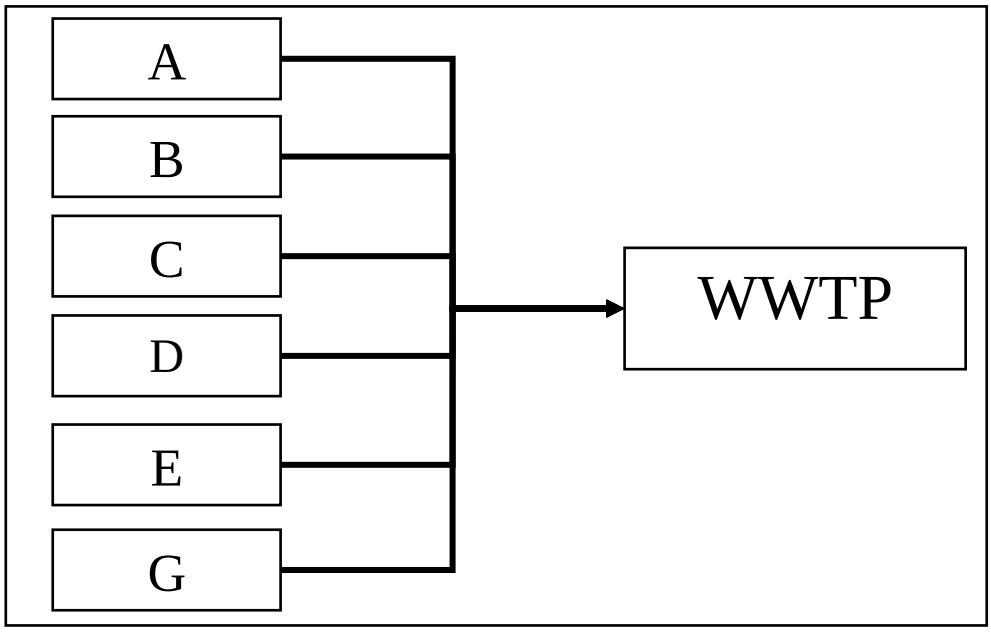

Figure A2-1. Schematic of connections within sewer system. Trunkline sites A, B, C, D, E, G, plus combined influent and treated effluent of the WWTP were sampled monthly.

Sample Preparation

Samples (200 mL of raw wastewater or 1 L of treated effluent) were filtered through a GF/F filter (0.45µm) which was extracted separately. Filtered samples were spiked with of a stable isotope labeled surrogate solution (Table A), and passed over an Oasis HLB cartridge (Waters, Massachusetts, USA), then eluted ethyl acetate followed by methanol, which were collected separately. Jars were rinsed with 3:1 hexane: acetone, which was combined with the ethyl acetate eluate and concentrated to 1 mL. Methanol eluate was also concentrated to 1 mL. Filters were air-dried and then extracted in a sonicating bath with 1:1 hexane/acetone, then concentrated to 1 mL. One LC extract for each sample was created from 0.5 mL of the ethyl acetate, methanol, and

hexane-acetone extracts, then concentrated to 0.2 mL and reconstituted to 1 mL with ultrapure water and spiked with the stable isotope labeled internal standard mix. Additionally, a GC extract was made from 0.5 mL of the ethyl acetate and hexane-acetone extracts, which was concentrated to 0.2 mL dibromooctafluorobiphenyl (DBOFB).

Liquid Chromatography and Mass Spectrometry

Data was acquired using an Agilent 1260 Infinity HPLC coupled to an Agilent 6530 QTOF-MS. Chromatographic separation was achieved with a Zorbax Eclipse Plus C18 column (100 mm, 2.5 mm, 1.8 µm, Agilent Technologies, Inc.) Ultra-pure water plus 0.1% (v/v) formic acid (A), and acetonitrile plus 0.1% (v/v) formic acid (B) were used as mobile phases for positive electrospray ionization. The initial gradient was held at 2% B for 1.5 minutes, followed by a linear increase to 100% B at 16.5 min and held for 4 min. A postrun column equilibrium time of 3 minutes was used resulting in a total run time of 23.5 minutes. Instrumental parameters are included in Table A1-1. For the single batch set (SB), only MS1 data was collected. For the multi-batch set (MB-unC/C), acquisition was done using *All-Ions* fragmentation method.

Gas Chromatography Mass Spectrometry

Extracts prepared for analysis on the GC-QTOF-MS (Agilent 7890B GC coupled to an Agilent QTOF/MS 7200B with a HP-5MS 30 m × 0.25 mm, 0.25 µm column, Agilent Technologies, Inc.) were run once in negative chemical ionization (NCI) mode using methane as collision gas and a second time in electron ionization (EI) mode.

Method Evaluation, Quality Assurance, and Quality Control Measures

Prior to applying this analytical method to the wastewater samples tested here, the performance of the method was evaluated for 22 pesticides in wastewater influent samples analyzed in positive electrospray ionization mode. Recoveries of spiked compounds ranged from

57-120% with an average of 89% recovery, and method detection limits were between 4 and 34 ng/L. Quality assurance and quality control measures applied during the study included preparation and analysis of one method blank sample and one matrix spike duplicate in each monthly batch of 8 samples. Performance of the overall method for nontarget feature extraction was evaluated by assessing the ability to align, recover spectra, and identify compounds in the matrix spike samples. When spiked at 100 ppb into wastewater influent, the alignment and deconvolution algorithms correctly isolated and identified 100% of the spiked compounds in both single and multi-batch data sets for 19/23 compounds, with high detection frequencies for most of the remaining compounds and was over 50% effective for 18/23 compounds spiked at 20 ppb in both data sets (Table A1-3).

Table A2-1: GC-QTOF-MS instrumental parameters

GC-NCI-MS Method	
Injection Volume	2.5 µL
Injection Mode	splitless
Purge Flow to Split Vent	33 mL/min at 0.75 min
Inlet Temperature	280 °C
GC Settings	
Column	HP-5MS (30m x 0.25mm, 025 µm)
Initial Oven Temperature	100 °C, hold 1 min
Ramp 1	15°C/min to 200 °C
Ramp 2	3.8 °C/min to 290 °C
Ramp 3	10 °C/min to 300 °C, hold 4 min
He Flow	1.35 mL/min, constant flow
Transfer Line Temperature	300 °C
MS Settings	
N2 Collision Gas	1.5 ml/min
Reactant Gas (Methane)	40%
Source Temperature	200 °C
Emmission Current Filament	90 µA
Electron Energy	70 eV

Scan Range	35-1000 m/z
Scan Speed	3 spectra/sec
Reference Mass Correction	internal mass correction after every second sample
GC-EI-MS Method	
Injection Volume	2.5 µL
Injection Mode	splitless
Purge Flow to Split Vent	33 mL/min at 0.75 min
Inlet Temperature	280 °C
GC Settings	
Column	HP-5MS (30m x 0.25mm, 025 µm)
Initial Oven Temperature	60 °C, hold 1 min
Ramp 1	40 °C/min to 120 °C
Ramp 2	5 °C/min to 310 °C
Optimized He Flow for RT locking	0.776 mL/min, constant flow
Transfer Line Temperature	280 °C
MS Settings	
N2 Collision Gas	1.5 ml/min
Source Temperature	300 °C
Emmission Current Filament	35 µA
Electron Energy	70 eV
Scan Range	35-1000 m/z
Scan Speed	4 spectra/sec
Reference Mass Correction	internal mass correction after every second sample

APPENDIX 3 SUPPORTING RESULTS CHAPTER 2

Table A3-1: GC Target Compounds Detection in Standards and Spikes

Compounds	Ion Mode	Detection Frequency in 250 ppb Standards (%)	Detection Frequency in 100 ppb Spikes[1] (%)	Detection Code[2]
Non-pyrethroid pesticides				
Chlorothalonil	GC-EI	67	0	C
Chlorpyrifos	GC-EI	100	30	C
Pyriproxyfen	GC-EI	100	90[3]	C
Pyrethroid Insecticides				
Bifenthrin	GC-EI	0	0	N
Bioallethrin	GC-EI	0	0	N
Cyhalothrin	GC-EI	100	20	C
Cypermethrin	GC-EI	67	0	C
Deltamethrin	GC-EI	0	0	N
Esfenvalerate	GC-EI	100	0	C
Etofenprox	GC-EI	0	0	N
Imiprothrin	GC-EI	0	0	N
Permethrin	GC-EI	100	70	C
Phenothrin	GC-EI	100	50	C
Prallethrin	GC-EI	0	0	N
Resmethrin	GC-EI	100	50	C
Tetremethrin	GC-EI	0	0	N

[1]Pyriproxyfen concentration: 600 ppb.
[2]C: Compounds identified correctly. N: Compounds that are not identified.
[3]More than one entry. Summed the numbers detected in all entries. (Total: 3 standards, 10 spikes)

Table A3-2: Suspect-annotated LC compounds and level of identification confidence, if achieved

Compound	**Use Category**	**ID Level of Confidence**	**Detection frequency[1] (n = 56)**
DEET / Diethyltoluamide	Pesticide	1	89%
Valsartan	Pharmaceutical- anti-hypertensive	1	73%
Caffeine	Food	1	68%
Paraxanthine	Metabolite- caffeine		66%
Prasterone enantate	Hormone		66%
Oleamide	Multi- food packaging;	1	61%

	lubricatns		
Ajmaline	Pharmaceutical- anti-arrythmic		59%
Atenolol	Pharmaceutical- beta blocker		59%
Acetaminophen	Pharmaceutical- NSAID	2a	57%
Mycophenolic acid	Pharmaceutical- immunosuppressant	2a	54%
Theobromine	Food- flavoring agent		48%
Tryptophan	Endogenous metabolite		45%
Hydrocortisone (Cortisol)	Pharmaceutical		43%
BTA / Benzotriazole	Cleaning product		41%
8-Hydroxyquinoline	antiseptic		38%
Benzoylecgonine	Metabolite- cocaine		36%
1-(3-Trifluoromethylphenyl)piperazine	Drug		32%
DEP / Diethyl phthalate	Plasticizer	1	32%
Octamylamine	Pharmaceutical- antispasmondic		30%
Gabapentin	Pharmaceutical		29%
Fexofenadine	Pharmaceutical- antihistamine	1	25%
Iohexol	Iodinated Xray Contrast	1	25%
Piperine	Natural product	2a	25%
Phenethylamine	Metabolite		21%
2,6-Xylidine	Metabolite		20%
TBEP / Tris(2-butoxyethyl) phosphate	Flame retardant	1	16%
Octyl methoxycinnamate	Fragrance		14%
Bis(2-ethylhexyl) phthalate (DEHP)	Plasticizer	1	13%
Ivabradine	Pharmaceutical- cardiac therapy		13%
Sulfamethoxazole	Pharmaceutical- antibiotic	1	13%
Metoprolol	Pharmaceutical- beta blocker	1	11%
Trimethoprim	Pharmaceutical- antibiotic	1	9%
Ivermectin B1a	Vet		7%
Diethofencarb	Fungicide		5%
Carbamazepine	Pharmaceutical- anti-seizure	1	4%

O-DT / O-Desmethyltramadol	Metabolite	1	2%
TEP / Triethyl phosphate	Flame retardant		2%

[1] In trunkline, WWTP influent and effluent

Table A3-3: GC suspect-identified compounds and detection frequencies

Compound	**Use Category**	**Mode**	**Detection frequency[1] (n = 56)**	**Groomer (n = 4)**	**Laundry (n = 4)**	**PCO (n = 4)**
Phenol, 2,2'-methylenebis[6-(1,1-dimethylethyl)-4-methyl-	Consumer product antioxidant	EI	39.3%	25%	0%	25%
Indole, 3-methyl-	Endogenous	EI	91.1%	25%	25%	0%
p-Cresol	Endogenous	EI	60.7%	25%	0%	0%
Hippuric acid	Endogenous	EI	44.6%	0%	25%	0%
Allopregnane-3.alpha.,20.alpha.-diol	Endogenous	EI	35.7%	0%	25%	75%
Cholestan-3-ol, (3.beta.,5.beta.)-	Endogenous	EI	30.4%	100%	75%	75%
TCPP	Flame retardant	EI	75.0%	50%	75%	0%
Oxybenzone	Flavoring; Fragrance; Personal care	EI	96.4%	25%	0%	0%
Benzoic acid	Flavoring; Fragrance; Personal care	EI	76.8%	25%	0%	0%
Heptasiloxane, hexadecamethyl-	Flavoring; Fragrance; Personal care	EI	75.0%	50%	100%	50%
Triclosan	Flavoring; Fragrance; Personal care	EI	64.3%	0%	25%	0%
o-Cymene	Flavoring; Fragrance; Personal care	EI	60.7%	0%	0%	0%
Methylparaben	Flavoring; Fragrance; Personal care	EI	50.0%	0%	25%	0%
Dimethyl phthalate	Flavoring; Fragrance; Personal care	EI	44.6%	25%	25%	50%
Methyl tetradecanoate	Flavoring; Fragrance; Personal care	EI	44.6%	100%	100%	50%
Benzene, 1-(1,1-dimethylethyl)-2-methoxy-4-methyl-	Flavoring; Fragrance; Personal care	EI	37.5%	0%	25%	0%

Benzoic acid, 2-hydroxy-, pentyl ester	Flavoring; Fragrance; Personal care	EI	37.5%	25%	0%	0%
Tetrasiloxane, decamethyl-	Flavoring; Fragrance; Personal care	EI	33.9%	25%	0%	25%
Isobutyl paraben	Flavoring; Fragrance; Personal care	EI	32.1%	0%	0%	0%
Ethanol, 2-(4-chlorophenoxy)-	Flavoring; Fragrance; Personal care	EI	30.4%	25%	75%	50%
1H-Indene, 2,3-dihydro-1,1,3-trimethyl-3-phenyl-	Flavoring; Fragrance; Personal care	EI	25.0%	50%	50%	25%
2(3H)-Furanone, 5-heptyldihydro-	Flavoring; Fragrance; Personal care	EI	21.4%	0%	25%	25%
D-Limonene	Food	EI	94.6%	25%	50%	0%
aR-Turmerone	Food	EI	35.7%	100%	75%	50%
Stigmasta-5,24(28)-dien-3-ol, (3.beta.,24Z)-	Food	EI	25.0%	25%	0%	0%
Phenol, 3-methyl-	Human xenobiotic metabolite	EI	96.4%	75%	100%	75%
2-Naphthalenol	Human xenobiotic metabolite	EI	30.4%	0%	50%	0%
1,2-Dichlorobenzene	Industrial	NCI	39.3%	50%	50%	50%
Lilial	Pesticide	EI	55.4%	0%	75%	0%
o-Hydroxybiphenyl	Pesticide	EI	50.0%	0%	0%	0%
Dichlorvos	Pesticide	NCI	48.2%	100%	100%	75%
Parathion-methyl	Pesticide	NCI	21.4%	25%	0%	25%
Etiracetam	Pharmaceutical	EI	82.1%	75%	100%	25%
Iminostilbene	Pharmaceutical	EI	76.8%	25%	25%	0%
Ibuprofen	Pharmaceutical	EI	51.8%	100%	100%	75%
Gabapentin	Pharmaceutical	EI	41.1%	0%	0%	0%
Guaifenesin	Pharmaceutical	EI	28.6%	0%	0%	0%
Stigmastanol	Pharmaceutical	EI	26.8%	0%	0%	0%
9,12,15-Octadecatrienol	Plastics	EI	69.6%	50%	50%	25%

[1] Trunkline, influent, & effluent

Targeted MS/MS structure results

Acetaminophen

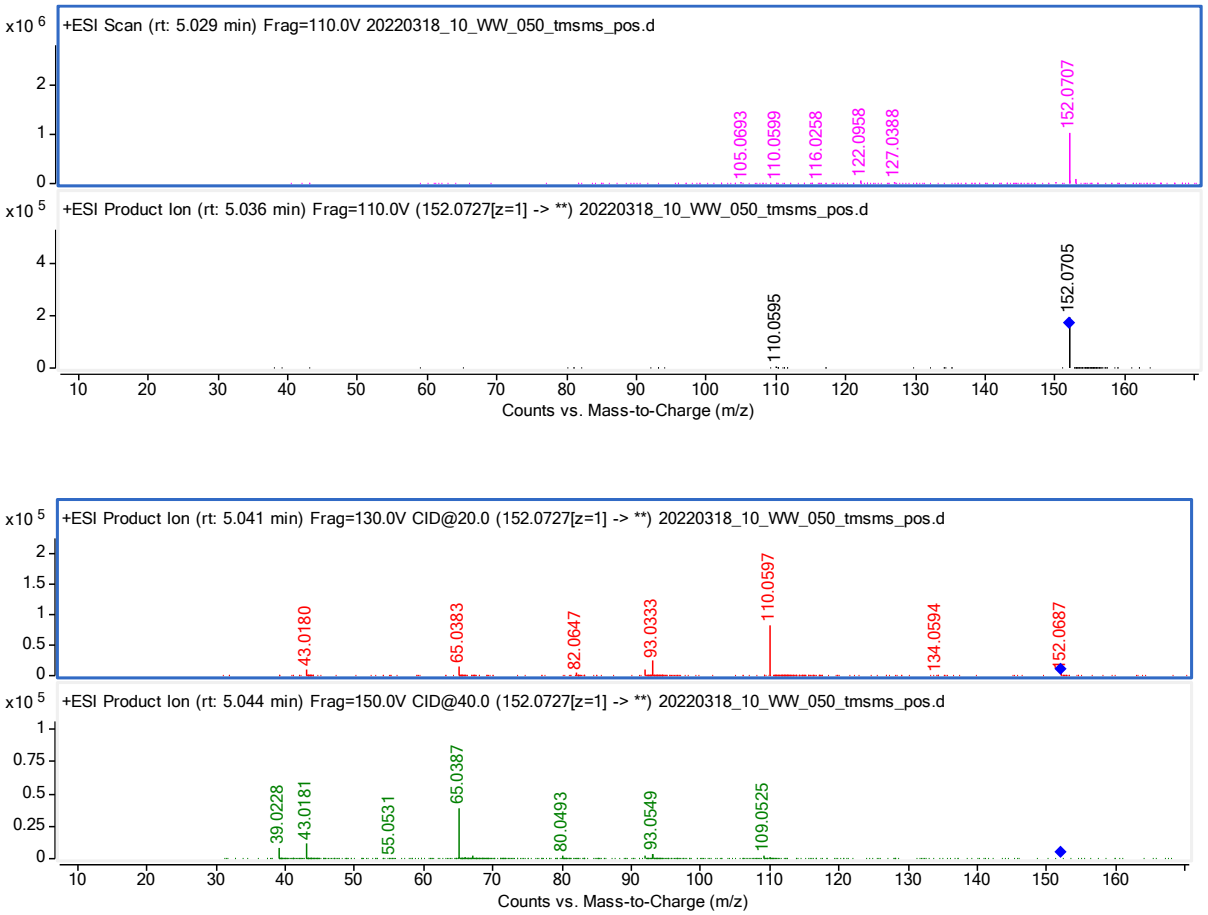

Figure A3-1. tMS/MS at collision energies of 0, 10, 20, and 40 eV for the feature identified at 2a confidence level as acetaminophen.

Table A3-4: Acetaminophen: library fragments and average mass error

Library Fragment m/z*	Average mass error (ppm)
152.0716	-6.58
110.0622	-23.62
65.0389	-6.15

*from MassBank Europe: https://massbank.eu/MassBank/Result.jsp?inchikey=RZVAJINKPMORJF-UHFFFAOYSA-N

Mycophenolic acid

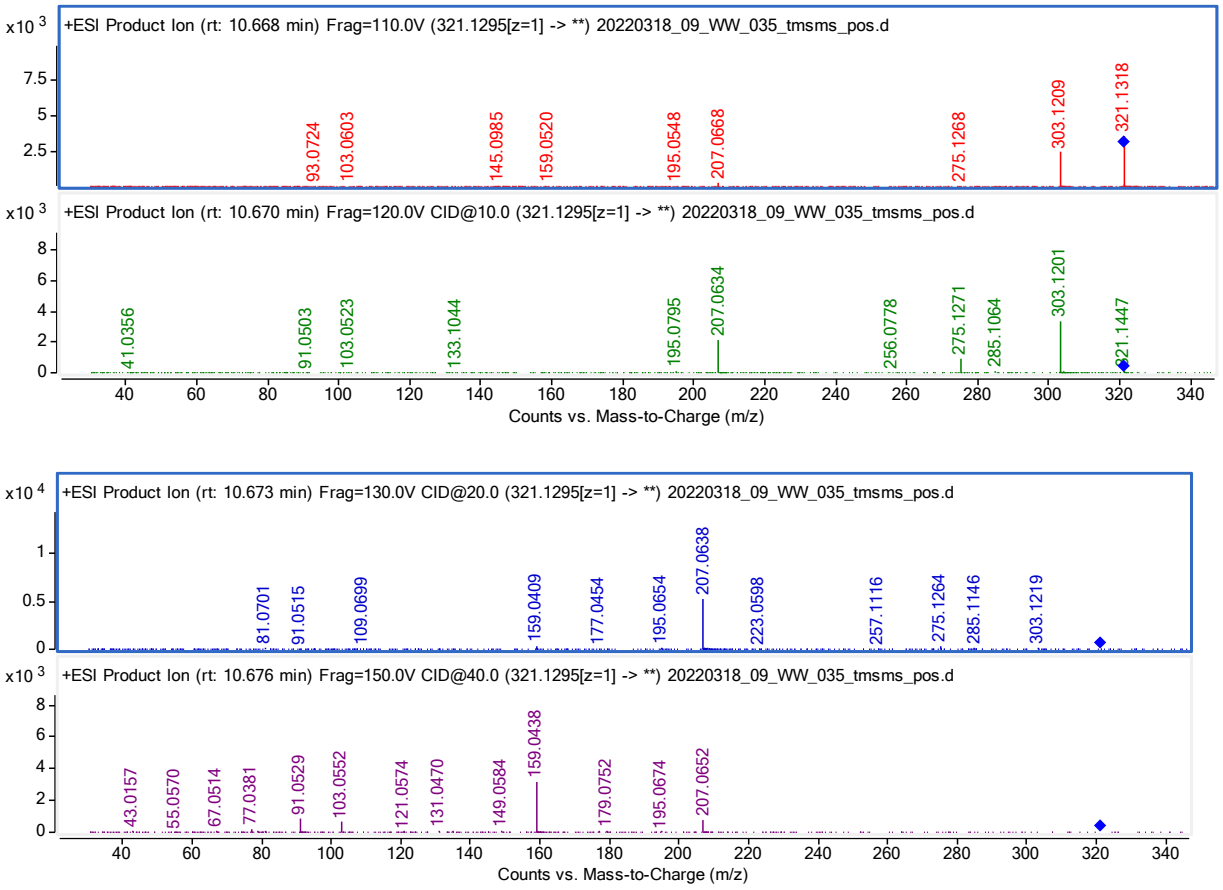

Figure A3-2. tMS/MS at collision energies of 0, 10, 20, and 40 eV for the feature identified at 2a confidence level as mycophenolic acid.

Table A3-5: Mycophenolic acid: library fragments and average mass error

Library Fragment m/z*	Average mass error (ppm)
321.1299	6.066082
303.1225	-6.48913
207.0644	-3.97461
159.0397	16.9266

*Library spectrum from Human Metabolome Database: https://hmdb.ca/metabolites/HMDB0015159#spectra

Piperine

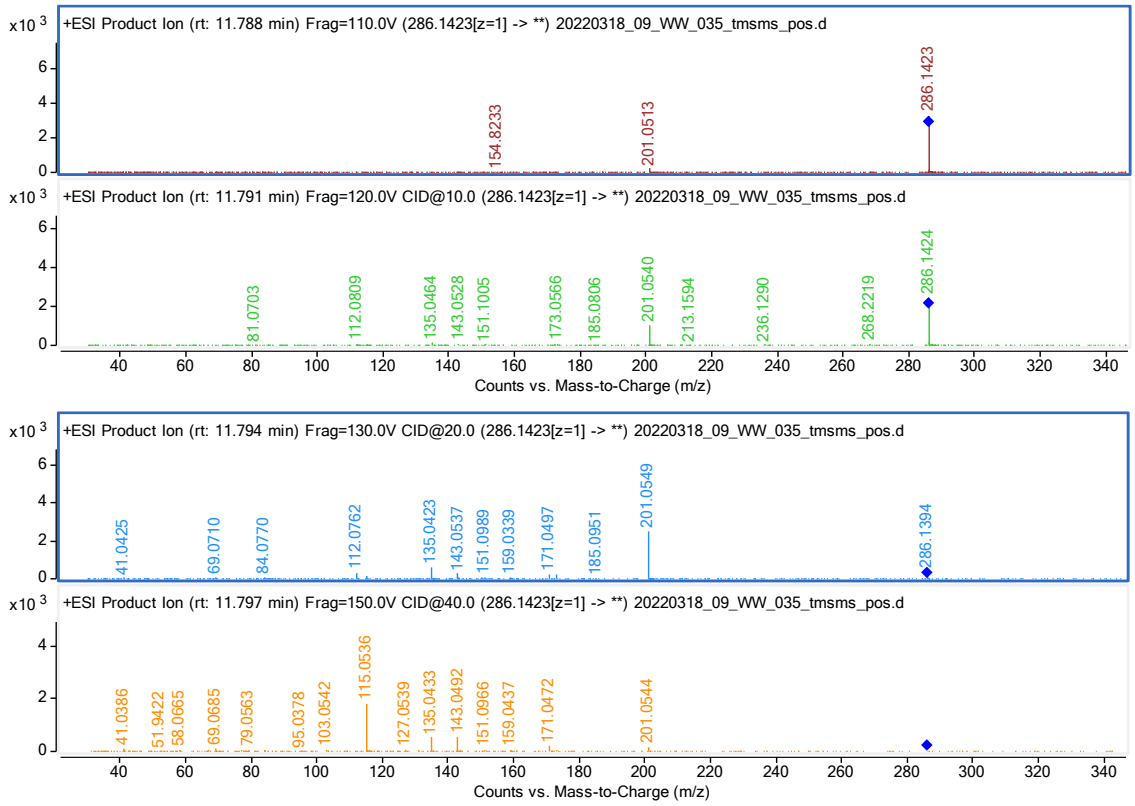

Figure A3-3. tMS/MS at collision energies of 0, 10, 20, and 40 eV for the feature identified at 2a confidence level as piperine.

Table A3-6: Piperine: library fragments and average mass error

Library Fragment m/z*	Average mass error (ppm)
286.1437	-4.71791
201.054	2.238205
135.0431	-2.22151

*Library spectrum from MassBank Europe: https://massbank.eu/MassBank/Result.jsp?inchikey=MXXWOMGUGJBKIW-YPCIICBESA-N

APPENDIX 4 SUPPORTING INFORMATION FOR CHAPTER 3

Table A4-1: MS-DIAL alignment parameters for SB and MB datasets

	SB	**MB-C; MB-UnC**
Project		
MS1 Data type	Profile	Profile
MS2 Data type	Centroid	Profile
Ion mode	Positive	Positive
Target	Metabolomics	Metabolomics
Mode	ddMSMS	diMSMS
Data collection parameters		
Retention time begin	4	0
Retention time end	100	100
Mass range begin	0	0
Mass range end	2000	5000
MS2 mass range begin	0	0
MS2 mass range end	2000	0
Centroid parameters		
MS1 tolerance	0.01	0.01
MS2 tolerance	0.025	0.025
Isotope recognition		
Maximum charged number	2	2
Data processing		
Number of threads	5	5
Peak detection parameters		
Smoothing method	LinearWeightedMovingAverage	LinearWeightedMovingAverage
Smoothing level	3	3
Minimum peak width	5	5
Minimum peak height	3000	3000
Peak spotting parameters		
Mass slice width	0.1	0.1
Exclusion mass list (mass & tolerance)		
Deconvolution parameters		
Sigma window value	0.5	0.5
MS2Dec amplitude cut off	0	0
Exclude after precursor	TRUE	TRUE
Keep isotope until	0.5	0.5
Keep original	FALSE	FALSE

precursor isotopes		
MSP file and MS/MS identification setting		
MSP file	MergedPCDL_AllSpectra_Positive.msp	MergedPCDL_AllSpectra_Positive.msp
Retention time tolerance	100	100
Accurate mass tolerance (MS1)	0.01	0.01
Accurate mass tolerance (MS2)	0.05	0.05
Identification score cut off	80	80
Using retention time for scoring	FALSE	TRUE
Using retention time for filtering	FALSE	FALSE
Text file and post identification (retention time and accurate mass based) setting		
Text file		
Retention time tolerance	0.1	0.1
Accurate mass tolerance	0.01	0.01
Identification score cut off	85	85
Advanced setting for identification		
Relative abundance cut off	0	0
Top candidate report	FALSE	TRUE
Adduct ion setting		
[M+H]+		
[M+NH4]+		
[M+Na]+		
Alignment parameters setting		
Reference file	170717_QC1.abf	160522_10_pos_Pest-STD-100.abf
Retention time tolerance	0.05	0.05
MS1 tolerance	0.015	0.015
Retention time factor	0.5	0.5
MS1 factor	0.5	0.5
Peak count filter	0	0
N% detected in at least one group	0	0

Remove feature based on peak height fold-change	FALSE	FALSE
Sample max / blank average	5	5
Sample average / blank average	5	5
Keep identified and annotated metabolites	TRUE	TRUE
Keep removable features and assign the tag for checking	TRUE	TRUE
Gap filling by compulsion	FALSE	TRUE
Tracking of isotope labels		
Tracking of isotopic labels	FALSE	FALSE
Ion mobility		
Ion mobility data	FALSE	FALSE

Table A4-2: Target compound detection in standards and spiked wastewater after MS-DIAL alignment

Compound	Detection Frequency in 100 ppb Standards[1] (%)		Detection Frequency in 20 ppb Spikes[2] (%)		Detection Code[3]	
	MB (n = 4)	SB (n = 7)	MB (n = 10)	SB (n = 12)	MB	SB
Azoxystrobin	100	100	90	100	C	C
Boscalid	100	100	90	100	U	C
Chlorantraniliprole	100	0	80	0	C	
Clomazone	100	100	90	92	C	I
Cyprodinil	100[4]	100	100[4]	100	U	C
DEET	100	100	90	100	C	I
Difenoconazole	100	100	90	100	C	C
Dimethoate	100	100	90	58	U	C
Diuron	100	86	90	50	U	C
Hexazinone	100	100	90	92	C	C
Imidacloprid	100	100	90	83	U	C
Methomyl	100	0	60	8	U	C
Methoxyfenozide	75	100	60	25	U	C
Metolachlor	100	100	90	100	C	C
Pendimethalin	100	100	40	33	U	C
Propanil	100	100	90	75	C	C
Propoxur	100	100	80	67	C	C
Pyriproxyfen	100	100	80	100	C	C
Simazine	100	100	90	67	C	I
Thiacloprid	100	100	90	92	U	C

Thiamethoxam	100	100	80	83	U	C
Thiobencarb	100	100	70	58	I	C
Triclocarban	100	100	40	67	U	C

[1] Triclosan concentration: 10 ppb.
[2] Fipronil concentration: 4 ppb. Pyriproxyfen concentration: 24 ppb. Triclosan concentration: 2 ppb.
[3] C: Compounds Identified correctly; I: Compounds identified as isomers; U: Compounds identified as Unknown but the correct compounds are in the top five hits under Compound Search.

Table A4-3: Results of feature filtering rules

Filter	Features in SB	Features in MB-unC/C
No filter	63,259	136,938
S/N Ratio	58,007	92,056
Blank	52,399	88,871
Retention time	51,934	85,697
Adduct joining	43,139	82,171
Detections in WW samples[a]	31,989	70,637
Split feature joining	29,772	66,790
Detection frequency at 60% cut-off	3,108	25,822

[a] Many samples were included in the alignment for the purpose of alignment quality control, such as blanks, standards, and spiked wastewater. As a result, some features were present only in these samples and not in the 56-sample subset that was ultimately considered.

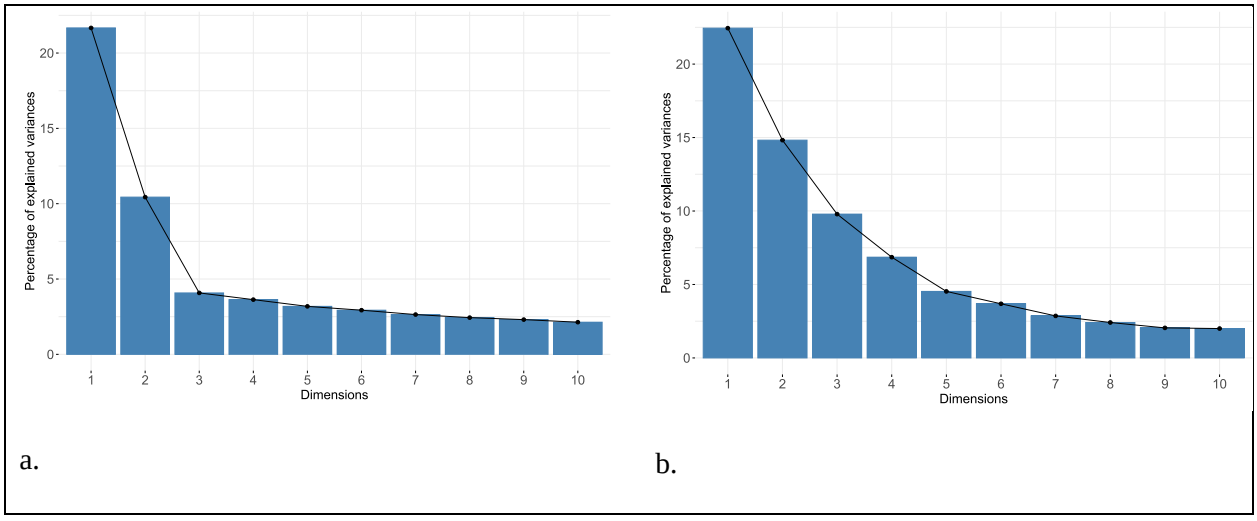

a. b.

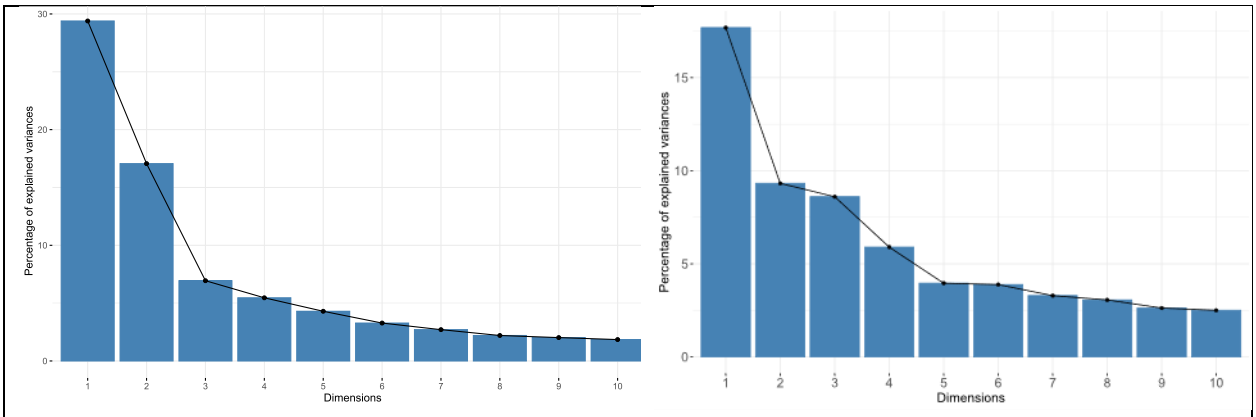

c. d.

Figure A4-1. PCA scree plots for a) single batch (SB), b) uncorrected multi-batch (MB-unC), c) median-ISTD scaled peak height (MB-IS), and d) ComBat-corrected multi-batch (MB-C) show good representation by first three principal components, although suggest that PC's 4 and 5 might be worth investigating as well.

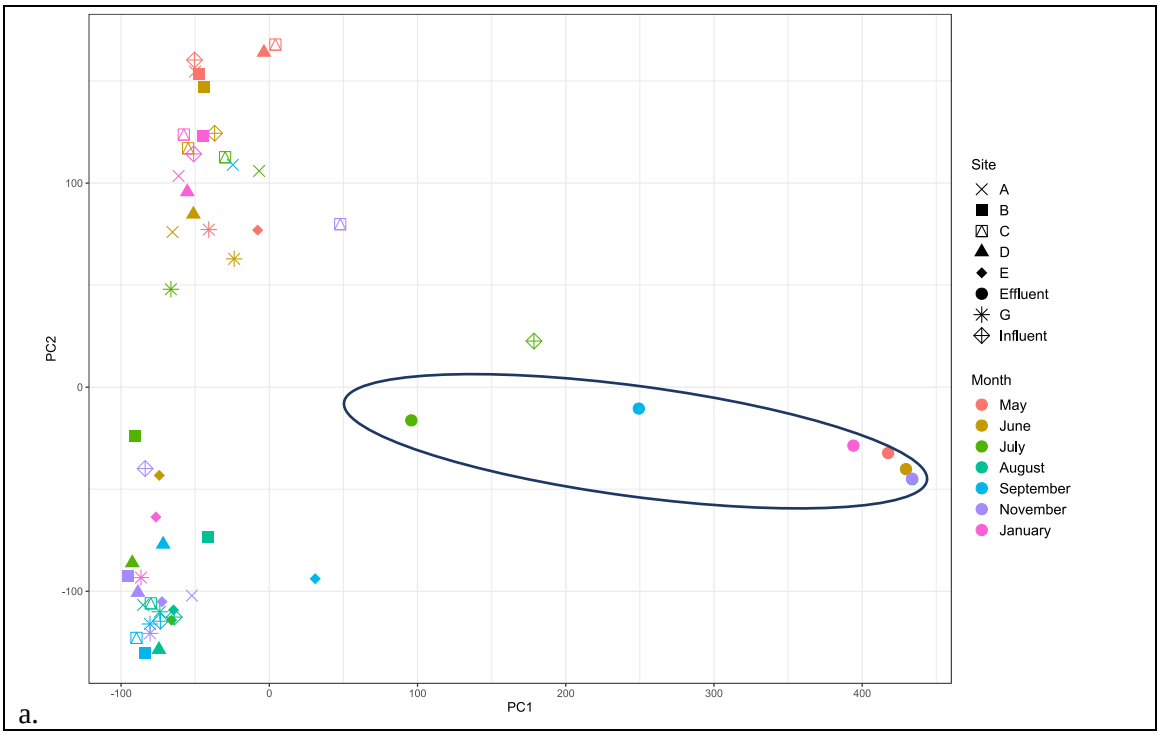

a.

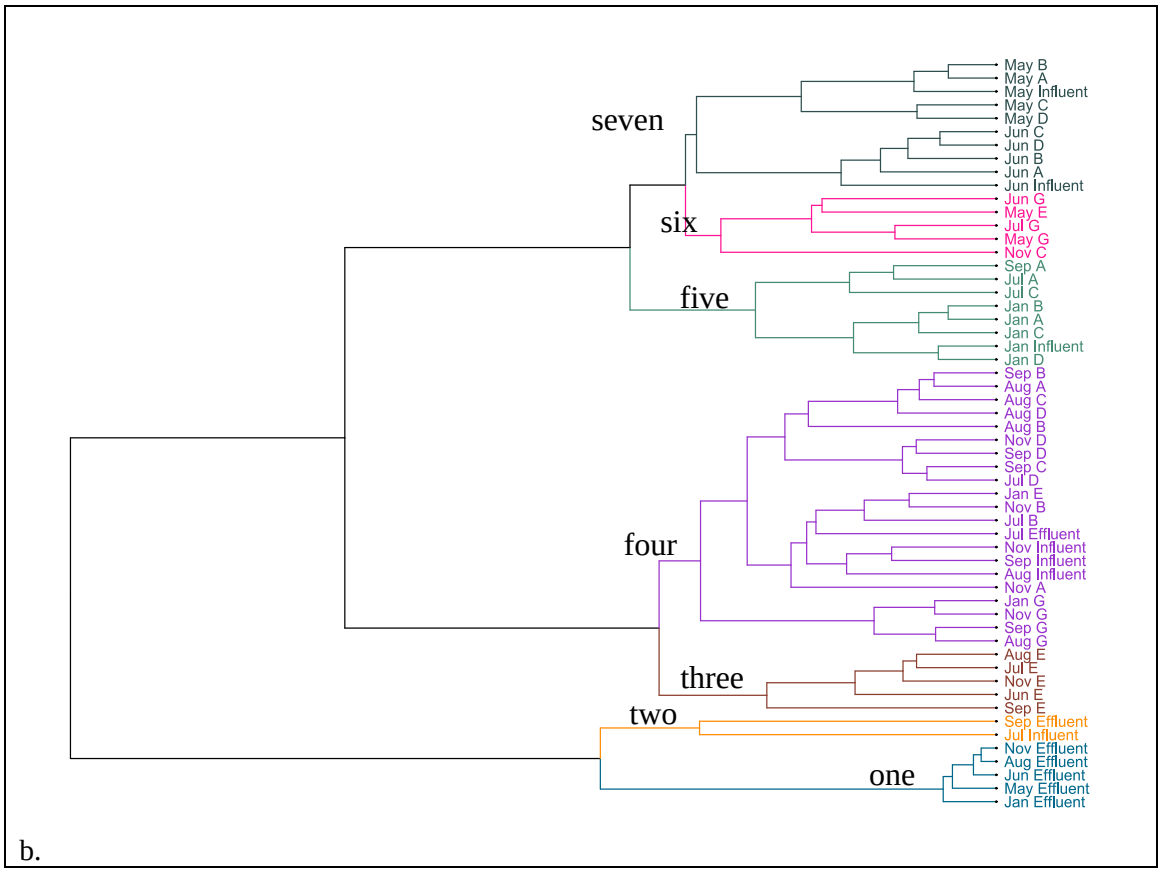

Figure A4-2. For SB, a) PCA showed little separation based off sampling month though effluent samples did form their own cluster in PC1 (denoted by oval) from raw WW samples, and b) HCA also shows that effluent samples are very different from influent and trunkline samples.

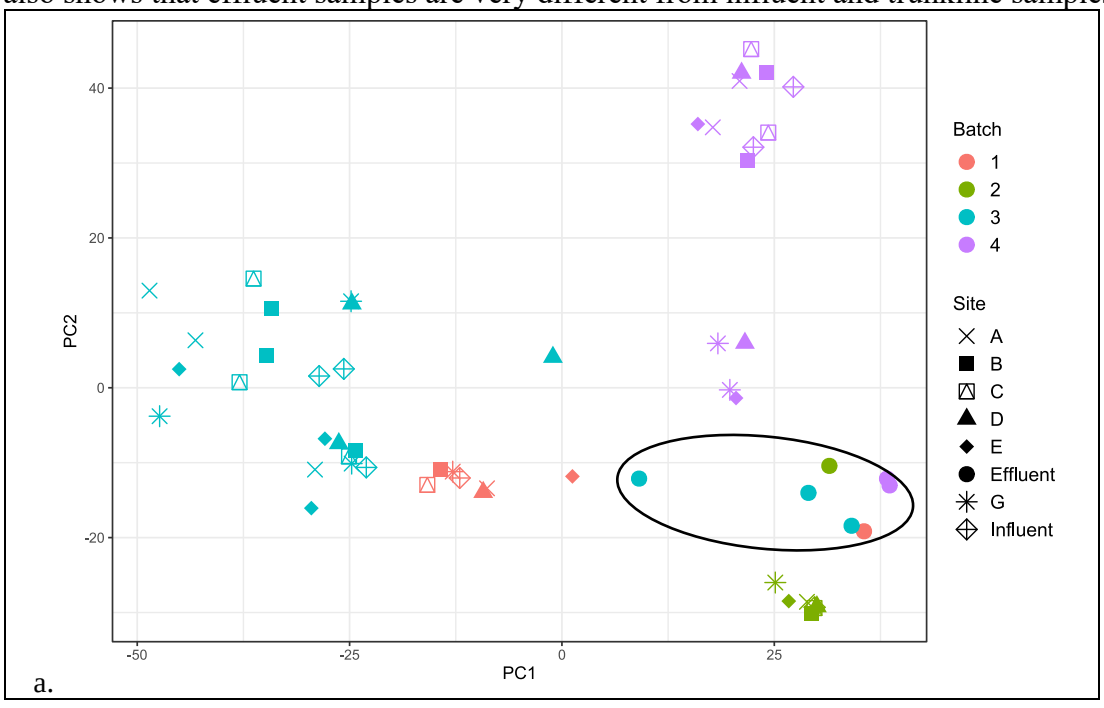

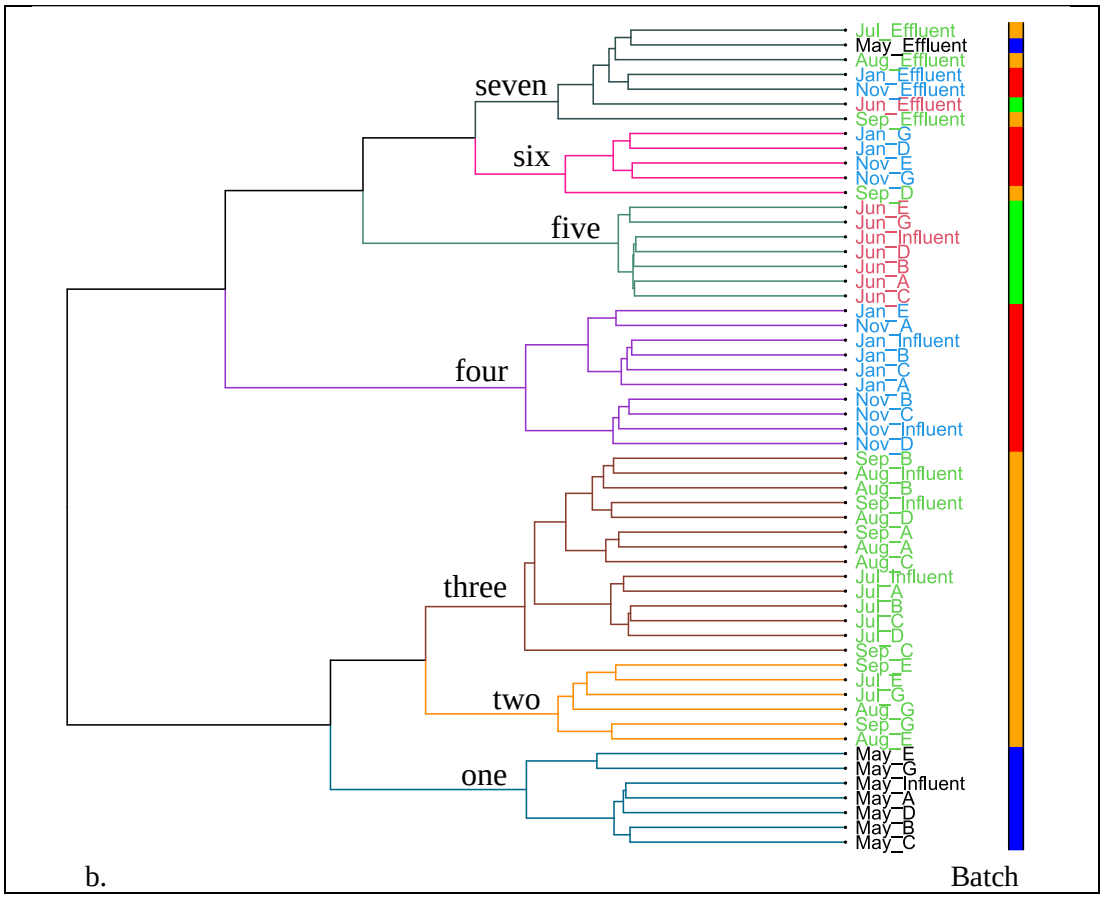

Figure A4-3. For MB-IS, a) PCA showed the grouping of effluent samples (circled), which were not entirely distinct in either PC1 or PC2, while raw-WW sample groupings by batch are conserved, and b) HCA shows almost exclusive clustering by batch (denoted by colored bar to right), except for treated effluent samples and cluster six.

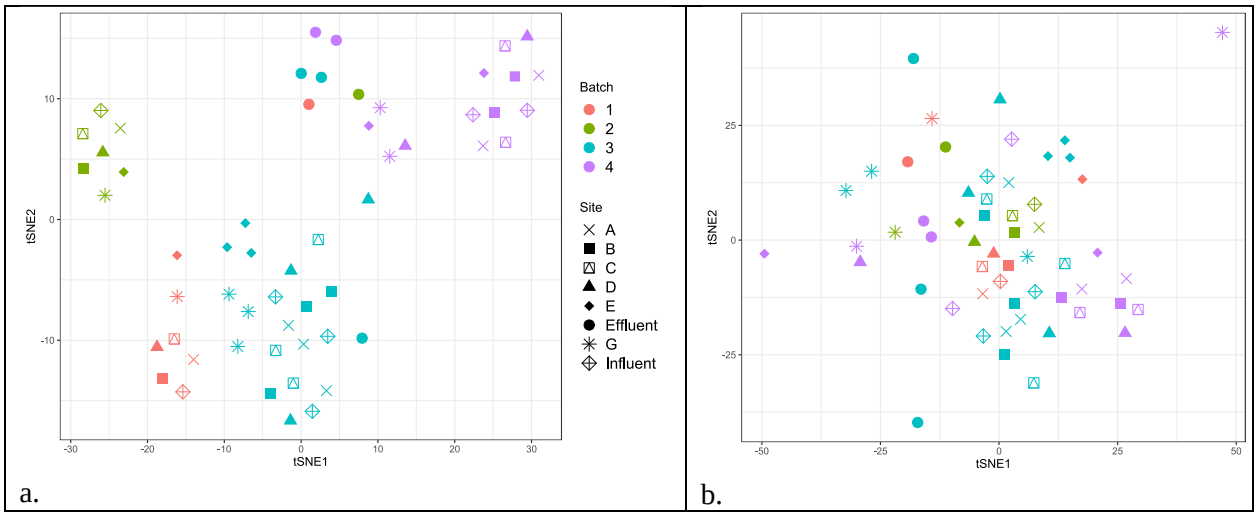

Figure A4-4. t-SNE plots (perplexity = 18) for a) MB-unC and b) MB-C show the organization of samples that becomes scrambled after the application of the ComBat correction method.

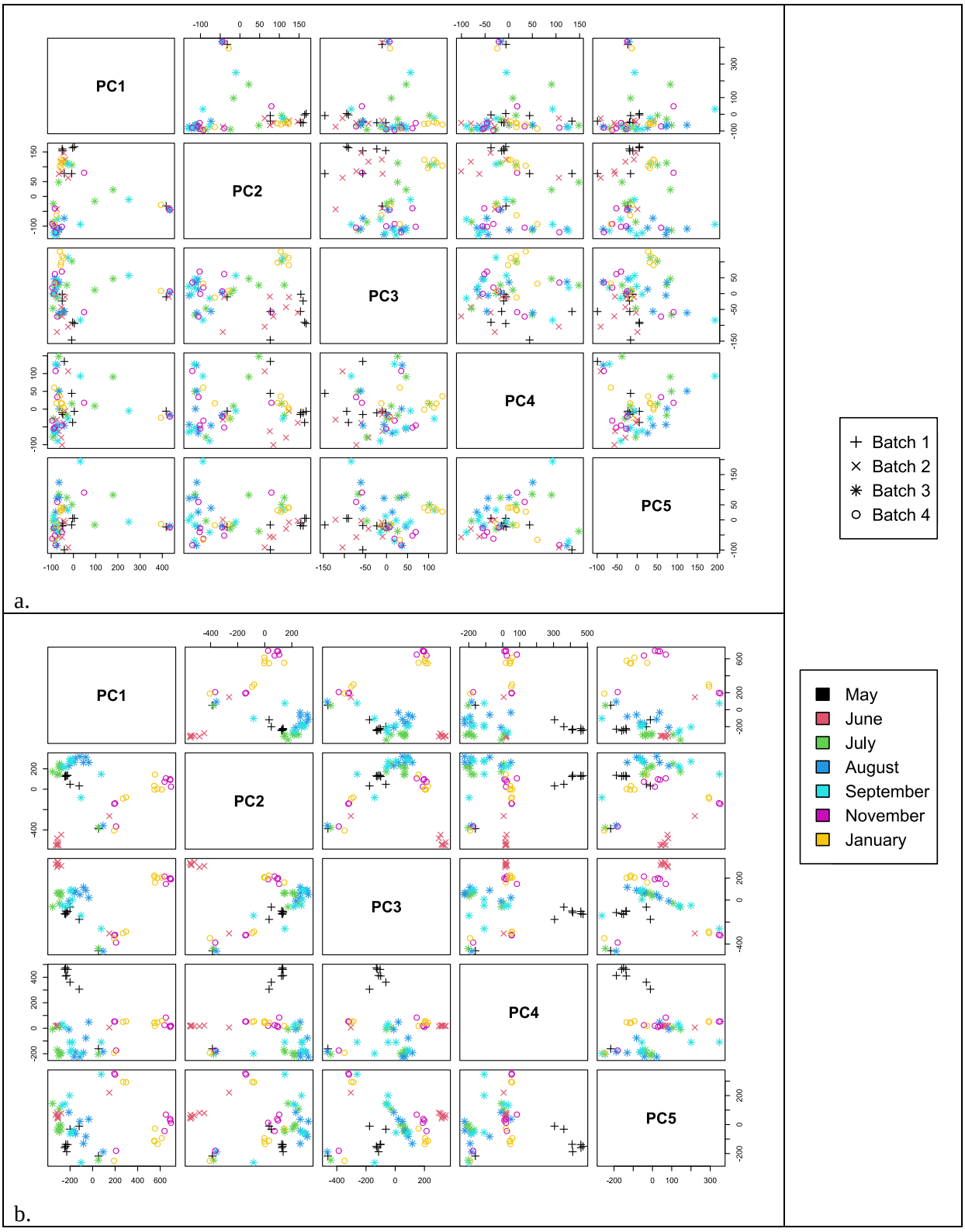
PC1
PC2
PC3
PC4
PC5
Batch 1
Batch 2
Batch 3
Batch 4
May
June
July
August
September
November
January

a.

b.

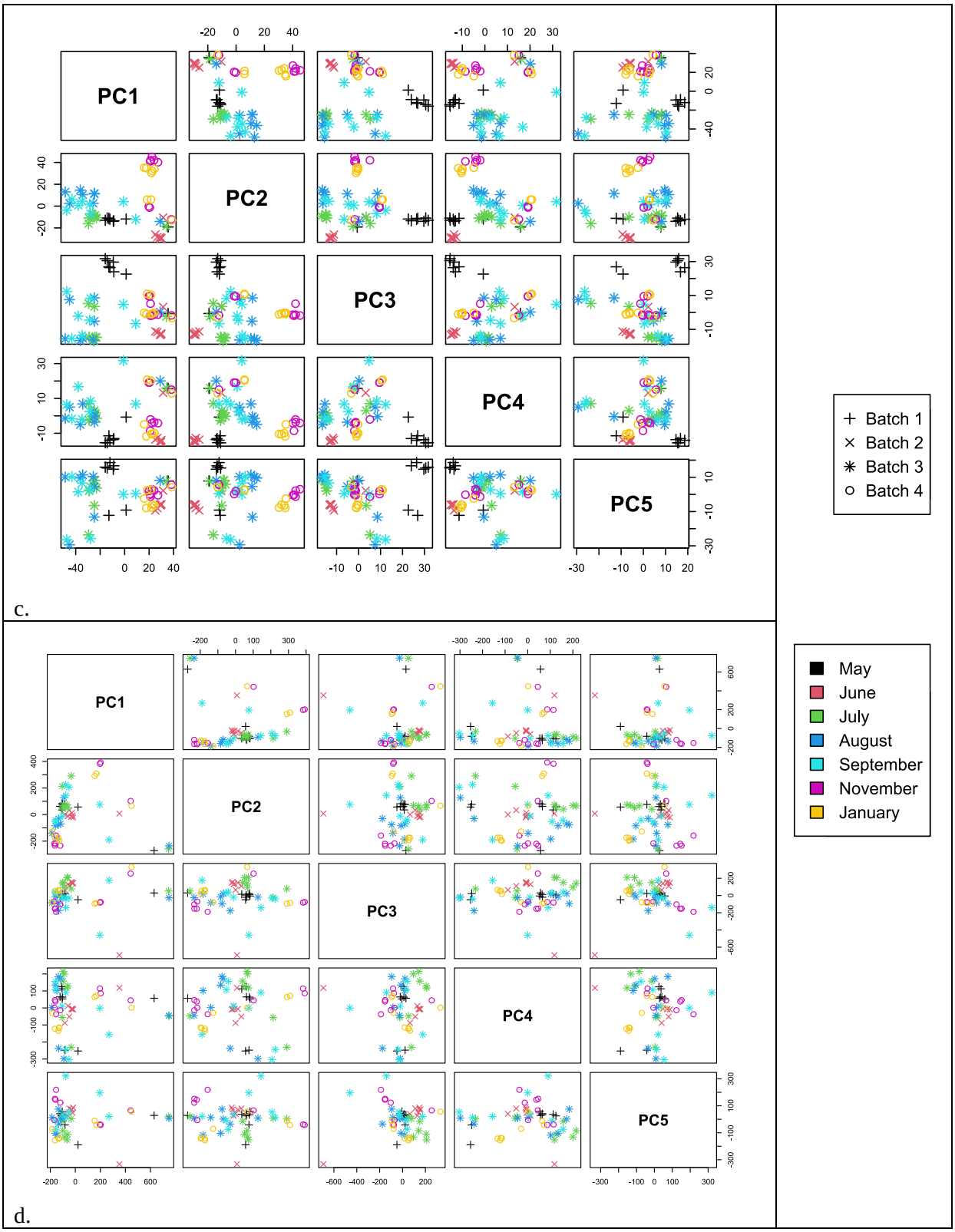

Figure A4-5. Matrix pair plots for principal components 1-5 for a) SB, b) MB-unC, c) MB-IS, and d) MB-C.

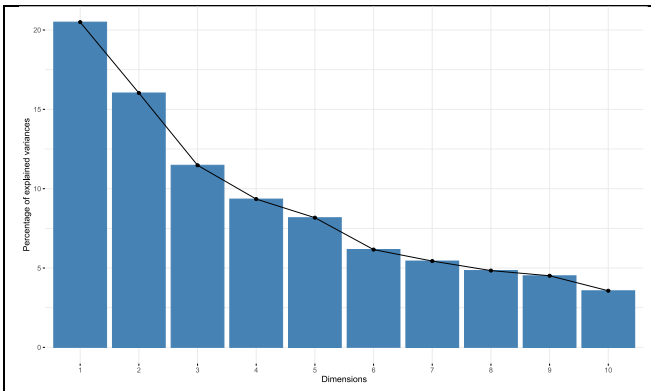

a.

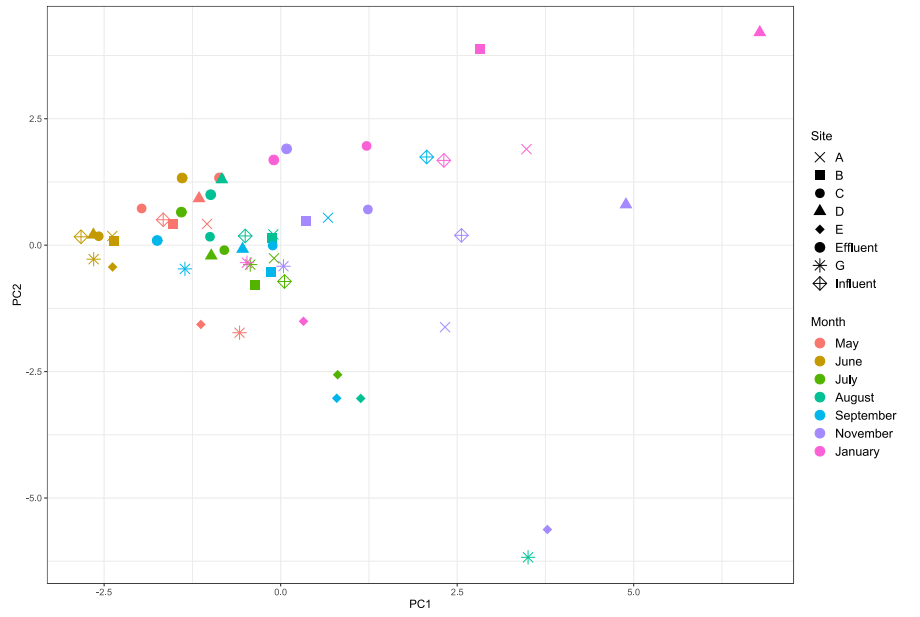

b.

Figure A4-6. Using only quantified target pesticides, a) showed approximately a similar explanation of variance as using nontarget features, b) plotting the first two PC's of wastewater samples primarily showed the separation of November and January samples from the rest, c) little separation in PC's 4 and 5.

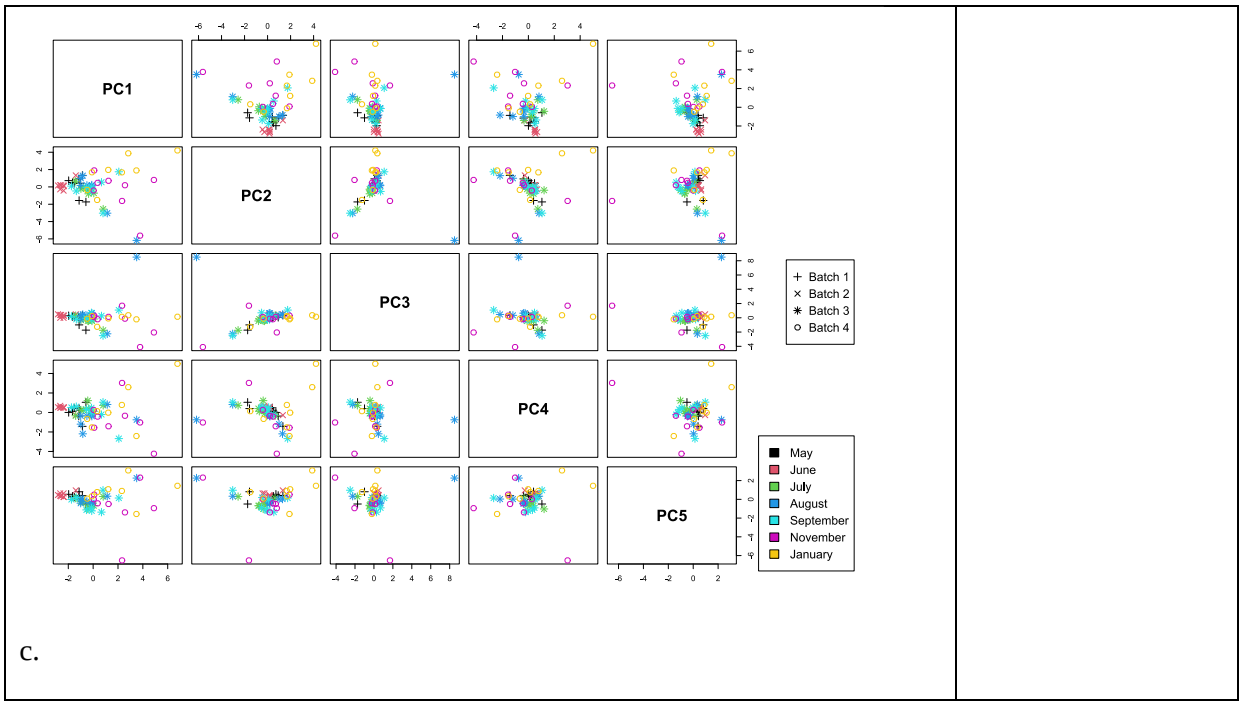

C.

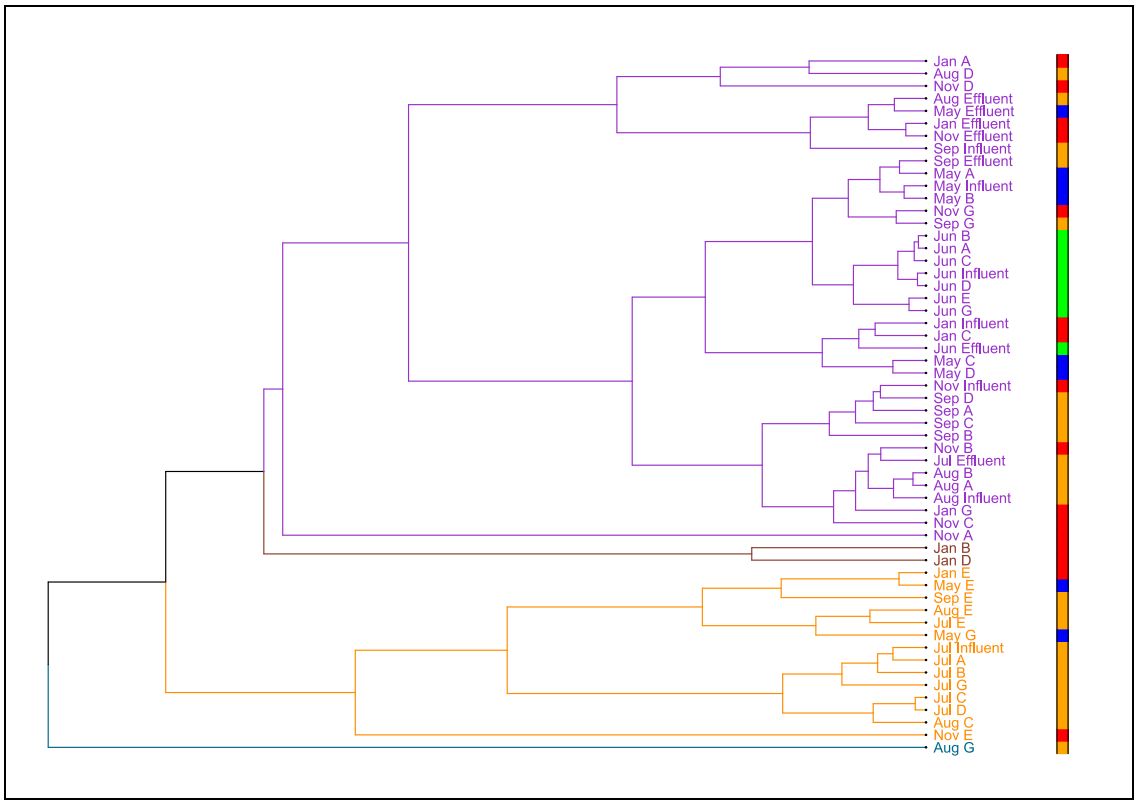

Figure A4-7. Conducting HCA with the first 5 principal components indicates (from left to right) one large cluster including trunkline, influent and effluent; a cluster containing a single August trunkline sample (the only detection of chlorothalonil); a cluster of six January and four November samples; and a cluster of four EPA 5-1 plus two other trunkline samples.

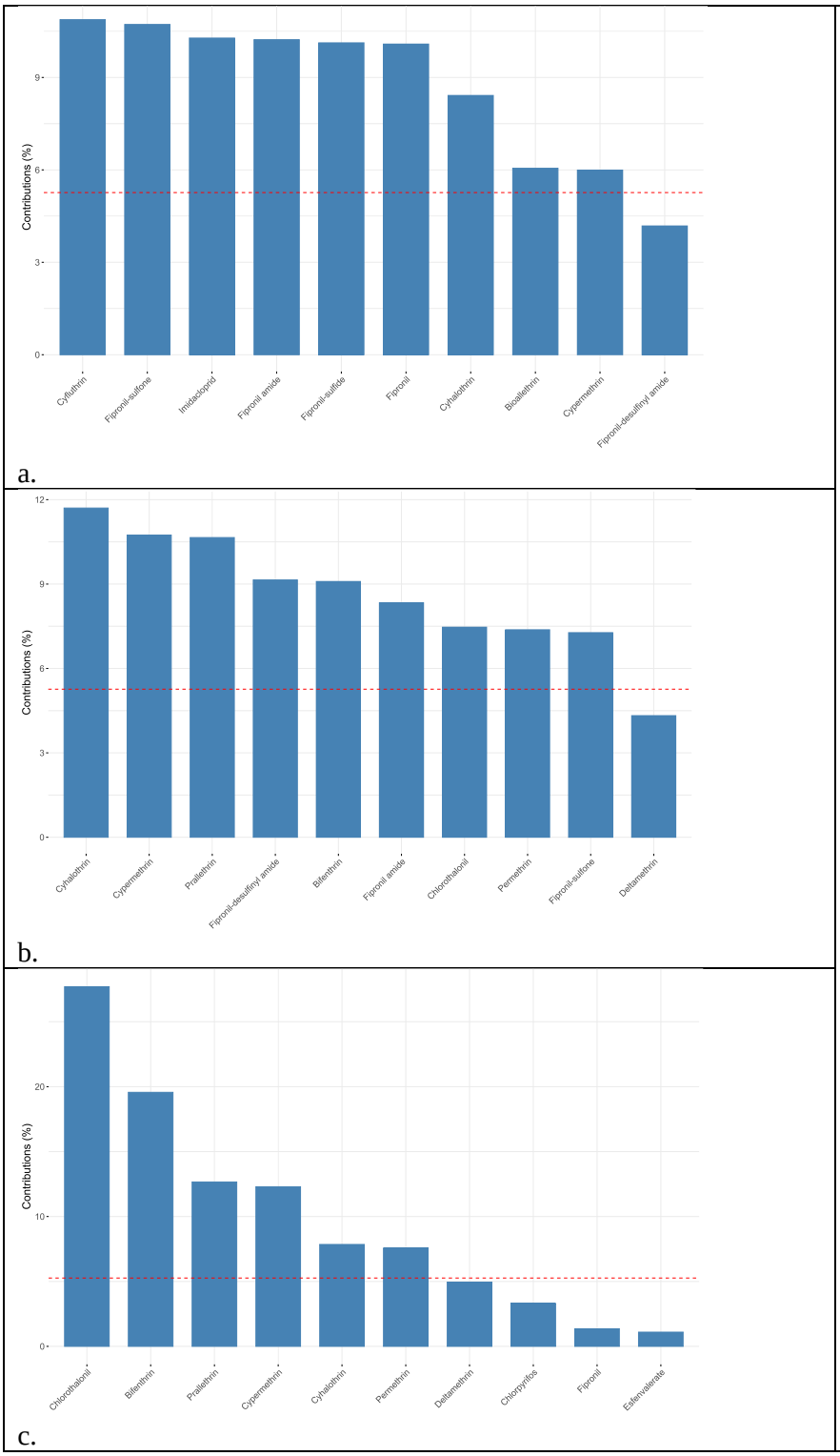

Figure A4-8. Top-ten highest variable contributions to principal components for PCA of wastewater set using only target-quantified pesticides in a) the first dimension, b) second dimension, and c) third dimension. The red line denotes the predicted value if variable contribution were uniform (Kassambra & Mundt, 2020).

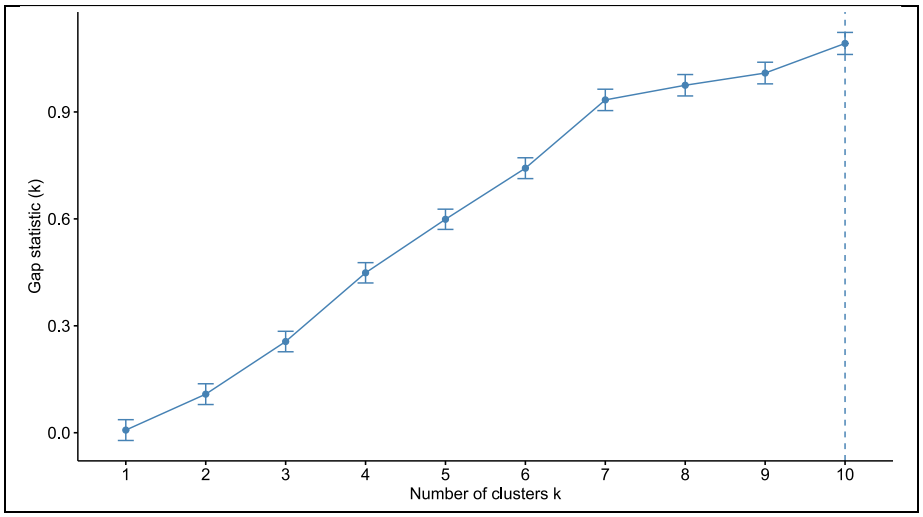

Figure A4-9. Gap-statistic plot for MB-unC to determine optimal number of clusters at about 10 clusters

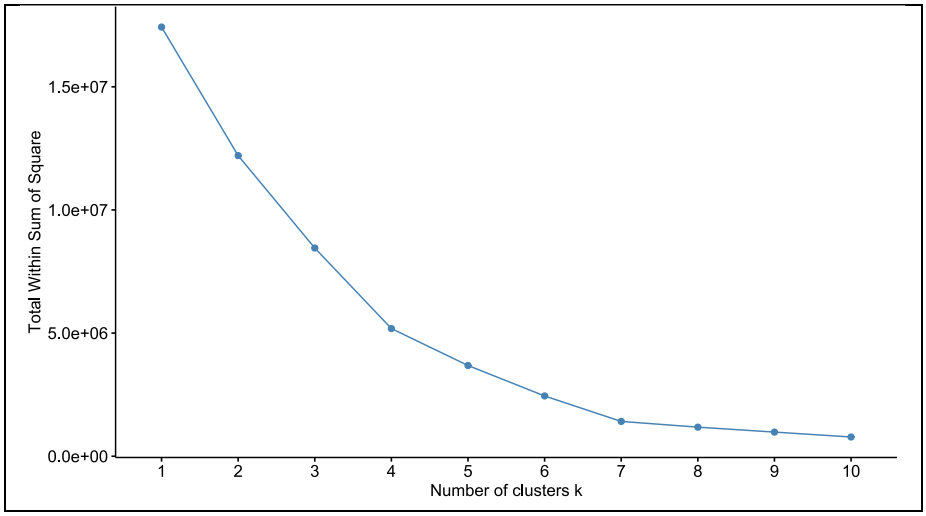

Figure A4-10. Total within cluster sum of squares for MB-unC to determine optimal number of clusters, about 7 or 8.

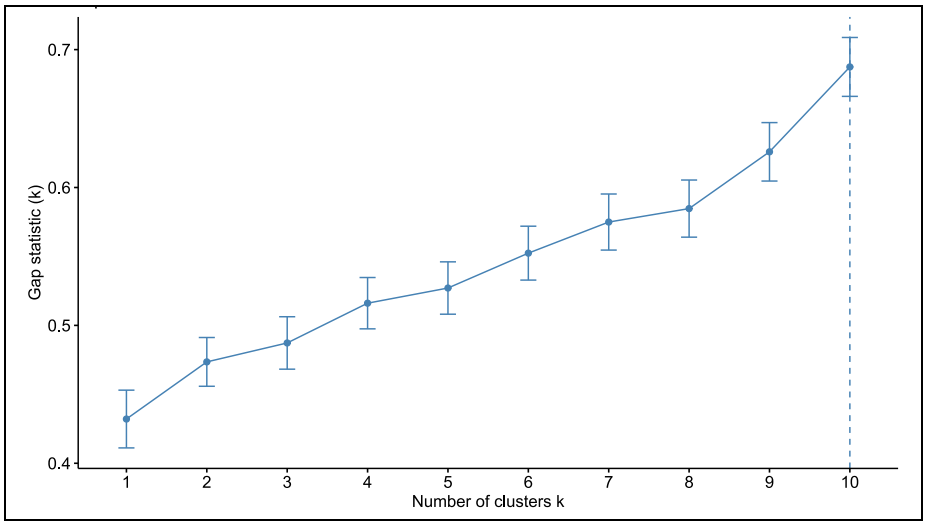

Figure A4-11. Gap-statistic plot for MB-C to determine optimal number of clusters at about 10 clusters

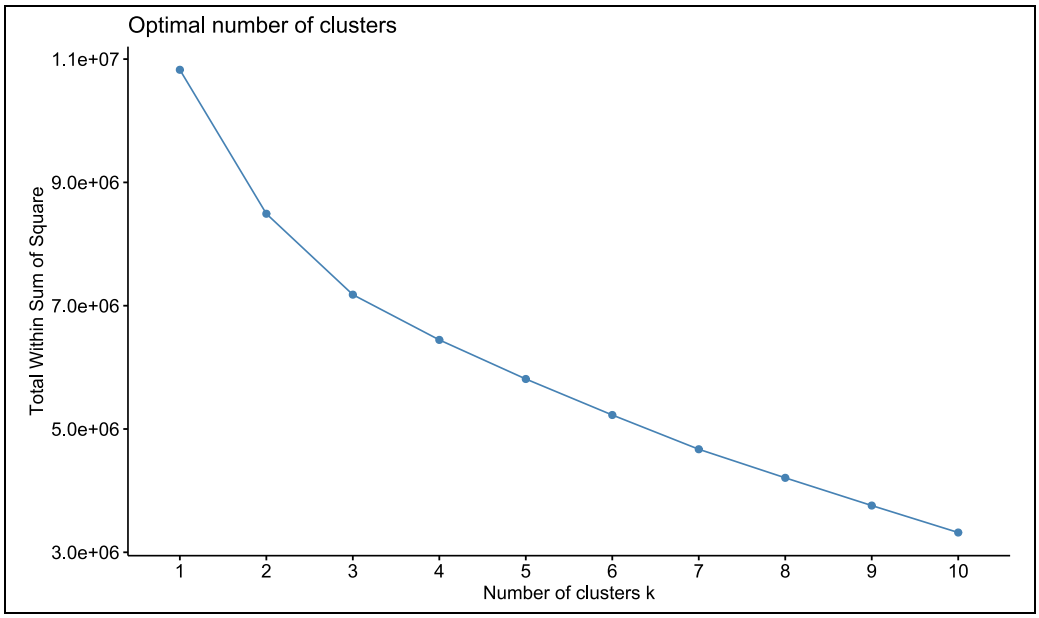

Figure A4-12. Total within cluster sum of squares for MB-C to determine optimal number of clusters at about 10 clusters

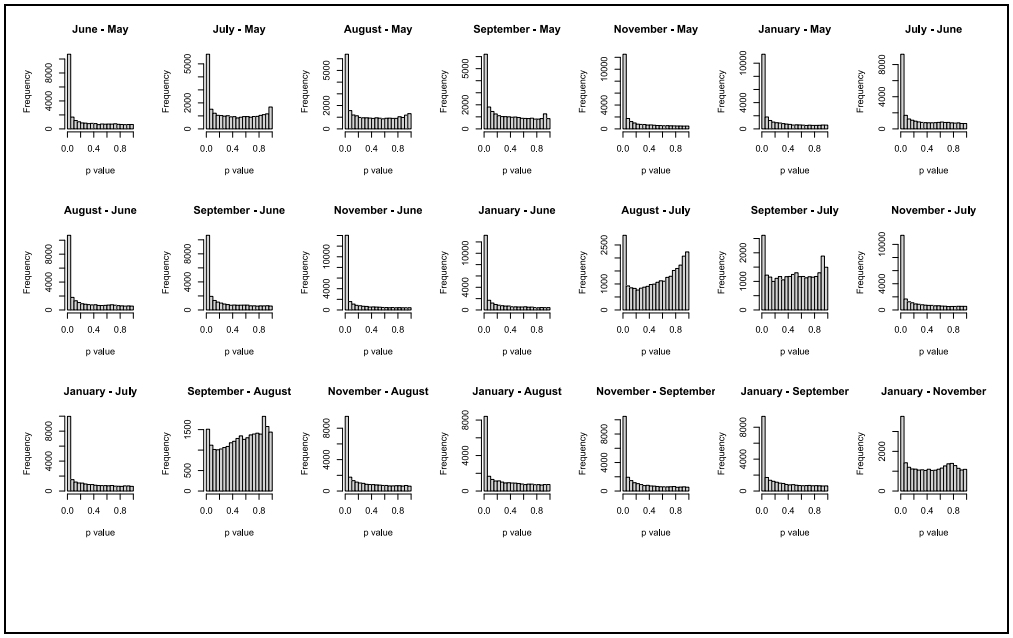

Figure A4-13. Histograms of p-values from contrasts by months of MB-unC shows many features are significantly different between months

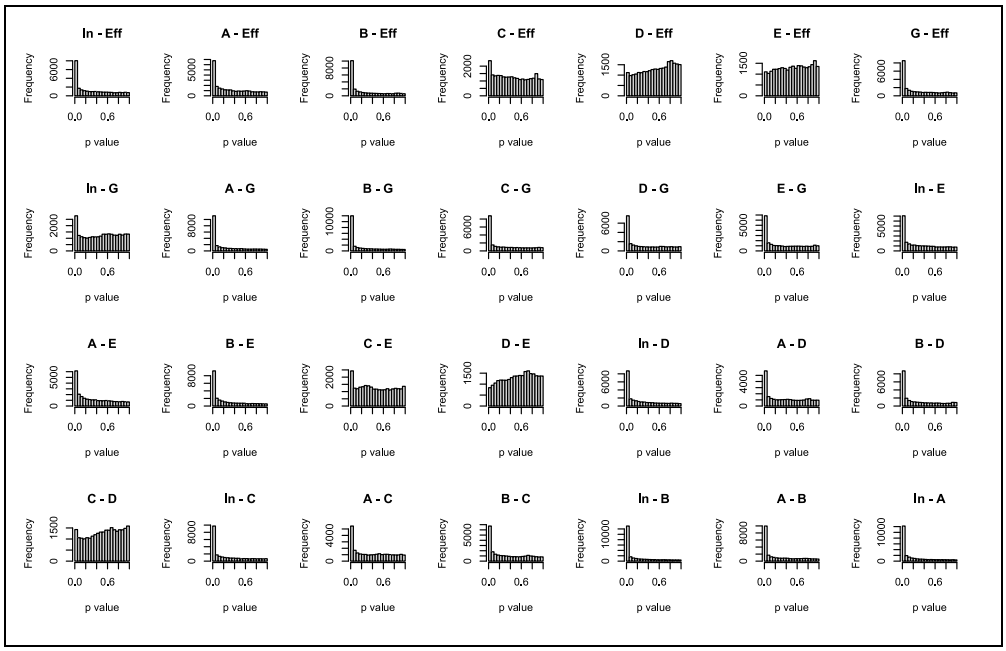

Figure A4-14. Histograms of p-values from contrasts by sampling site of MB-unC shows significant differences between sampling sites, but also that samples such as C, D, and E are more like effluent, and C – D and D – E are similar.

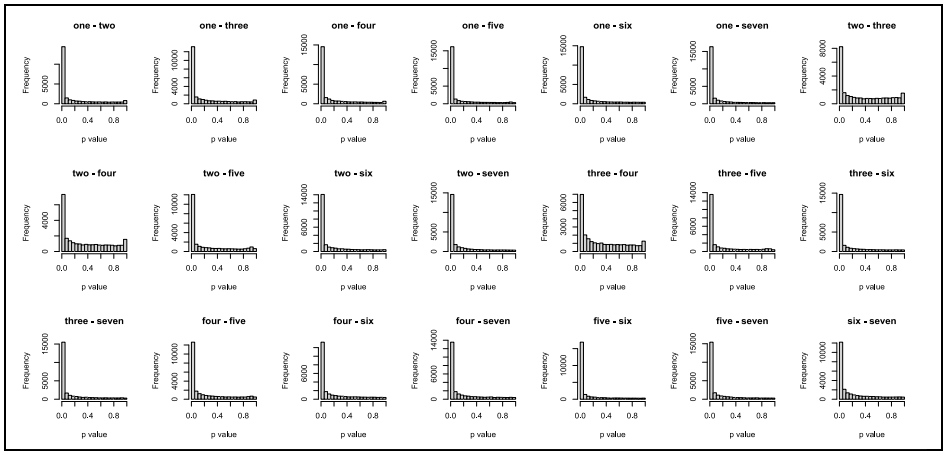

Figure A4-15. Histograms of p-values from contrasts by HCA cluster shows high numbers of significantly different features for MB-unC.

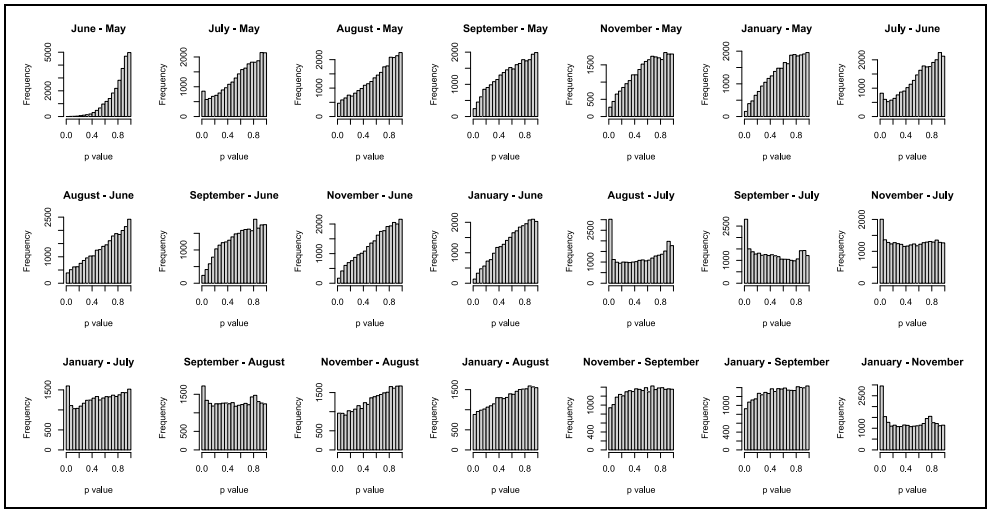

Figure A4-16. Histograms of p-values from contrasts by month of MB-C shows only a few months with a large number of significantly different features, unlike for MB-unC (Figure S7).

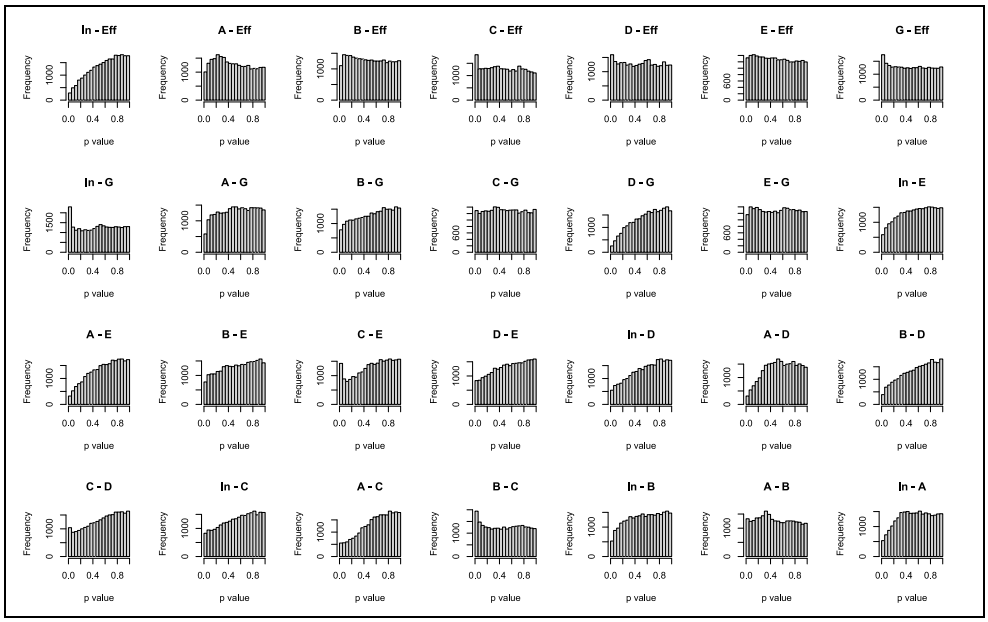

Figure A4-17. Histograms of p-values from contrasts by site for MB-C shows very few significantly different features, dissimilar from MB-unC (Figure S8).

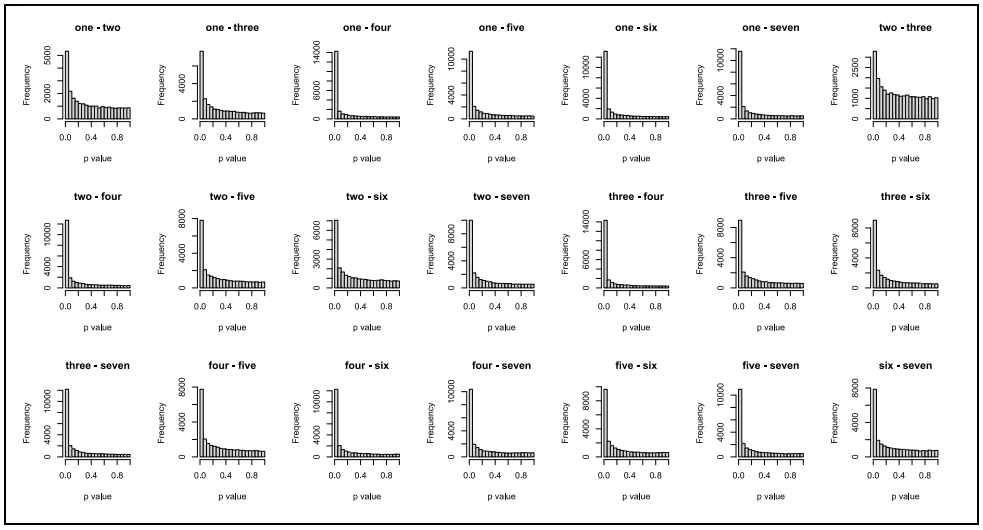

Figure A4-18. Histograms of p-values from contrasts by HCA cluster shows high numbers of significantly different features for MB-C.

Table A4-4. Counts of features with $p_{adj} < 0.05$ for MB-unC and MB-C, by HCA cluster, Site, and Month

Contrast	MB-unC	MB-C
In - A	1434	
In - B	1658	
In - C	1016	
In - D	837	
In - E	486	
In - G	42	1
In - Eff	691	
A - B	1155	
A - C	353	
A - D	353	
A - E	403	
A - G	1245	
A - Eff	556	
B - C	530	
B - D	856	
B - E	948	
B - Eff	1092	
C - E	61	
C - G	1714	
C - Eff	43	
D - G	643	
E - G	529	
G - Eff	755	5

Contrast	MB-unC	MB-C
January - November	179	14
January - September	917	
January - August	821	
January - July	1062	2
January - June	1677	
January - May	1300	
November - September	1012	
November - August	931	
November - July	1286	
November - June	1823	
November - May	1471	
September - August	8	5
September - July	98	88
September - June	1275	
September - May	498	
August - July	154	136
August - June	1276	
August - May	519	
July - June	1071	
July - May	457	
June - May	1290	

Contrast	MB-unC	MB-C
one - two	1825	123
one - three	1509	464
one - four	1699	2046
one - five	2191	1243
one - six	1949	1782
one - seven	2220	1406
two - three	848	7
two - four	613	1687
two - five	1607	628
two - six	2031	656
two - seven	1941	1077
three - four	492	2052
three - five	1804	816
three - six	2212	1011
three - seven	2143	1508

Contrast	MB-unC	MB-C
four - five	1620	761
four - six	1898	1524
four - seven	1856	1177
five - six	2412	945
five - seven	2166	1198
six - seven	1513	760

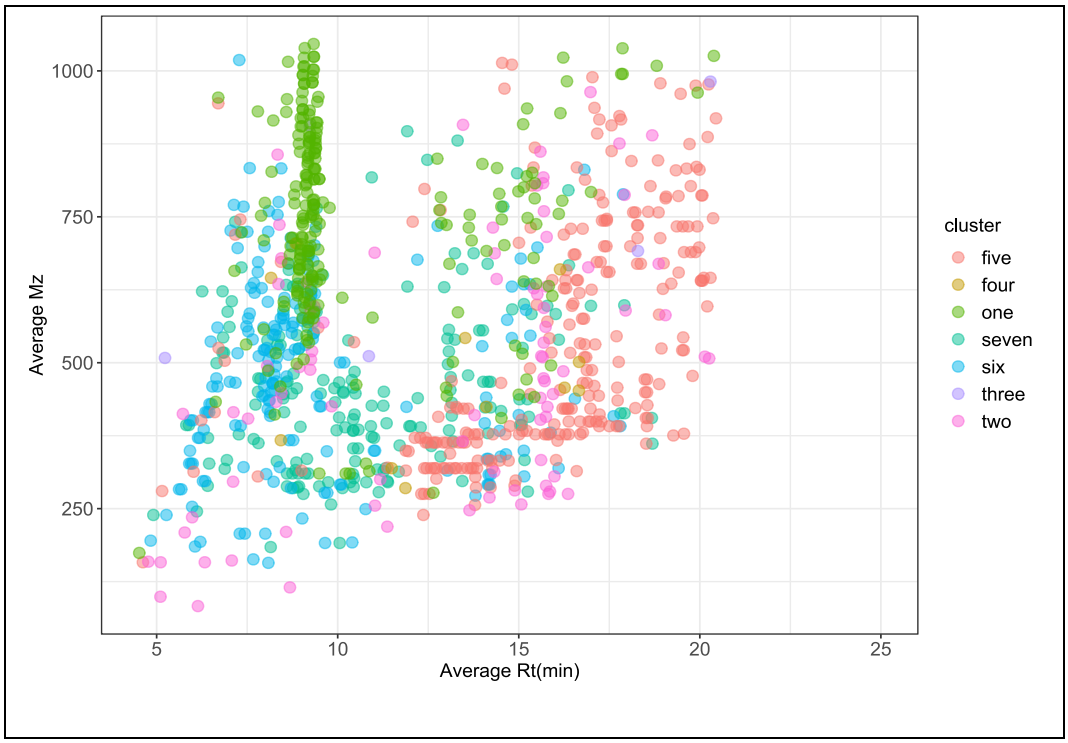

Figure A4-19. M/z to RT plot of features found to be significantly lower in a single cluster (denoted by color) in MB-unC dataset.

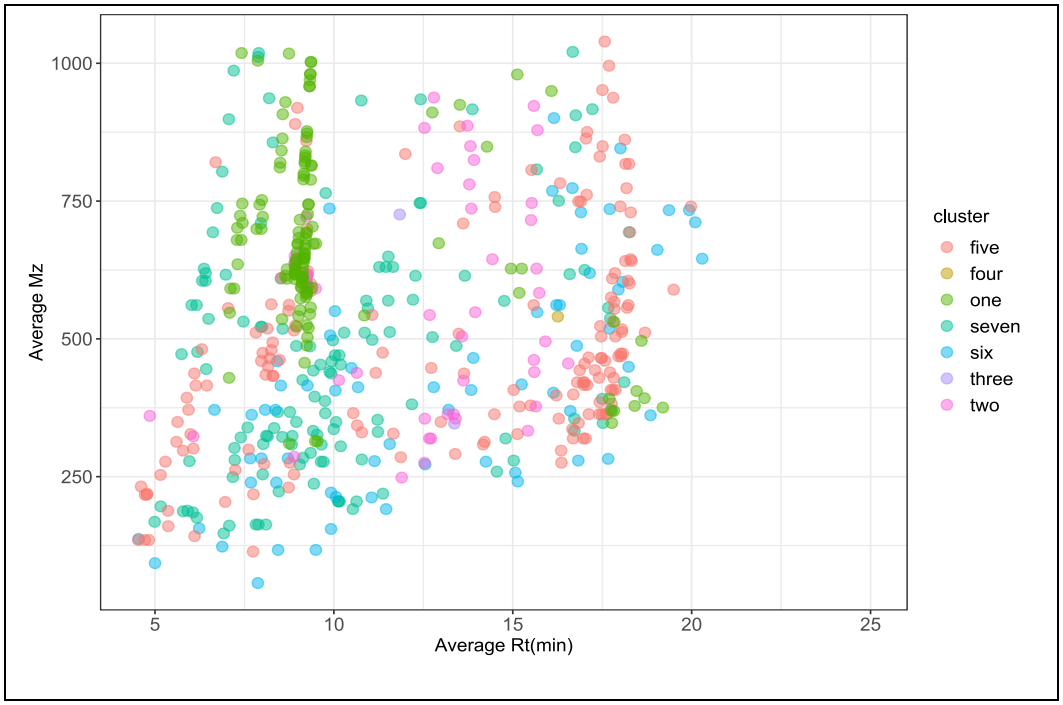

Figure A4-20. M/z to RT plot of features found to be significantly higher in a single cluster (denoted by color) in MB-unC dataset.

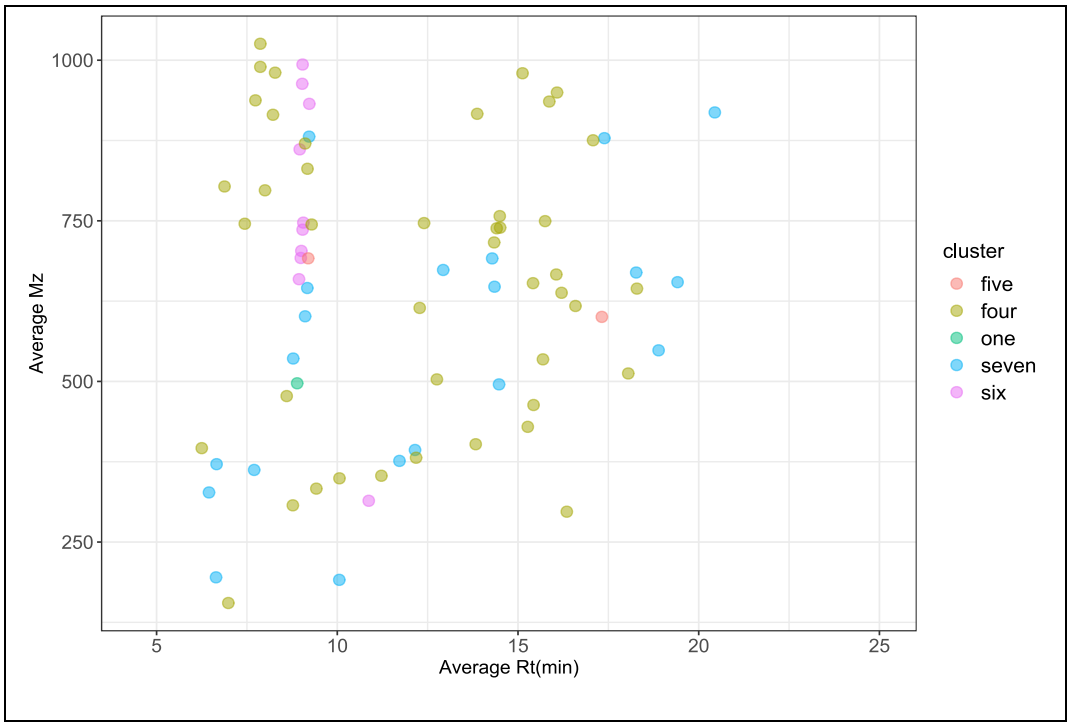

Figure A4-21. M/z to RT plot of features found to be significantly higher in a single cluster (denoted by color) in MB-C dataset.

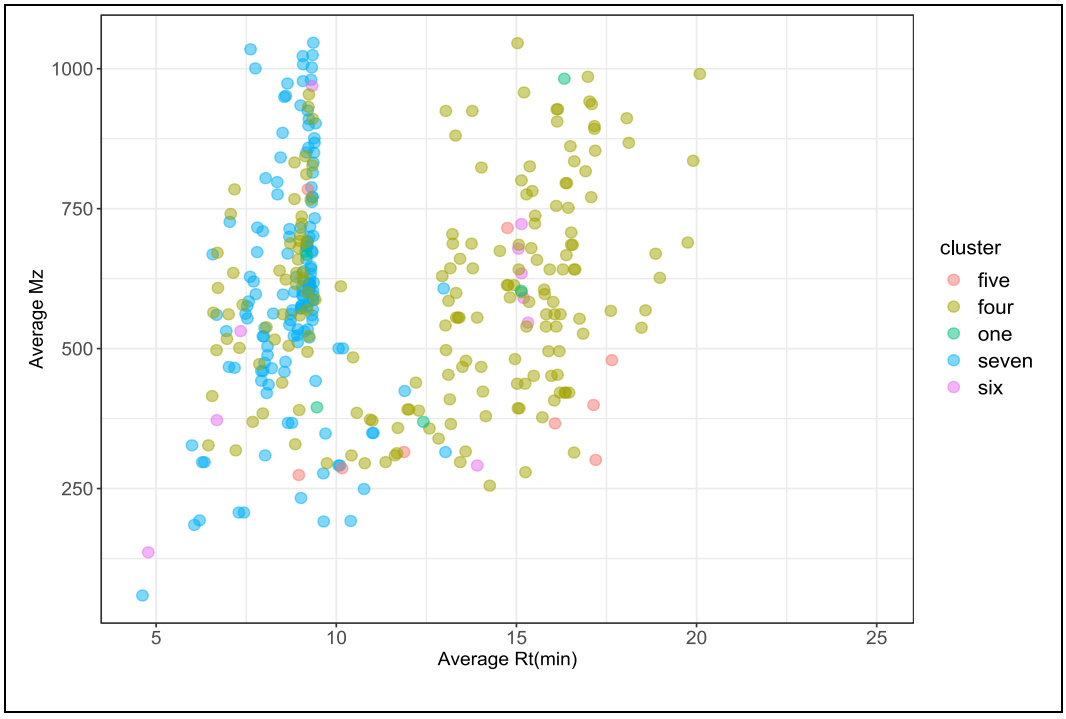

Figure A4-22. M/z to RT plot of features found to be significantly lower in a single cluster (denoted by color) in MB-C dataset.

References

Kassambara, A. and Mundt, F. (2020). factoextra: Extract and Visualize the Results of Multivariate Data Analyses. R package version 1.0.7. https://CRAN.R-project.org/package=factoextra

APPENDIX 5 SUPPORTING INFORMATION FOR CHAPTER 4

Equations

$$Rank\ Score = 0.5\left(\frac{1}{MSFinder\ Rank}\right) + 0.5\left(\frac{1}{SIRIUS\ Rank}\right) \quad \text{Eq. A1}$$

$$Match\ Score = 0.5\left(\frac{MSFinder\ Score}{10}\right) + 0.5\left(\frac{10}{|CSI\ Score|}\right) \quad \text{Eq. A2}$$

$$Overall\ Score = 0.4(Match\ Score) + 0.6(Rank\ Score) \quad \text{Eq. A3}$$

Abbreviations:

Experiments

I-1: first imidacloprid-spiked microcosm; I-2: second imidacloprid-spiked microcosm; D: diuron-spiked microcosm

Experimental groups

NWC: no-woodchip control; MC: microbially suppressed control with woodchips; TB: microbially active woodchips

Statistically determined patterns

Ads: Adsorbed; Deg: degraded microbially; Des: desorbed; Met: microbial metabolite; MC: chemical that desorbs but would be degraded microbially in TB

Table A5-1: Spearman's rho and p-values for PubChemLite and Envipath-matched features, I-1

		NWC		MC		TB		
Average Mz	Average Rt (min)	ρ	p	ρ	p	ρ	p	Pattern
100.0765	5.06	-0.46	0.06	**0.95**	**0.00**	0.19	0.44	MC
102.0916	5.60	0.33	0.18	**0.96**	**0.00**	-0.29	0.25	MC
130.1602	6.34	-0.12	0.63	**-0.76**	**0.00**	**-0.77**	**0.00**	Ads
146.0586	8.38			**0.90**	**0.00**			MC
162.0550	8.24	0.35	0.16	**0.93**	**0.00**	0.55	0.019	Des
176.0705	8.69	0.27	0.29	**0.97**	**0.00**	-0.24	0.33	MC
188.0706	5.98	-0.02	0.93	**0.60**	**0.01**	0.02	0.95	MC
188.0707	5.71	-0.20	0.43	**0.90**	**0.00**	-0.23	0.37	MC
192.1399	10.78	0.48	0.04	-0.24	0.35	-0.19	0.45	
193.122	7.26	-0.07	0.79	**0.89**	**0.00**	0.26	0.29	MC
208.0992	7.72	-0.23	0.35	**0.85**	**0.00**	-0.20	0.43	MC
209.1171	7.44	-0.01	0.98	**0.92**	**0.00**	0.00	0.99	MC
227.1278	7.41	-0.09	0.72	**0.92**	**0.00**	-0.13	0.59	MC
237.1118	9.15	-0.41	0.09	**0.71**	**0.00**	0.19	0.45	MC
239.0597	10.87	-0.05	0.85	**-0.47**	**0.05**	**-0.51**	**0.03**	Ads
256.0603	8.10	0.03	0.89	**-0.77**	**0.00**	**-0.74**	**0.00**	Ads
281.2484	15.86	0.20	0.42	**0.59**	**0.01**	0.01	0.97	
281.2484	15.90	0.63	0.01	**0.73**	**0.00**	-0.32	0.19	MC

284.2958	18.23	-0.45	0.06	**-0.54**	**0.02**	**-0.49**	**0.04**	Ads
299.2589	15.88	0.69	0.00	**0.76**	**0.00**	-0.37	0.13	MC
301.1823	12.44	0.04	0.86	**0.56**	**0.02**	0.37	0.13	MC
313.1548	12.90	0.17	0.50	**0.67**	**0.00**	**0.70**	**0.00**	Des
321.2407	15.88	-0.01	0.97	**0.57**	**0.01**	-0.22	0.37	MC
334.238	12.35	-0.35	0.15	**-0.72**	**0.00**	**-0.58**	**0.01**	Ads
347.2218	11.50	0.16	0.53	0.03	0.89	-0.08	0.77	
390.1091	11.11	0.14	0.58	0.40	0.10	0.42	0.08	
403.2469	15.89	0.06	0.82	-0.08	0.76	-0.17	0.50	
454.9981	13.07	-0.30	0.22	0.15	0.54	**0.71**	**0.00**	Met
473.013	10.99	0.21	0.40	-0.03	0.91	**-0.88**	**0.00**	Deg
481.9777	11.67	-0.23	0.35	0.36	0.14	0.42	0.09	
549.281	19.7	-0.34	0.17	**0.72**	**0.00**	**0.65**	**0.00**	Des
549.2865	19.62	0.03	0.90	**0.56**	**0.01**	-0.36	0.15	MC

Table A5-2: Spearman's rho and p-values for PubChemLite and Envipath-matched features, D

		NWC		MC		TB		
Average Mz	Average Rt (min)	ρ	p	ρ	p	ρ	p	Pattern
73.0648	4.91			0.25	0.33	-0.15	0.55	
73.0654	5.81			-0.19	0.47	0.04	0.87	
73.0659	5.02			0.00	0.99	-0.08	0.74	
100.0765	5.06	0.27	0.29	0.04	0.88	0.24	0.35	
102.0916	5.60	0.25	0.33	-0.10	0.70	0.03	0.91	
130.1602	6.34	0.37	0.14	0.44	0.08	**-0.69**	**0.00**	Deg
146.0586	8.38	-0.28	0.27	**0.90**	**0.00**	**0.49**	**0.04**	Des
162.0550	8.24	-0.11	0.67	**0.94**	**0.00**	0.14	0.58	MC
176.0705	8.69	-0.02	0.93	**0.97**	**0.00**	0.24	0.33	MC
188.0693	5.24			0.34	0.18	-0.25	0.32	
188.0705	5.84			0.26	0.32	-0.06	0.81	
188.0706	5.98	0.34	0.18	**0.52**	**0.03**	-0.17	0.49	MC
188.0707	5.71	-0.66	0.00					
188.0714	4.97			0.24	0.35	0.30	0.23	
192.1399	10.78	0.04	0.89	**0.63**	**0.01**	0.07	0.78	MC
193.122	7.26	-0.46	0.06	0.47	0.06	0.22	0.37	
208.0992	7.72	-0.03	0.91	0.32	0.21	-0.16	0.52	
209.1171	7.44	-0.28	0.27	**0.66**	**0.00**	-0.01	0.98	MC
227.1263	7.27			-0.26	0.31	0.06	0.80	
227.1278	7.41	-0.24	0.35	**0.82**	**0.00**	0.45	0.06	MC
227.1287	7.18			0.36	0.15	-0.23	0.37	
237.1118	9.15	-0.38	0.13					
239.0597	10.87	0.23	0.37	-0.36	0.16	0.27	0.29	
256.0603	8.1	0.04	0.89	**-0.64**	**0.01**	**-0.48**	**0.04**	Ads

281.2484	15.86	-0.09	0.72	**0.74**	**0.00**	**-0.55**	**0.02**	
281.2484	15.9	-0.15	0.57	0.44	0.08	-0.46	0.06	
284.2958	18.23	-0.28	0.27	-0.20	0.43	-0.27	0.29	
293.1727	9.68			0.24	0.36	0.36	0.14	
299.2589	15.88	-0.03	0.92	**0.74**	**0.00**	**-0.62**	**0.01**	
301.1823	12.44	0.65	0.00					
313.1548	12.9	0.18	0.49	**0.66**	**0.00**	0.34	0.17	MC
321.2407	15.88	-0.04	0.89	**0.74**	**0.00**	-0.05	0.83	MC
334.238	12.35	0.09	0.73	**-0.53**	**0.03**	-0.25	0.32	
347.2218	11.50	0.07	0.79	**0.59**	**0.01**	-0.10	0.69	MC
390.1091	11.11	0.21	0.41	**0.97**	**0.00**	0.91	0.00	MC
403.2469	15.89	0.02	0.95	**0.80**	**0.00**	0.38	0.12	MC
454.9981	13.07	0.52	0.03	0.28	0.27	**0.61**	**0.01**	Met
473.013	10.99	0.21	0.43	**0.64**	**0.01**	0.70	0.00	MC
481.9777	11.67	0.26	0.32	**0.53**	**0.03**	0.45	0.06	MC
549.281	19.7	0.25	0.33					
549.2865	19.62	0.23	0.37	-0.29	0.26	0.06	0.82	

Table A5-3: Spearman's rho and p-values for PubChemLite and Envipath-matched features, I-2

		NWC		MC		TB		
Average Mz	Average Rt (min)	ρ	p	ρ	p	ρ	p	Pattern
100.0765	5.06	-0.16	0.55	**0.89**	**0.00**	0.10	0.70	MC
102.0916	5.6025	-0.16	0.55	**0.94**	**0.00**	-0.15	0.56	MC
130.1602	6.34	-0.19	0.47	-0.07	0.78	0.30	0.23	
162.0550	8.24	0.11	0.68	**0.99**	**0.00**	0.32	0.20	MC
176.0705	8.69	0.15	0.56	**0.79**	**0.00**	0.35	0.15	MC
188.0706	5.98	0.17	0.52	**0.86**	**0.00**	**0.53**	**0.02**	Des
188.0707	5.7125	0.09	0.73	**0.94**	**0.00**	0.40	0.10	MC
192.1399	10.775	0.30	0.25	0.19	0.45	0.44	0.07	
193.122	7.26	0.06	0.83	**0.92**	**0.00**	-0.40	0.10	MC
208.0992	7.72	-0.21	0.43	0.39	0.11	0.12	0.65	
209.1171	7.44	-0.08	0.77	**0.92**	**0.00**	0.36	0.15	MC
227.1278	7.41	-0.15	0.57	**0.92**	**0.00**	0.39	0.11	MC
239.0597	10.87	-0.06	0.83	-0.04	0.87	0.30	0.22	
281.2484	15.86	0.14	0.60	0.29	0.25	-0.29	0.24	
281.2484	15.9	-0.20	0.44	**0.69**	**0.00**	-0.04	0.86	MC
284.2958	18.23	0.35	0.17	0.40	0.10	0.44	0.07	
293.1727	9.68	0.31	0.22	0.30	0.22	**0.53**	**0.02**	Met
297.1448	12.32	-0.18	0.49	**0.67**	**0.00**	0.38	0.12	MC
299.2589	15.88	0.26	0.32	**0.98**	**0.00**	-0.26	0.31	MC
313.1548	12.9	0.11	0.67	**0.56**	**0.02**	**0.74**	**0.00**	Des
321.2407	15.88	0.31	0.23	**0.97**	**0.00**	0.04	0.87	MC

390.1091	11.11			**0.73**	**0.00**	**0.85**	**0.00**	Des
403.2469	15.89	0.25	0.34	0.19	0.45	-0.19	0.46	
454.9981	13.07	-0.08	0.75	**0.76**	**0.00**	0.35	0.15	MC
473.013	10.99	-0.08	0.76	**0.47**	**0.05**	0.29	0.25	MC
549.281	19.7	-0.17	0.51	0.20	0.43	0.35	0.15	

Table A5-4: Prioritized features for tMS/MS and results

Avg Mz	Avg Rt (min)	Source[1]	Exact-mass match name	Suspect description	tMS/ MS[2]	Identification Level[3]	PUR 2016-2018[4]	RTI Pred Box[5]
73.0659	5.02	E	Butanone	Predicted TP: Butopyronoxyl	A		No	
100.0765	5.06	P	1-methyl-2-pyrrolidine	inert	A		NA	
102.0916	5.60	P	4,4-dimethyloxazolidine	microbiocide	B		No	
130.1602	6.34	P	Dibutylamine	TP (carbosulfan)	A		No	
146.0586	8.38	E		Predicted TP: Aldimorph	A		No	
162.055	8.24	MoNA	Indole carboxylic acid		A	2a	NA	2
176.0705	8.69	P	Indole-3-acetic acid	Growth hormone	A	3	NA	3
188.0714	4.97	E		Predicted TP: Atrazine	A		No	
192.1399	10.78	P	DEET	Insecticide	A	2a	No	2
193.122	7.26	P	4-tert-Butylphenylacetic acid	TP (fenazaquin)	C		No	
208.0992	7.72	P	S-Metolachlor Metabolite CGA 50720	TP (metolachlor)	A	2b	Yes	1
209.1171	7.44	P	SCHEMBL7753233	TP (etofenprox)	A		No	
227.1287	7.18	E		Predicted TP: Butopyronoxyl	C		No	
237.1118	9.15	P	Fenazaquin metabolite NN4	TP (fenazaquin)	D		No	
281.2484	15.9	P	(Z,Z)-Gossyplure	Insect attractant	B		No	
284.2958	18.23	P	Aldimorph	Fungicide	A		No	
293.1727	9.68	E		Predicted TP: MCPA-isooctyl	B		No	
297.1448	12.32	P	2,4-dinitro-6-(1-methylheptyl)phenol	TP (meptyldinocap)	D		No	
299.2589	15.88	P	Ricinoleic acid	inert (emulsifying)	A		NA	2
301.1823	12.44	P	Prallethrin	Insecticide	A		No	
313.1548	12.9	P	MCPA-isooctyl	Herbicide	A		No	
334.238	12.35	P	Fenpropimorphic Acid	TP (fenpropimorph)	A		No	
347.2218	11.5	P	AKM 18	TP (acequinocyl)	A		Yes	
390.1091	11.11	P	Azoxystrobin acid	TP (azoxystrobin)	A	2a	Yes	1

Avg Mz	Avg Rt (min)	Source[1]	Exact mass match name	Suspect description	tMS/ MS[2]	Identification Level[3]	PUR 2016-2018[4]	RTI Pred Box[5]
403.2469	15.89	E		Predicted TP: antimycin A1	D		No	
454.9981	13.07	E	IN-J9Z38	Predicted TP: Cyantraniliprole	A	2a	Yes	2
473.013	10.99	P	Cyantraniliprole	Insecticide	A	2a	Yes	1
481.9777	11.67	P	Chlorantraniliprole	Insecticide	A	2a	Yes	2
549.2865	19.62	P	Antimycin A1	Piscicide	A		No	

[1] E = Envipath predicted; P = PubChemLite with Agrochemical information; MoNA = Mass Bank of North America (http://mona.fiehnlab.ucdavis.edu), used for suspect screening during alignment step
[2] Success of tMS/MS experiment: peak captured with good shape (A), peak captured but noisy or poor peak shape (B), peak missed but good shape (C), or peak missed with bad shape (D)
[3] As described in (Schymanski et al., 2014)
[4] Reported applications in fields draining to the PG&E bioreactor, from CDPR Pesticide Use Reporting Database, 2016-2018 (*Pesticide Use Reporting, Annual 2016-2018*, n.d.)
[5] Using RTI prediction tool, accepting "Exp. & Pred. tR are accepted for this candidate (box1)" and "Although there is error, exp. & pred. tR are accepted for this candidate (box2)" (Aalizadeh et al., 2021)

MS/MS and Weight of Evidence Confirming Structures of Prioritized Features

m/z = 162. 055 (Indole carboxylic acid)

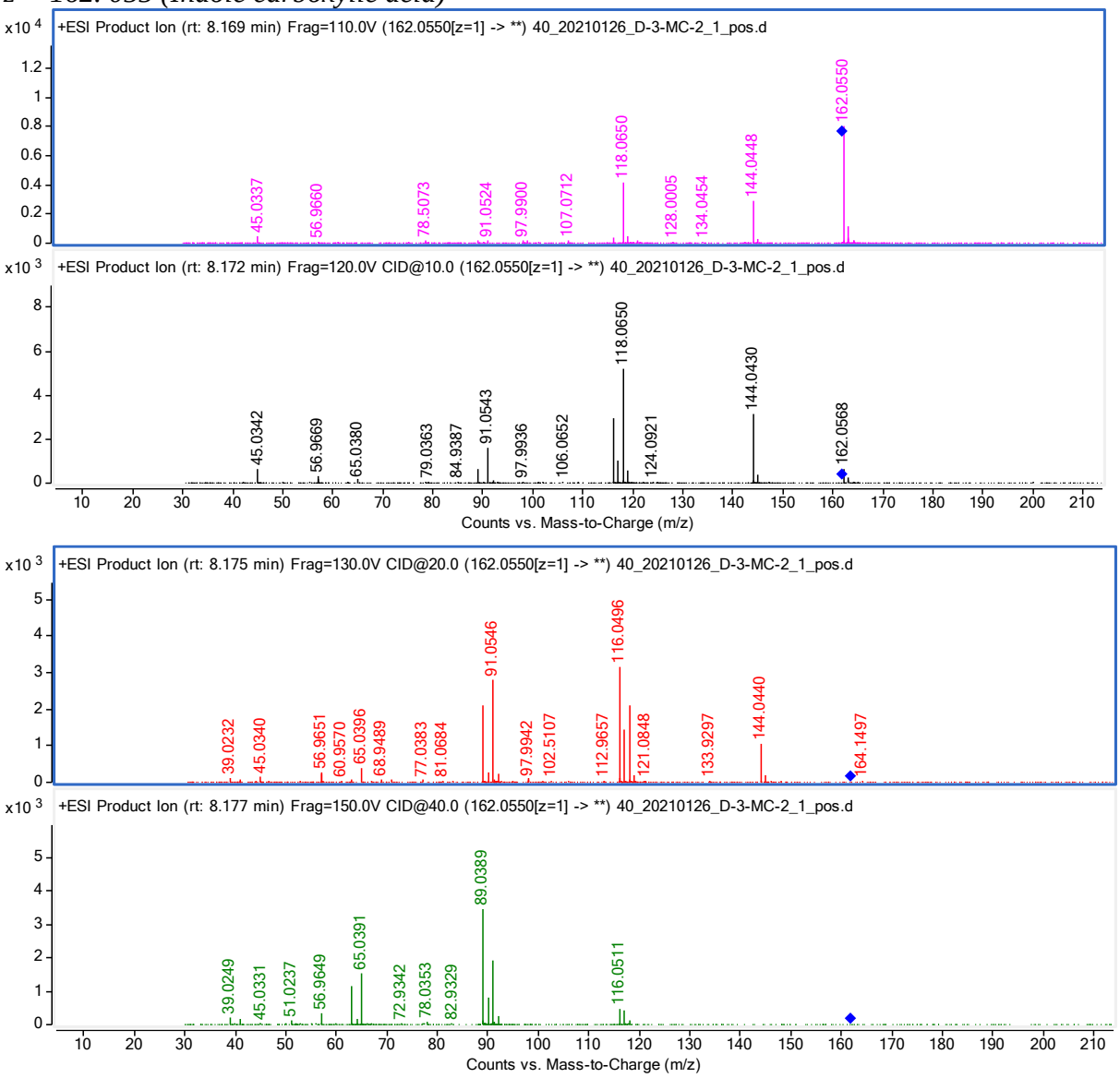

Figure A5-1. Targeted MS/MS results for m/z = 162.055 at collision energies 0, 10, 20 and 40 eV.

Table A5-5: Fragment m/z and average mass error

Fragment m/z*	Average mass error (ppm)
162.06	-25.3
144.045	-7.4
118.068	-25.4

*from indole-3-carboxylic acid spectra recorded in MassBank Europe (https://massbank.eu/MassBank/Result.jsp?inchikey=KMAKOBLIOCQGJP-UHFFFAOYSA-N)

m/z = 176.0705 (Indole acetic acid or methyl indole-3-carboxylic acid)

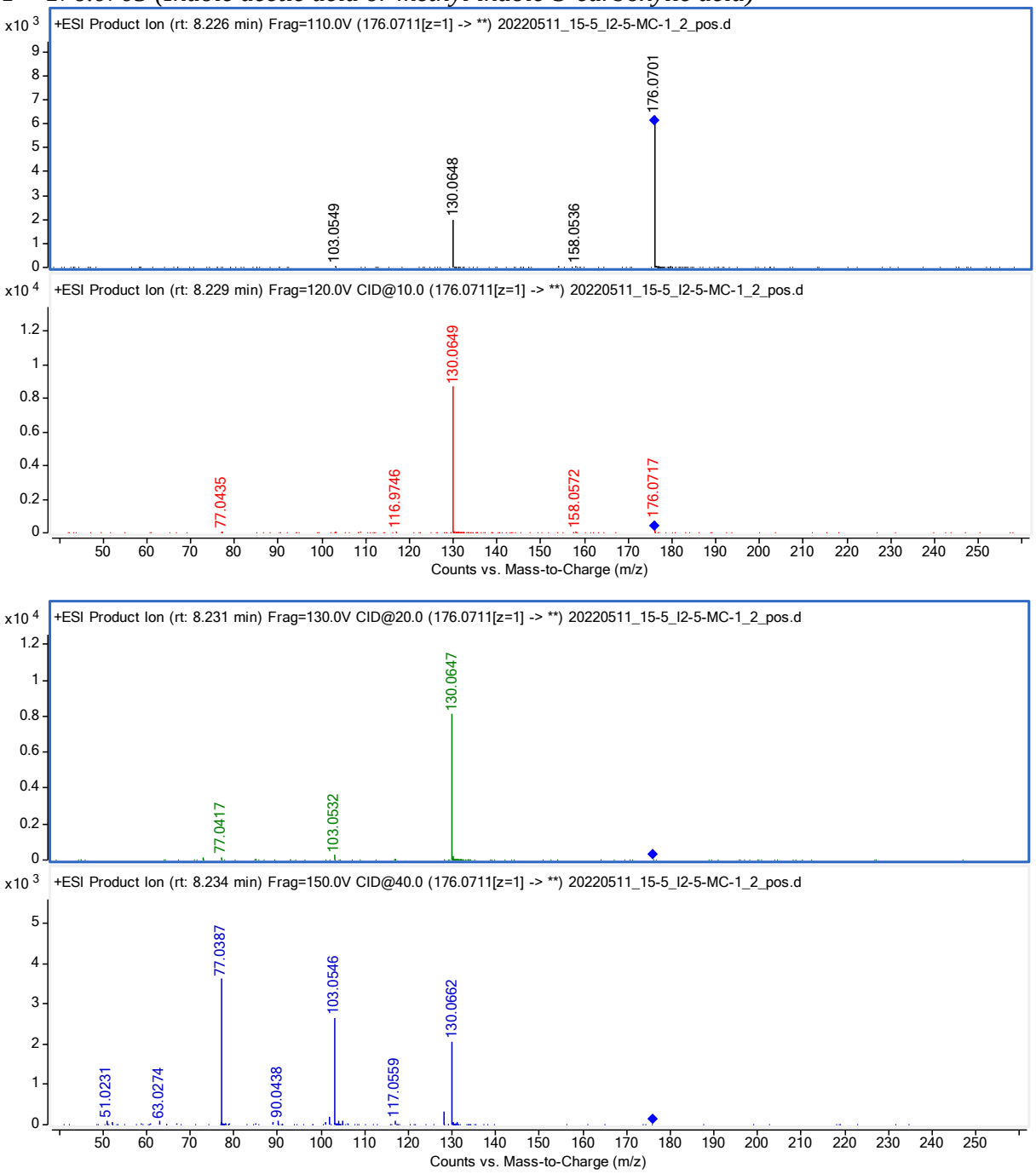

Figure A5-2. Targeted MS/MS results for m/z = 176.0705 at collision energies 0, 10, 20 and 40 eV.

m/z = 192.1388 (DEET)

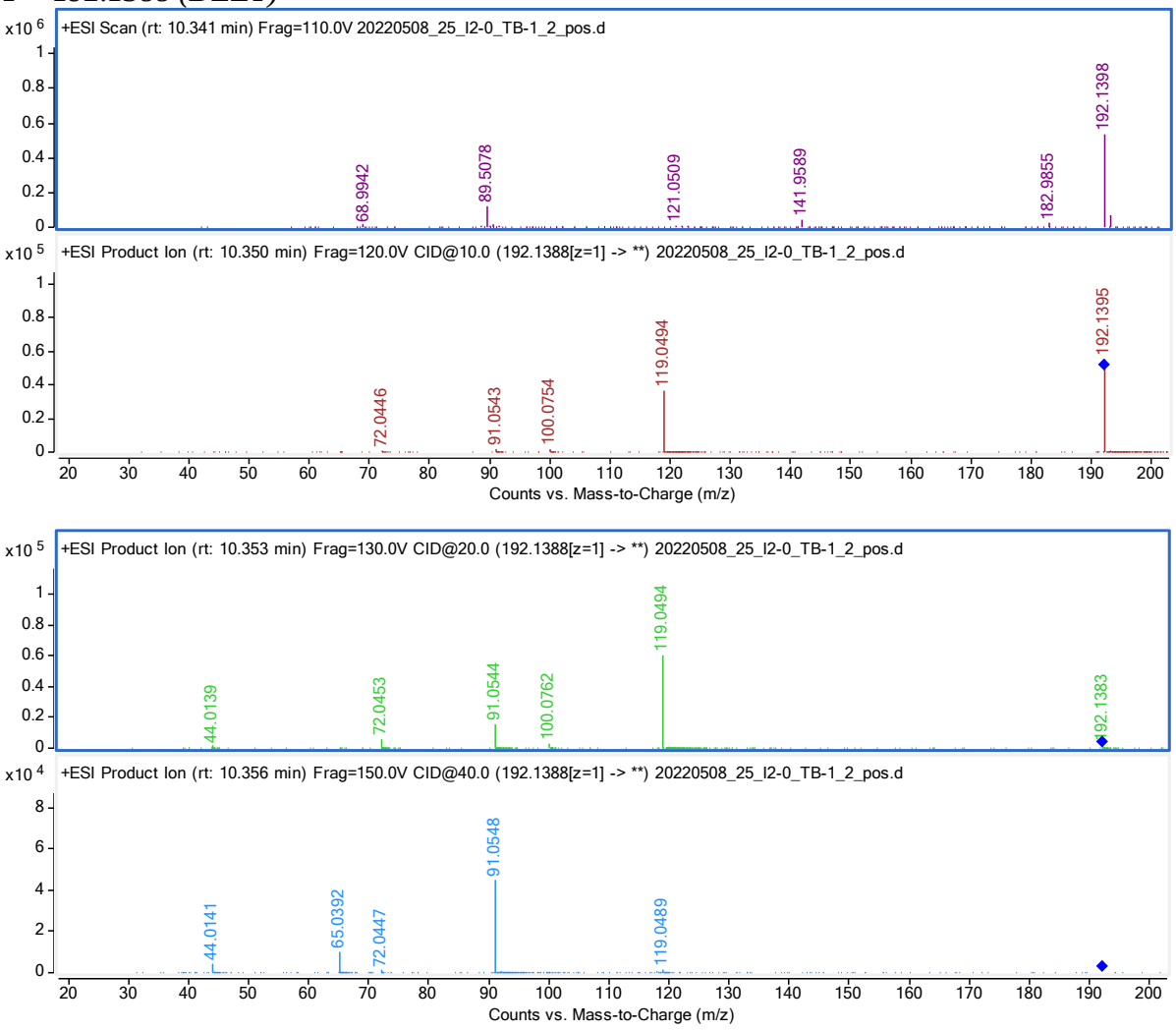

Figure A5-3. Targeted MS/MS results for m/z = 192.1388 at collision energies 0, 10, 20, and 40 eV.

Table A5-6: Fragment m/z and average mass error

Fragment m/z*	Average mass error (ppm)
192.1388	4.42
119.049	3.36
91.0543	5.49

* Fragments from 500 ng/mL DEET standard, Figure A5-4

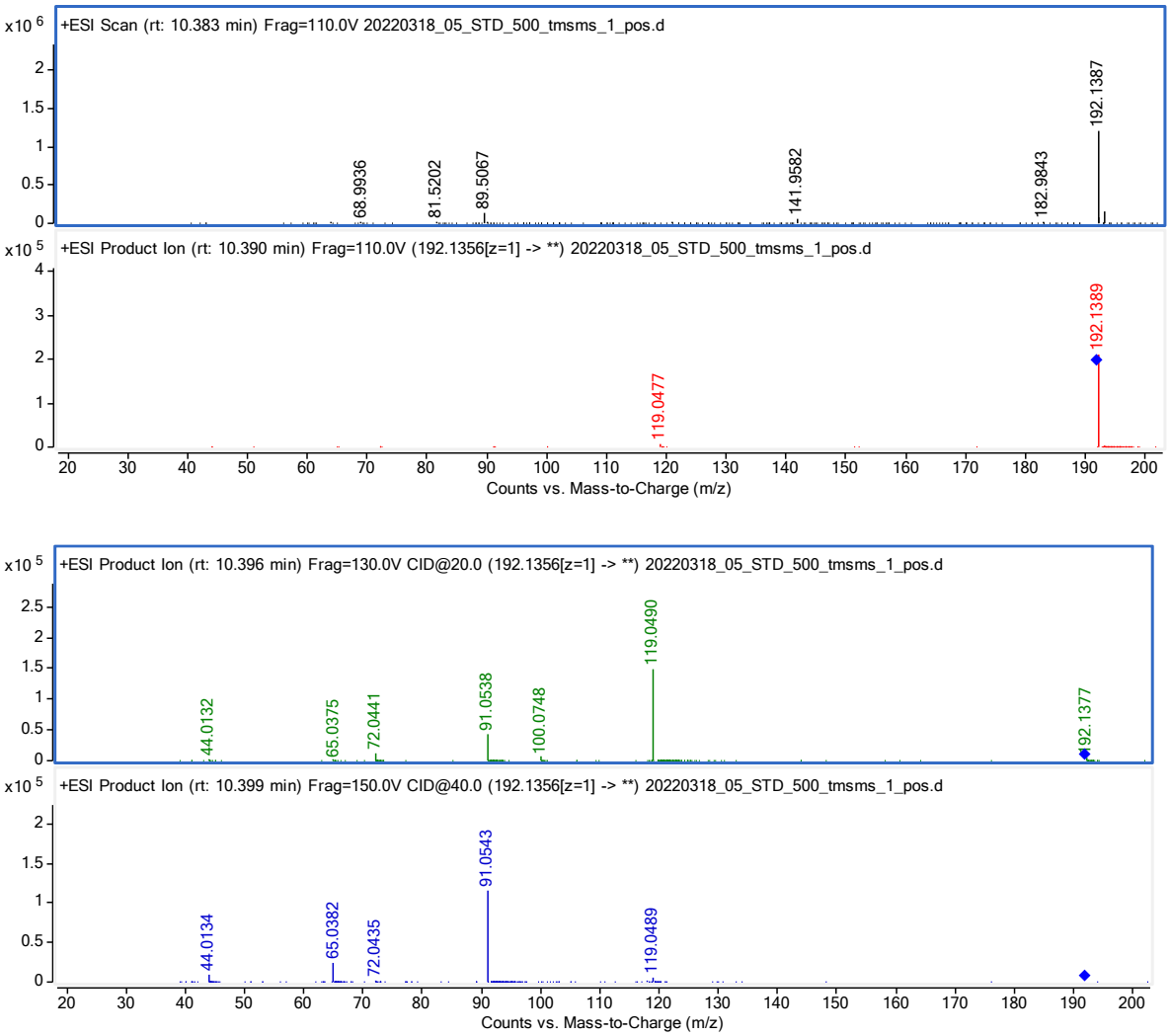

Figure A5-4. Targeted MS/MS results for 500 ng/mL DEET standard at collision energies 0, 10, 20, and 40 eV.

m/z/ = 208.0973 (S-Metolachlor metabolite CGA 50720)

Figure A5-5. Targeted MS/MS results for m/z = 208.0973 at collision energies 0, 10, 20, and 40 eV

Table A5-7: Fragment m/z and average mass error, CGA 50720 (SAWXESXDACFEPC-UHFFFAOYSA-N)

CFM-ID fragment m/z	Average mass error (ppm)
208.0968	1.35
190.0863	3.37
162.0913	-1.48
120.0808	-1.08
103.0542	2.13

m/z = 390.1090 (Azoxystrobin acid)

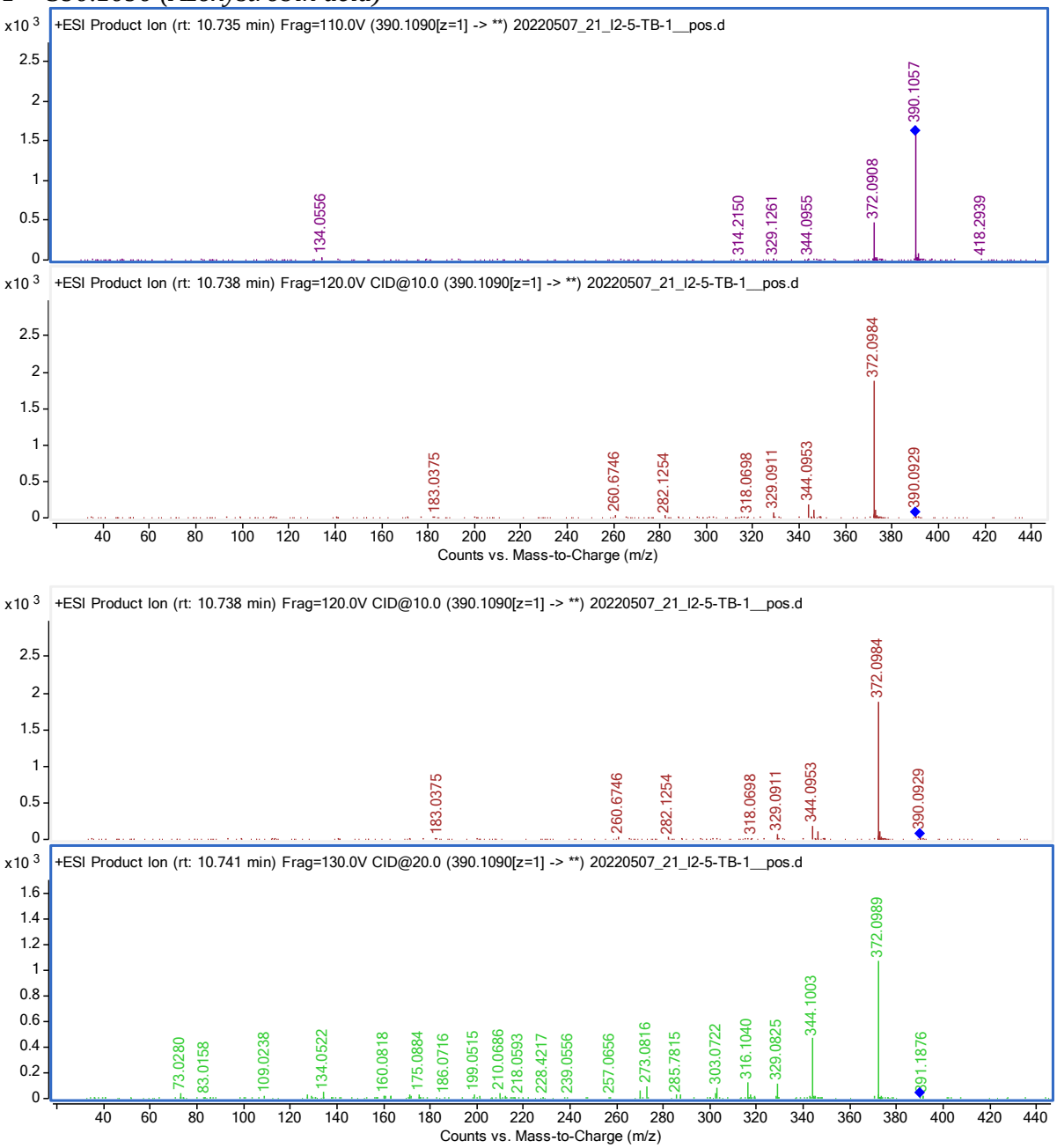

Figure A5-6. tMS/MS for m/z = 390.1090 at 0, 10, 20, and 40 eV collision energies.

Table A5-8: Fragment m/z and average mass error for azoxystrobin acid

Library fragment m/z*	Average mass error (ppm)
390.1086	-7.43
372.0981	-3.96
344.1026	-13.95

*Library spectrum from MassBank Europe:
https://massbank.eu/MassBank/Result.jsp?inchikey=IKCXDZCEWZARFL-FOWTUZBSSA-N

m/z = 473.0130 (Cyantraniliprole)

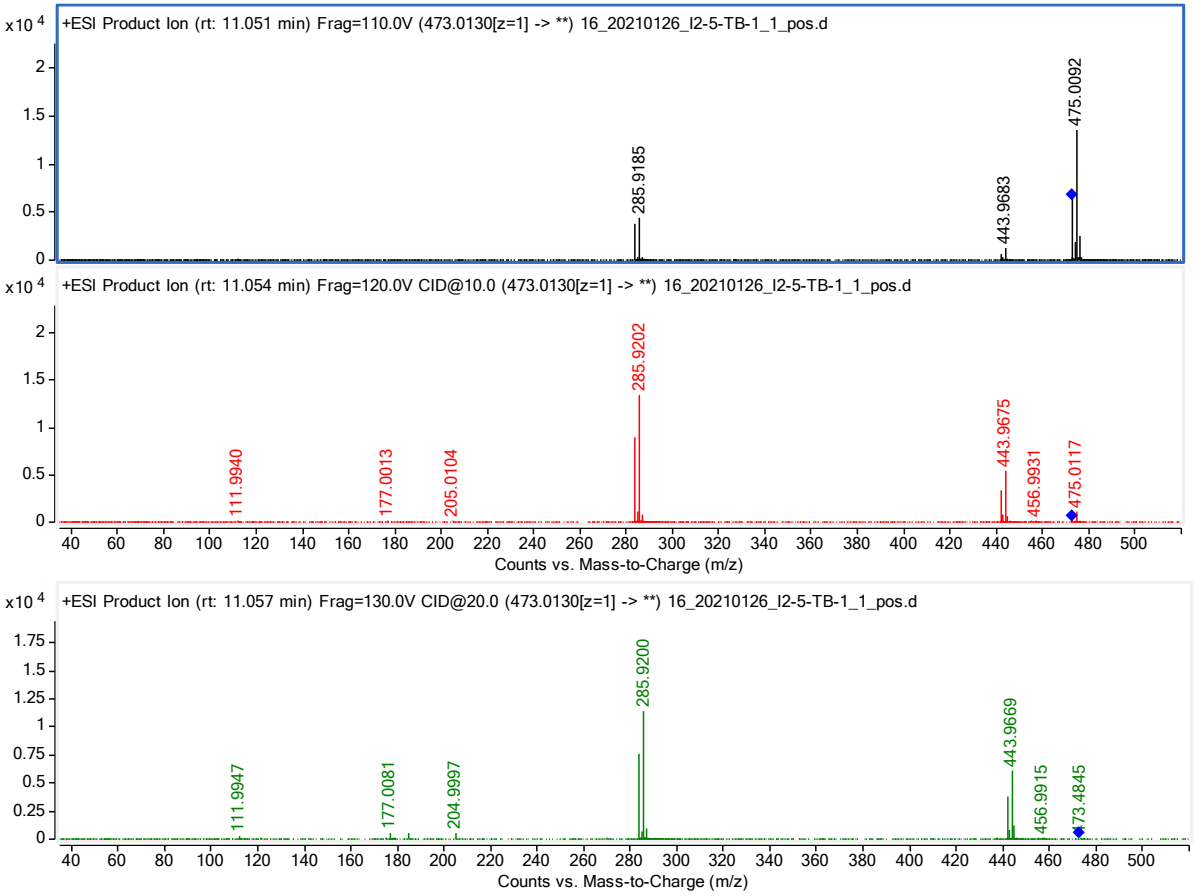

Figure A5-7. tMS/MS for m/z = 473.0130 at 0, 10, and 20 eV collision energies.

Table A5-9: Previously reported fragment m/z and experimental mass error

Fragment m/z*	Average mass error (ppm)
475.0102	-2.11
443.9686	-3.15
285.9204	-2.91

*Fragments reported by (Zhang et al., 2021)

m/z = 481.9786 (Chlorantraniliprole)

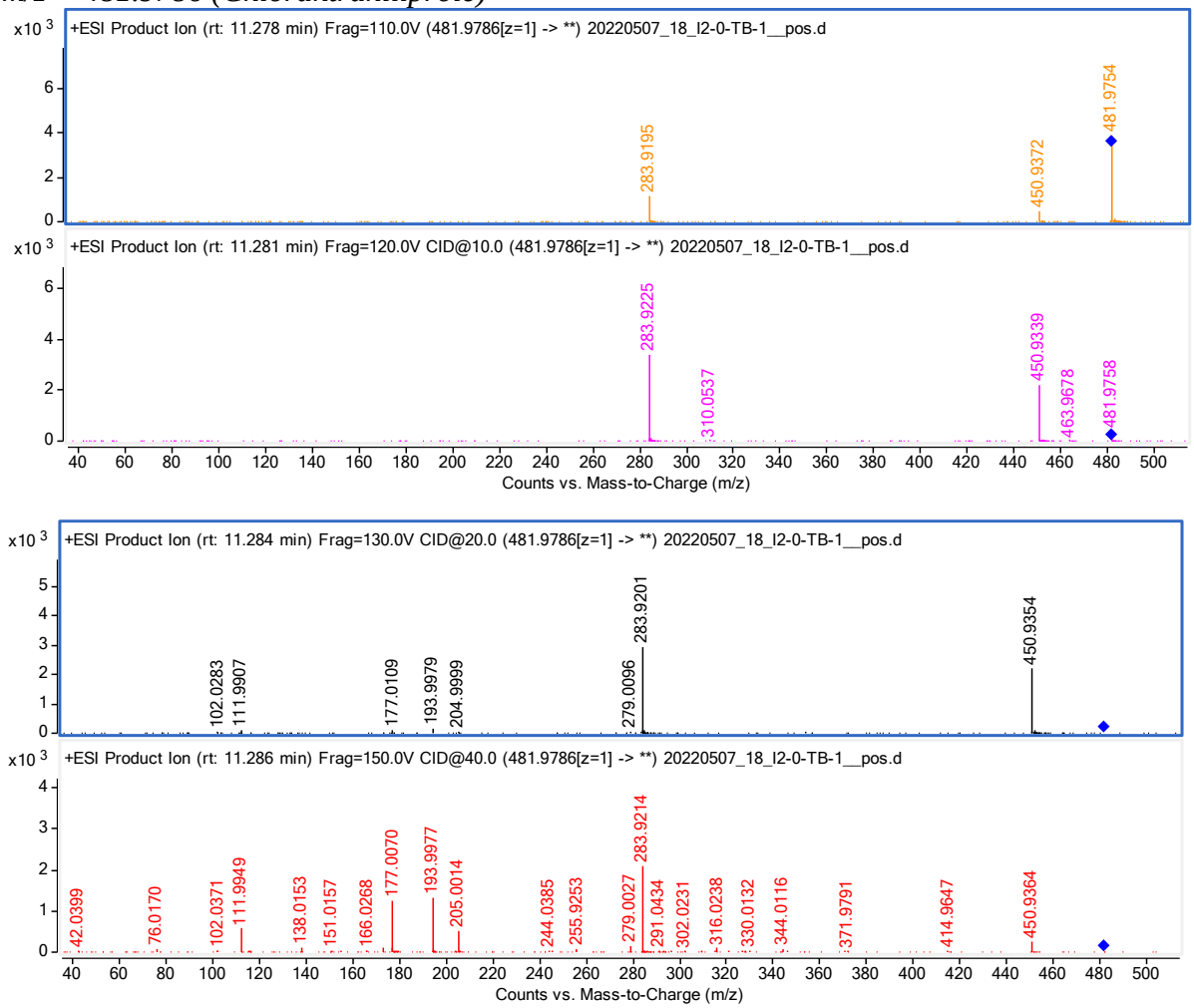

Figure A5-8. tMS/MS for m/z = 481.9786 at 0, 10, and 20 eV collision energies.

Table A5-10: Library fragment m/z and mass errors for chlorantraniliprole

Library fragment m/z*	Average mass error (ppm)
450.9384	-8.42
283.9208	0.24
205.0041	-13.04
193.9998	-11.07
177.0091	-11.91

*Library spectrum accessed through Massbank of North America: https://mona.fiehnlab.ucdavis.edu/spectra/browse?query=compound.metaData%3Dq%3D%27name%3D%3D%22InChIKey%22%20and%20value%3D%3D%22PSOVNZZNOMJUBI-UHFFFAOYSA-N%22%27

References

Aalizadeh, R., Alygizakis, N. A., Schymanski, E. L., Krauss, M., Schulze, T., Ibáñez, M., McEachran, A. D., Chao, A., Williams, A. J., Gago-Ferrero, P., Covaci, A., Moschet, C., Young, T. M., Hollender, J., Slobodnik, J., & Thomaidis, N. S. (2021). Development and Application of Liquid Chromatographic Retention Time Indices in HRMS-Based Suspect and Nontarget Screening. *Analytical Chemistry*, *93*(33), 11601–11611. https://doi.org/10.1021/acs.analchem.1c02348

Pesticide Use Reporting, Annual 2016-2018. (n.d.).

Schymanski, E. L., Jeon, J., Gulde, R., Fenner, K., Ruff, M., Singer, H. P., & Hollender, J. (2014). Identifying small molecules via high resolution mass spectrometry: Communicating confidence. In *Environmental Science and Technology*. https://doi.org/10.1021/es5002105

Zhang, Y., Si, W., Chen, L., Shen, G., Bai, B., & Zhou, C. (2021). Determination and dietary risk assessment of 284 pesticide residues in local fruit cultivars in Shanghai, China. *Scientific Reports*, *11*(1), 9681. https://doi.org/10.1038/s41598-021-89204-5